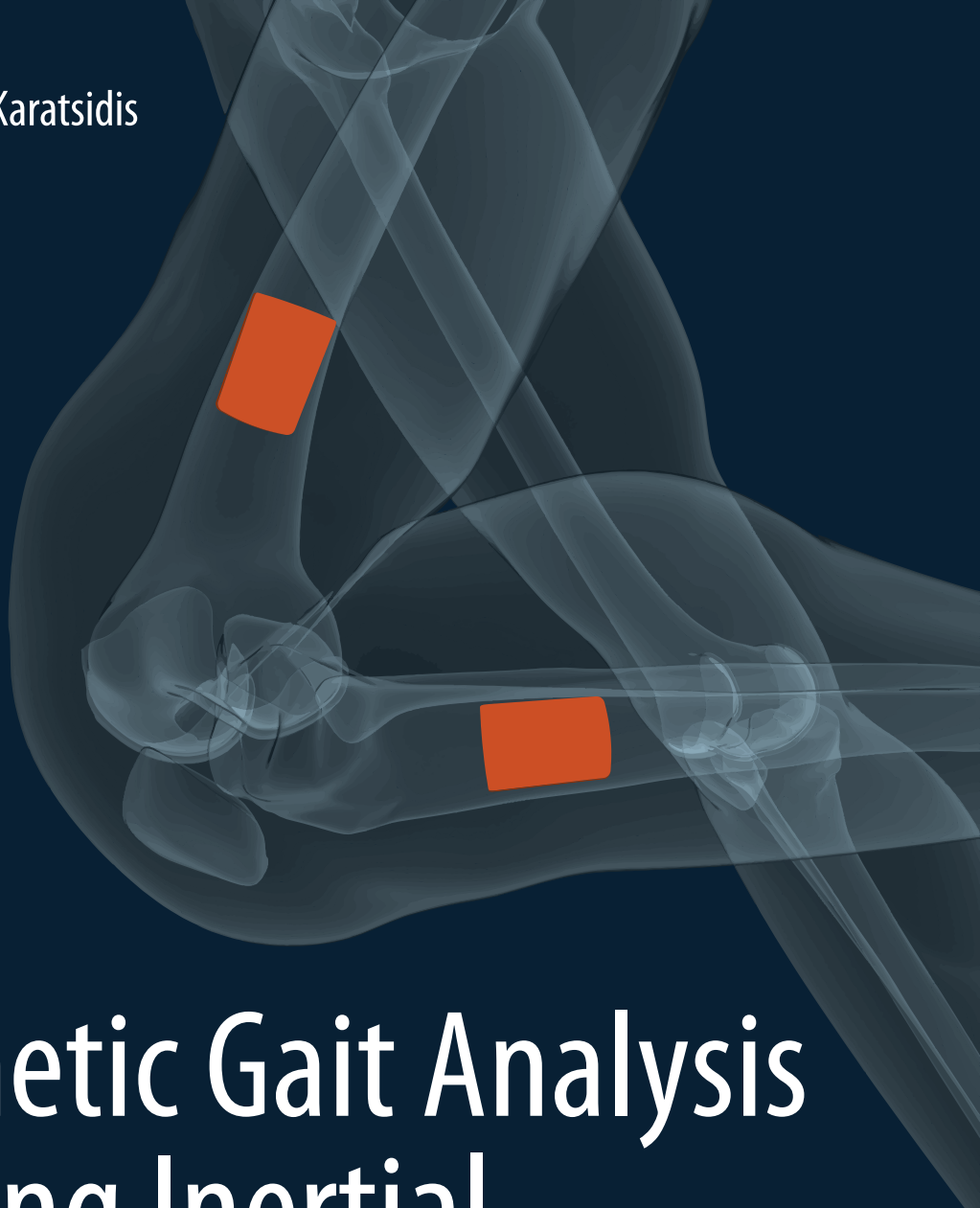


Angelos Karatsidis



Kinetic Gait Analysis Using Inertial Motion Capture

New Tools for Knee Osteoarthritis

KINETIC GAIT ANALYSIS
USING INERTIAL MOTION CAPTURE

NEW TOOLS FOR KNEE OSTEOARTHRITIS

Angelos Karatsidis

UNIVERSITY | TECHMED
OF TWENTE. | CENTRE

Department of Biomedical Signals and Systems, Faculty of Electrical Engineering, Mathematics, and Computer Science, Technical Medical Center, University of Twente



This work is part of the KNEEMO Initial Training Network for knee osteoarthritis funded by the European Union's Seventh Framework Programme for research, technological development and demonstration under grant agreement no. 607510.



The publication of this thesis was financially supported by Xsens Technologies B.V.

Paronymphs:

Frank J. Wouda and Matteo Giuberti

Cover:

Angelos Karatsidis

Printing:

Ipskamp Printing

ISBN

978-90-365-4602-7

DOI:

10.3990/1.9789036546027

© Angelos Karatsidis, 2018 - All rights reserved

No part of this publication may be reproduced or transmitted in any form or by any means, electronic or mechanical, including photocopying, recording, or any information storage or retrieval system, without written permission from the author.

KINETIC GAIT ANALYSIS USING INERTIAL MOTION CAPTURE
-
NEW TOOLS FOR KNEE OSTEOARTHRITIS

DISSERTATION

to obtain
the degree of doctor at the University of Twente,
on the authority of the Rector Magnificus,
Prof. dr. T. T. M. Palstra,
on account of the decision of the graduation committee,
to be publicly defended
on Friday the 14th of September 2018, at 12:45

by

Angelos Karatsidis

born on the 29th of October, 1990
in Didymoteicho, Greece

This dissertation has been approved by:

The supervisors: Prof. dr. ir. P. H. Veltink

Prof. dr. ir. J. Harlaar

The co-supervisor: Dr. ir. G. Bellusci

Composition of the Graduation Committee:

Chairman and secretary:

Prof. dr. J. N. Kok University of Twente

Supervisors:

Prof. dr. ir. P. H. Veltink University of Twente
Prof. dr. ir. J. Harlaar VUMC Amsterdam
Delft University of Technology

Co-supervisor:

Dr. ir. G. Bellusci Xsens Technologies B.V.

Members:

| | |
|------------------------------------|--|
| Prof. dr. ir. N. J. J. Verdonschot | University of Twente Radboud University Nijmegen |
| Prof. dr. ir. H. J. Hermens | University of Twente Roessingh Research and Development |
| Prof. dr. M. P. M. Steultjens | Glasgow Caledonian University |
| Prof. dr. L. H. V. van der Woude | University of Groningen |

Referee:

Dr. M. Kok Delft University of Technology

Contents

| | | |
|----------|---|-----------|
| 1 | Introduction | 1 |
| 1.1 | Human Movement: A story from Aristotle to Newton | 3 |
| 1.2 | Biomechanical Analysis: Definitions and Techniques | 5 |
| 1.2.1 | Human Body Kinematics | 5 |
| 1.2.2 | Human Body Kinetics | 8 |
| 1.3 | Biomechanics in Knee Osteoarthritis | 12 |
| 1.3.1 | Prevalence and Burden | 12 |
| 1.3.2 | Treatments and Management of Knee Osteoarthritis | 12 |
| 1.3.3 | Towards Subject-specific Biomechanical Interventions in Clinical Practice | 13 |
| 1.3.4 | The KNEEMO Initial Training Network | 13 |
| 1.4 | Thesis Objectives | 14 |
| 1.5 | Thesis Outline | 15 |
| 2 | Estimation of Ground Reaction Forces and Moments | 17 |
| 2.1 | Introduction | 19 |
| 2.2 | Methods | 20 |
| 2.2.1 | Experimental Protocol | 20 |
| 2.2.2 | Data Processing: IMC System | 22 |
| 2.2.3 | Data Analysis: Reference Lab System | 26 |
| 2.3 | Results | 29 |
| 2.3.1 | Accuracy Analysis | 29 |
| 2.3.2 | Sensitivity Analysis | 30 |
| 2.4 | Discussion | 32 |
| 2.4.1 | Comparison with Reported Optical-Based Estimation | 32 |
| 2.4.2 | Limitations and Sources of Error | 35 |
| 2.4.3 | Future Work | 37 |
| 2.5 | Conclusions | 38 |
| 2.A | Appendix | 39 |
| 3 | Assessment of Knee Adduction and Flexion Moments | 41 |
| 3.1 | Introduction | 43 |
| 3.2 | Materials and methods | 44 |
| 3.2.1 | Subjects | 44 |
| 3.2.2 | Instrumentation | 44 |
| 3.2.3 | Experimental procedures | 45 |

| | | |
|----------|---|-----------|
| 3.2.4 | Computational procedures | 45 |
| 3.2.5 | Data analysis | 47 |
| 3.3 | Results | 47 |
| 3.4 | Discussion | 48 |
| 3.5 | Conclusion | 56 |
| 4 | Ambulatory Musculoskeletal Inverse Dynamic Analysis | 57 |
| 4.1 | Introduction | 59 |
| 4.1.1 | Subjects | 60 |
| 4.1.2 | Instrumentation | 60 |
| 4.1.3 | Experimental protocol | 61 |
| 4.1.4 | Overall description of the components in the musculoskeletal models | 61 |
| 4.1.5 | Scaling and kinematics analysis of the musculoskeletal models | 62 |
| 4.1.6 | Inertial and geometric scaling of the musculoskeletal models | 63 |
| 4.1.7 | Muscle recruitment | 63 |
| 4.1.8 | Ground reaction force and moment prediction | 64 |
| 4.1.9 | Data Analysis | 64 |
| 4.2 | Results | 64 |
| 4.2.1 | Estimated kinematics of the musculoskeletal model | 64 |
| 4.2.2 | Predicted kinetics using inertial and optical motion capture | 65 |
| 4.3 | Discussion | 66 |
| 4.4 | Conclusion | 71 |
| 5 | Wearable Visual Feedback on Foot Progression Angle | 73 |
| 5.1 | Background | 75 |
| 5.2 | Methods | 76 |
| 5.2.1 | Subjects | 76 |
| 5.2.2 | Instrumentation | 77 |
| 5.2.3 | Experimental procedures | 78 |
| 5.2.4 | Computational procedures | 80 |
| 5.2.5 | Data Processing and Statistical Analysis | 80 |
| 5.3 | Results | 81 |
| 5.4 | Discussion | 82 |
| 5.5 | Conclusion | 87 |
| 6 | General Discussion | 89 |
| 6.1 | Overall Insights and Conclusions | 90 |
| 6.2 | Sensors | 91 |
| 6.2.1 | Number of Sensors | 91 |
| 6.2.2 | Types of Sensors | 92 |
| 6.2.3 | Size and Power Autonomy of Sensors | 93 |
| 6.3 | Modeling and Algorithms | 93 |
| 6.3.1 | Subject-specific Anthropometry | 93 |
| 6.3.2 | Idealization of Biomechanical Models | 94 |
| 6.3.3 | Sensor-to-Segment Calibration | 94 |
| 6.3.4 | Consistent Inertial and Magnetic Motion Tracking | 94 |
| 6.4 | Biofeedback | 95 |

| | |
|--|------------|
| 6.5 Towards healthcare application and beyond in the internet of moving things | 95 |
| 6.6 Concluding Remarks | 96 |
| Bibliography | 97 |
| Summary | 121 |
| Samenvatting | 125 |
| Acknowledgements | 129 |
| Biography | 131 |
| List of Publications | 133 |

Chapter 1

Introduction

Human movement analysis is an important field enabling us to understand the nature of several musculoskeletal disorders. For instance, altered mechanical loading of the affected knee joint has been demonstrated as an important risk factor of knee osteoarthritis, leading to high rates of disability in the elderly population. In this context, assessing loading is essential to develop new, patient-specific, conservative, non-pharmacological treatments for the effective management of joint pathologies. However, to date, analysis of human movement in terms of both kinematics and kinetics is traditionally performed within a laboratory environment, equipped with optical motion capture and force plate systems. Despite the robust performance of these systems, their laboratory dependence, increased costs, operation complexity, and time are important limitations, obstructing the translation of state-of-the-art clinical biomechanics research into routine clinical practice. Therefore, there is an emerging need for new tools for biomechanical analysis capturing both kinematics and kinetics in a flexible and convenient, but still accurate and reliable manner. In this thesis, we propose the use of high-end inertial motion capture systems to build and evaluate ambulatory methods for estimating kinetics, as well as to provide real-time biofeedback to the subject.

1.1. Human Movement: A story from Aristotle to Newton

1.1 Human Movement: A story from Aristotle to Newton

Analysis of human movement comprises a long-standing science, tracing its roots back to the ancient times. Our knowledge about the field has been influenced by discoveries and inventions made through the passage of centuries across several disciplines, including, but not limited to medicine, physics, and mathematics [1].

As early as about two and a half millennia ago, Aristotle (c. 384 - c. 322 B.C.) wrote his observations in the book *Περὶ ζώων κινήσεως* (English: *On the Movement of Animals*), which are considered the first writings about animal movement [2, 3]. For the first time locomotion generated from rotational movements, resulting in translations was described and analyzed. Many principles formulated back then composed fundamental knowledge for Newton's three laws of motion.

About a century later, the most notable mathematician of antiquity, Archimedes (c. 287 - c. 212 BC), developed several principles of mechanics. In his treatise, *Επιπέδων ἴσορροπίαν* (English: *On the Equilibrium of Planes*) [4, 5], Archimedes introduced the Law of Levers, where magnitudes are in equilibrium at distances reciprocally proportional to their weights, often considered as the first ever mathematical formulation of mechanical torque.

In the Roman era, Claudius Galen of Pergamon (c. 130 - c. 210 A.D.) researched the musculoskeletal system for the first time, among other systems. In his work, *De motu muscularum*, Galen made a distinction between motor and sensory nerves, as well as described the difference between agonist and antagonist muscles. Muscle contractions were explained by Galen as “animal spirits”, which are generated in the brain and reach the muscles via the nerves.

The next considerable scientific contributions in human movement science came in the Renaissance period. Leonardo da Vinci (1452-1519) became the first to study anatomy taking into account the mechanical aspects (Figure 1.1) [6]. Da Vinci examined the function of joints and described muscle forces as acting along lines from insertion to origin.

The founder of modern physics, Galileo Galilei (1564-1642) focused on the strength of materials. In this context, he explained that bones are hollow in order to achieve maximum strength while maintaining a minimum weight. A number of notes related to his eventually unpublished book on human movement *De Animalium Motibus* have been retrieved. Among other topics, Galileo described from a biomechanical aspect, how the length of the foot influences the height of a jump.

In 1680, the work *De Motu Animalium* of Giovanni Alfonso Borelli (1608-1679) was published (Figure 1.2), influenced by Aristotle's ancient work with the same title [7]. Borelli proposed that actions of muscles can only contract or rest and driven by Galileo's analytical techniques in mechanics, he became the first to calculate joint forces. Due to his pioneering contributions in applying mechanical principles on the human body, Borelli is considered the father of biomechanics.

Eventually, in the 17th century, Sir Isaac Newton (1642-1727) introduced the three laws of motion that comprise the most influential theory in modern dynamics [8]. Among the three laws, Newton's second law is the most essential in human movement analysis and in this thesis, since it is describing that acceleration is proportional to the force, therefore, linking kinematics to kinetics.

1. Introduction

1

Figure 1.1: Leonardo Da Vinci's sketches on human anatomy. [9]

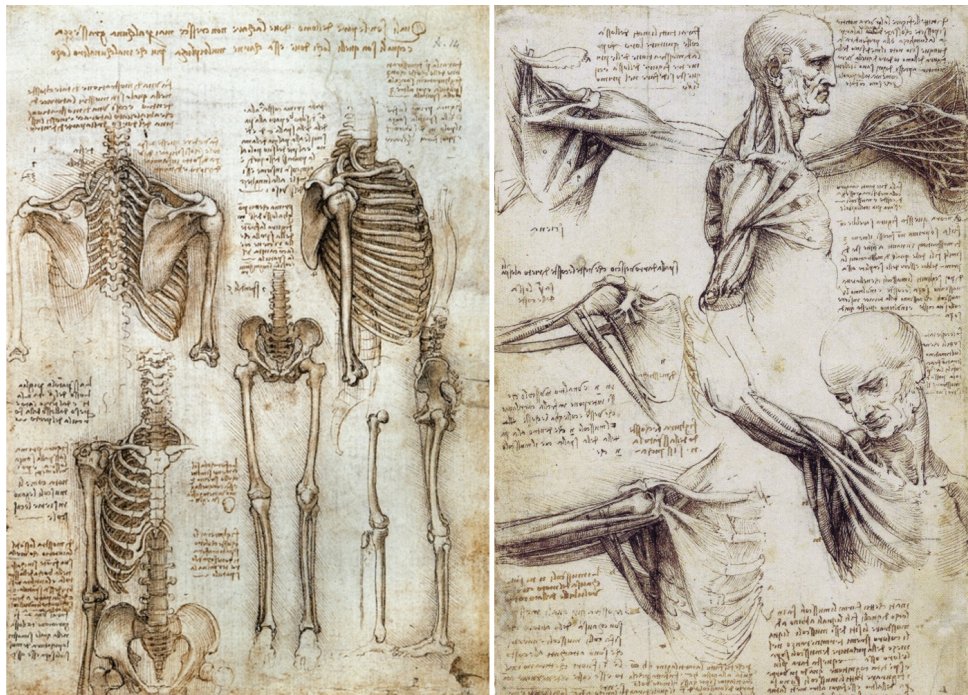
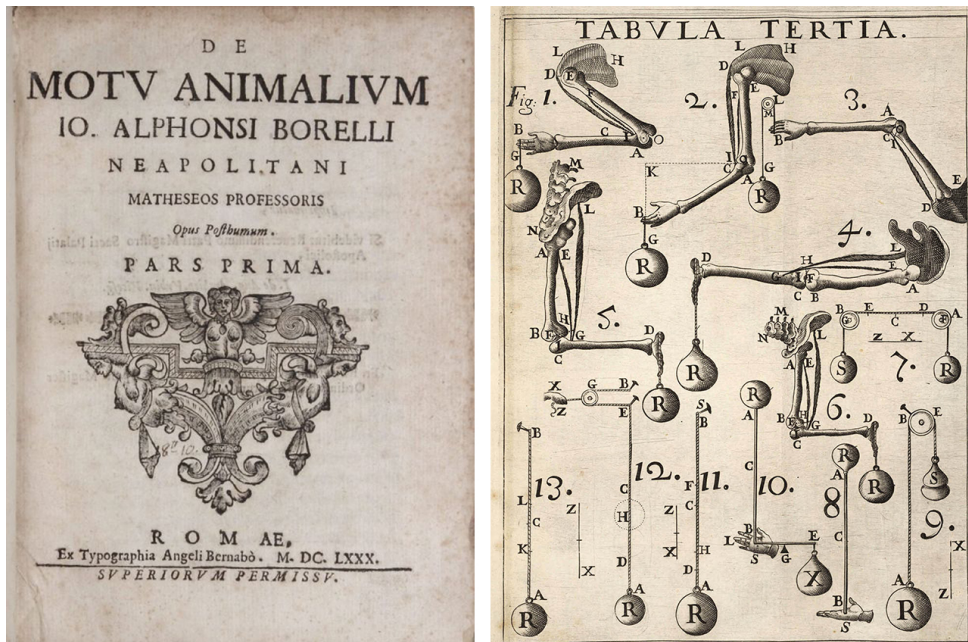


Figure 1.2: Giovanni Alfonso Borelli's *De Motu Animalium* [7].

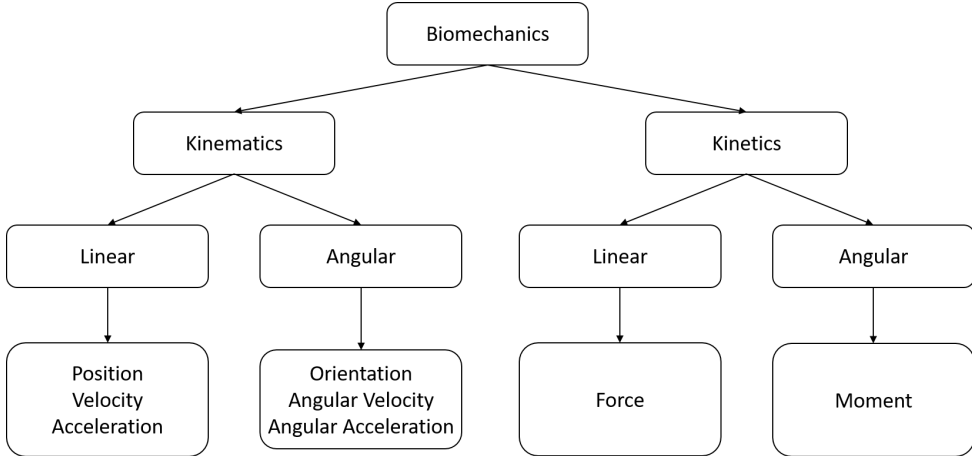


1.2. Biomechanical Analysis: Definitions and Techniques

1.2 Biomechanical Analysis: Definitions and Techniques

Biomechanical analysis can be performed either from the perspective of kinematics or kinetics [10]. In the following section we present what both branches represent and which techniques currently exist to assess the related quantities.

Figure 1.3: The components of biomechanical analysis [10].



1.2.1 Human Body Kinematics

Human body kinematics describes the motion of the body segments without considering masses or causal forces [11]. Three-dimensional kinematic quantities can be either linear (linear acceleration, linear velocity, and position) or angular (angular acceleration, angular velocity, and orientation) as shown in Figure 1.3. Typically, human body kinematics are assessed using motion capture systems. In most cases, these technologies are divided in optical (camera-based) and inertial motion capture systems. In the following sections, we present the main characteristics, as well as advantages and disadvantages of each approach.

Laboratory Method - Optical Motion Capture

Optical motion capture systems utilize a number of cameras to assess the human body kinematics [12]. Conventional optical systems track the trajectories of active or passive markers placed on the skin, and subsequently use computational techniques to reconstruct the segment kinematics [13]. Alternatively, unconventional optical systems, track the human body segments without the use of markers [14], using depth-camera sensors, contained in devices such as the Microsoft Kinect [15, 16]. The latter markerless approach has a significantly lower setup time and cost, but it is shown to be less accurate than marker-based methods, especially for fast motions and low range of motion [17, 18].

Marker-based optical systems (Figure 1.4b) perform well in tracking marker trajectories, with often reported sub-millimeter accuracy [19, 20, 21]. However, they introduce several important limitations in human motion analysis. Marker trajectory assessment typically requires time-consuming setup preparation, data collection, and post-processing.

Precise placement of the markers on anatomical landmarks is necessary, which has been shown to have low inter-session reliability, even within the same rater and same subject [22]. In order to track three translational and three rotational degrees of freedom of a body in space, at least three markers placed on the body are required. Due to the fact that markers are placed on the skin and not on the bone, soft tissue artifacts driven by the rigid body assumptions, may increase the position and orientation errors in optical motion capture systems radically. For instance, assuming that one of the three markers placed on a 40 cm long tibia is misplaced towards the anterior direction by 1 cm, these would lead to an orientation error equal up to the inverse tangent of the ratio between the two values, which is approximately $\text{atan}(1/40) = 1.4$ degrees on the sagittal plane. Such differences introduce greater impact when they occur in planes where the range of motion is already small [23].

Post-processing of the data includes tasks such as marker labeling, gap-filling of incomplete trajectories, and filtering. These tasks may be further prolonged when markers are occluded or fall off the body. Occlusion typically occurs when line of sight between the camera and marker is obstructed by a third body, such as the subject's own segments or other external environmental objects. Marker occlusion and falls may result in marker label swapping within a trial which demands for cautious treatment to avoid erroneous kinematic estimates.

Spatial limitations, and mainly the dependence on a laboratory setup are another important restriction of optical systems. For gait analysis, a common 8-camera setup requires a dedicated area larger than 25 square meters, which results to an actual capture volume much smaller than the total space volume. In addition to the small measurement volume, one of the most essential limitations of optical motion capture systems is the overall inability to capture motion in realistic environments, outside the laboratory.

Even though they are often mistakenly perceived as gold standard for kinematics assessment, optical motion capture systems in combination with the methods and assumptions used to reconstruct body kinematics, may introduce several errors [23]. In addition, their inapplicability in daily life due to limited capture volume, as well as time-consuming and complex preparation, data collection, and post-processing tasks prevent the translation of human movement analysis in routine clinical practice. In this context, ambulatory motion capture systems could provide a potential solution.

Ambulatory Method - Inertial Motion Capture

Inertial motion capture (IMC) utilizes inertial measurement units (IMU) to describe human motion [24]. Typical sensing components contained in an IMU such as the one depicted in Figure 1.5b, are primarily accelerometers and gyroscopes, and often magnetometers. Among others, the most significant advantage of IMC is that it does not require a dedicated laboratory space to operate and can be used in various environments, both indoors and outdoors (Figure 1.5a).

Accelerometers are convenient and well-established measurement devices used to

1.2. Biomechanical Analysis: Definitions and Techniques

(a) Gait Laboratory with optical motion capture and force plates.



(b) Qualisys Oqus infrared camera.
Source: www.qualisys.com



(c) AMTI OR6-7 force plate.
Source: www.amti.biz

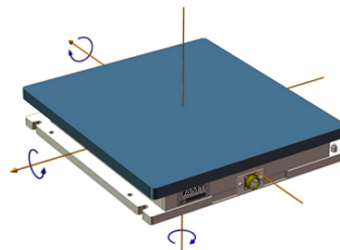
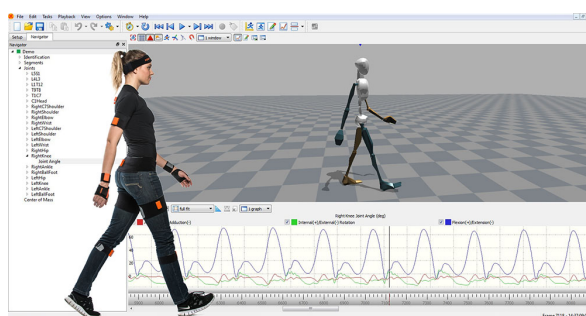


Figure 1.4: Laboratory-based systems for assessment of human body kinematics and kinetics.

(a) Xsens MVN Awinda inertial motion capture system.
Source: www.xsens.com



(b) Xsens MTw IMU. Source: www.xsens.com



Figure 1.5: Inertial motion tracking solutions.

assess not only kinematic, but can be also extended to extract kinetic information. In fact, a single-axis accelerometer uses both Hooke's law ($F = kx$) and Newton's laws ($F = ma$) to derive acceleration (a) given a mass (m) and a force (F) found

from a known stiffness factor (k) and deformation (x) of a spring. Similarly, by replicating a single-axis accelerometer three times, in a formation of three orthogonal axes defining a sensor frame, a triple axis accelerometer can be constructed [25]. The measurement of a three-axis accelerometer provides a three-dimensional acceleration \mathbf{a} plus gravitational acceleration \mathbf{g} in the sensor coordinate frame. However, in order to remove the gravitational component from the accelerometer measurements, these have to be transformed to an earth-based coordinate frame, by deriving sensor orientation.

Orientation of the sensor frame with respect to an external frame is typically estimated using a sensor fusion technique, such as an Extended Kalman Filter [26]. In this way, the three-dimensional signals from accelerometers, rate gyroscopes, and magnetometers are fused to assess an accurate drift-free orientation estimate [27].

A biomechanical model is used to derive inter-segment positions and orientations from sensor orientations. The segment lengths of a subject are measured and subsequently input to the model [28]. Commonly, sensors are assumed to be rigidly placed on the human body, therefore an orientation difference between segment and sensor has to be found through a calibration process. To find this sensor-to-segment alignment, typically each sensor is initially mapped to a segment and a static assumed *a-priori* known pose is used [29]. In this way the sensor orientations can drive the segment orientations, assuming a fixed orientation difference between the two. Based on the admission that segments of known length are linked by joints, inter-segment positions can also be derived using forward kinematics [30].

A challenging task in IMC is to obtain the position of a subject with respect to an external environment-fixed frame (global position). The most straightforward way to do this is via inertial dead-reckoning, where accelerations are numerically integrated twice to derive position, based on a known initial position and velocity. However, the effect of numerical integration drift results in a rapidly increased uncertainty over time, which can result in highly erratic position and velocity estimates, even after a short period of a few seconds [27]. To limit these effects and maximize the accuracy of absolute position estimations, advanced IMC systems exploit the interactions with the environment. For instance zero velocity (stillness) or height updates of the feet segment during walking or running can be used to minimize the inaccuracies [31].

Traditionally, the most prominent source of error in IMC systems is due to the reliance on magnetometer measurements [32]. Typically, the fusion models assume that the magnetic field within the environment of use is homogeneous. However, this assumption was shown to be invalid for several indoor environments, in the presence of ferromagnetic material. Typical example of these environments are gait laboratories, which often contain several metallic objects. Recent advances in the field are improving these measurements and provide consistent kinematic data regardless of external factors, such as the measured magnetic field [33].

1.2.2 Human Body Kinetics

In classical mechanics, the field of kinetics focuses on the relation between the motion and its causes [34]. Similarly to kinematics, the causes of motion can be linear or angular, namely forces and torques, respectively. Thus human body kinetics examines these forces and torques applied on the segments and joints of the human body. For instance, as we describe in the next section of this thesis, moments about

1.2. Biomechanical Analysis: Definitions and Techniques

the knee joint can be a convenient measure to quantify knee joint loading. Typically joint kinetic measures are assessed using the inverse dynamic approach, in which the human body is modelled as a chain of segments connected by joints, and a free-body diagram can be solved for each one of them given the external loads and kinematics [35].

Gait analysis is commonly limited to conditions where the main interaction between a subject and the environment is present between the feet and the ground [36]. In this case the external loads are completely described by the ground reaction forces and moments (GRF&M). Therefore assessing the joint loads, in terms of net forces and net moments, requires the assessment of GRF&M and kinematics. The assessment of kinematics was described in the previous section, thus below we focus on conventional and alternative techniques to assess the GRF&M.

Laboratory Methods

Traditionally, kinetic gait analysis is performed in a gait laboratory (Figure 1.4a). Such laboratories are commonly equipped with optical motion capture systems and force plates [37]. Force plates or force platforms are measurement devices embedded in the floor of a laboratory [12] as depicted in Figure 1.4c. Even though force plates are highly accurate with reportedly sub-Newton accuracy, they introduce several limitations.

Similarly to optical motion capture systems, the requirement of a gait laboratory limits the application in daily life activities. This dependency on a dedicated room, together with the high costs and complex setup of the instrumentation prevent biomechanical applications in clinical routine practice.

In terms of application, overground force plates are embedded in the floor of a lab and their measurement area is typically small (commonly around 0.5 m x 0.5 m). Requirement for a usable measurement is that the subject steps with only one foot entirely on the force plate. To fulfill this requirement subjects often tend to subconsciously alter their gait pattern [38]. In addition, the small measurement area does not allow overground force plates to capture many consecutive steps. For that reason, force plates have been embedded under treadmill belts. However the latter can only capture walking or running in a straight line which is not the case in real life situations.

The inconvenience of laboratory-based force plates directed research towards alternative assessment methods. For instance, predicting GRF&M from kinematics of laboratory systems has been examined several times in the last decades. In these techniques, externals loads are assessed through the full-body kinematics combined with additional modelling assumptions [39, 40, 41, 42, 43]. The entire human body is typically modeled as a chain of rigid body segments linked with joints. When the chain interacts with the environment through only one segment, then the external loads triggered from this interaction can be calculated by solving the Newton-Euler equations, serially starting from the open ends towards the only closed end [39]. However, when more than one segments are in contact with the environment then the system of equations becomes under-determinate.

A typical situation when under-determinacy occurs, is the double stance phase of gait, where two feet are in contact with the ground. Several methods have been proposed to solve the under-determinacy during the double stance phase of gait. An

empirical function proposed by Ren *et al* called smooth transition assumption was demonstrated to work during gait [39]. Methods based on machine learning [40, 41] showed to work as well by mapping kinematic parameters to distribution ratios of the external forces. Finally, methods where contact points modeled as actuators become part of a muscle recruitment problem, aimed at minimizing the body's fatigue to perform the underlying motions showed to perform independently of a database for daily living activities and sports tasks [42, 43].

To the best of our knowledge, prior to this thesis, all proposed and validated methods examined the prediction of three-dimensional forces and moments from kinematics using optical motion capture input [44]. The dependency on optical motion capture decreases the value of these predictive techniques, since the application area remains coupled to the limited capture volume. Exploiting the full-potential of these techniques could be achieved by obtaining the kinematics from inertial measurement units that are not bounded by a laboratory space and therefore can capture unlimited areas. In addition, a significant advantage of accelerometers contained in inertial measurement units is that they directly measure accelerations, which are linearly related to forces through Newton's second law ($F = ma$).

Ambulatory Methods

Given the incapability of laboratory systems to capture kinetics in daily life conditions, alternative approaches featuring ambulatory methods for assessing GRF&M have been investigated in several studies [44], using either force and torque sensors or pressure insoles placed above or beneath the actual sole of a shoe (Figure 1.6).

Instrumented force shoes can be constructed with force sensors placed beneath the sole of a shoe in order to measure directly the three-dimensional GRF&M components [45, 46]. In the early 2000's, Veltink *et al* developed the first version of an instrumented force shoe [45], with two force sensors, rigidly placed beneath the anterior and posterior parts of an orthopedic shoe. Schepers *et al* further developed the shoe capabilities by integrating an inertial measurement unit with each force sensor to derive the orientation of the forces [47]. In addition, each force and IMU sensor was mounted separately on a rigid body. However, the height and weight of the force sensors, may influence the gait pattern and does not allow for applications in daily life or clinical practice [48, 49].

A less obtrusive system proposed in other studies is composed of pressure insoles. Such devices are typically placed between the sole of a shoe and the foot, and provide a foot pressure distribution. This distribution can be used to reconstruct the complete GRF&M utilizing mathematical models [50, 51, 52, 53, 54, 55]. Despite their compact size and unobtrusive use, pressure insole measurements suffer from repeatability and durability limitations [56]. In addition, pressure distribution depends highly on the subject-specific anatomy, and therefore developing a generalized model is challenging.

The direction of this thesis was influenced by the limitations of the aforementioned ambulatory approaches for kinetics; as well as the potential showcased in motion-based techniques applied in laboratory systems and the recently increased performance of IMC systems. The apparent potential towards the ambulatory application of motion-based assessment of kinetics, with the use of inertial sensors was identified and utilized to define the aims of this project.

1.2. Biomechanical Analysis: Definitions and Techniques



(a) The Xsens ForceShoe - an orthopedic shoe instrumented with force/torque sensors. Source: www.NASA.gov



(b) TekScan in-shoe pressure measurement technology.

Figure 1.6: Ambulatory methods to assess human body kinetics.

1.3 Biomechanics in Knee Osteoarthritis

1.3.1 Prevalence and Burden

Osteoarthritis (OA) is a degenerative disease in which the articular cartilage surrounding a joint gradually wears away [57]. Typical symptoms of pain, swelling, and stiffness of the affected joint result in significant mobility impairment in the elderly more than any other condition [58]. According to the World Health Organization, about 10-15% of the global population aged over 60 years old is affected by some form of OA [59]. Furthermore, the effects of disability on the patients and their families have financial, psychological, and social consequences [60, 61, 62, 63].

Several risk factors are associated with OA that are categorized to individual factors such as age, gender, obesity, diet, and genetics, and joint-level factors, such as previous trauma or abnormal loading of the joint [64]. With age being one of the main risk factors of OA, the prevalence and incidence of OA are expected to rise due to an increase in life expectancy. Recent figures from Eurostat estimate the percentage of people in the European Union aged 65 and over to increase to 28.1% by 2050 from 18.9% in 2015 [65]. Moreover, modern society routines, characterized by sedentary lifestyles and poor dietary habits, result in an increased obesity rate that predicts higher prevalence of the disorder in the near future [66, 67]. The most common form of the disease is knee OA that comprises 41% of limb OA, followed by 30% hands and 19% hip OA [68].

1.3.2 Treatments and Management of Knee Osteoarthritis

To date, there is no cure available for OA that restores the joint to its original condition [69]. Management of the disease is achieved through surgical and conservative options [70]. Surgical treatments include cartilage repair, arthroscopy, osteotomy, and joint arthroplasty. However, these are only considered when conservative approaches fail to relieve the symptoms of the disease and typically at the most severe stages [71]. Conservative management can be either pharmacological or non-pharmacological [72]. The former approach includes medications, such as paracetamol, non-steroidal anti-inflammatory drugs, topical treatments and aim at alleviating symptoms of pain and swelling [73, 74]. On the other hand, conservative non-pharmacological therapies target the biomechanics of the problem, in an attempt to alter the mechanical loading, one of the important factors of the disease [75]. This fact, makes the biomechanical approach suitable for use in early and mid severity stages of the disease.

Several conservative biomechanical treatments have been proposed for the management of knee OA, including, but not limited to knee braces, footwear insoles or canes, programs for muscle strengthening and weight loss, as well as gait modifications [76]. The goal of these interventions is to decrease or redistribute the knee joint loading, which is quantified through the contact forces on the medial compartment of the knee joint. However, measurement of the knee contact forces is practically challenging and is only possible in patients with instrumented knee implants, following total knee replacement. For this reason, research has proposed surrogate non-invasive measures, such as the knee adduction moment, which showed a significant positive correlation with the internal contact forces [77, 78, 79].

1.3. Biomechanics in Knee Osteoarthritis

1.3.3 Towards Subject-specific Biomechanical Interventions in Clinical Practice

Among the aforementioned biomechanical treatment examples, gait modifications can be highly advantageous due to the fact that they do not require external devices to unload the knee joint, but instead utilize one's own movement strategy [80]. Typical examples of gait modifications include walking with a gait pattern characterized by toes pointing inwards [81] or outwards [82, 83], medial knee thrust[84, 85], as well as lateral trunk lean [86, 87, 88]. Combining gait modifications with a muscle strengthening and weight loss program can have positive outcomes [89]. Regarding gait modifications though, a generic approach does not suit all individuals and there is a general consensus and strive towards patient-specific interventions [84]. Such tailored approaches require accurate real-time assessment of the human movement in terms of kinematics and kinetics.

Current methods used to capture the biomechanics to date are only applied in research-oriented gait laboratories with complex, time-consuming and expensive set-ups [90]. These drawbacks hinder the wider application of patient-specific gait modifications in clinical practice [91]. Understanding the effect of gait modifications on each individual knee OA patient is essential and can only be achieved via translation of research into practice. To this end, in order to boost clinical adoption, it is necessary to introduce new measurement techniques and methodologies that are easier in use, more flexible, more scalable, and more affordable.

1.3.4 The KNEEMO Initial Training Network

The research described in this thesis was performed in the context of the KNEEMO project; an Initial Training Network for knee OA research, funded through the European Commission's Framework 7 Programme. The project ran from April 2014 until April 2018 and included 15 research fellows based at 8 institutions. [92]

The topic of KNEEMO ITN research is “towards targeted and tailored interventions for knee OA” with a focus on investigating and matching patient profiles, timing, and treatments. A broad range of research areas were involved including epidemiology, anatomy, musculoskeletal modelling, measurement techniques, orthotics, intervention studies, prevention and early identification of patients.

Overall, KNEEMO ITN aimed at understanding the non-pharmacological conservative management of knee OA through early identification and tailored interventions. The objectives of KNEEMO ITN are: 1) to provide personalized biomechanical knee models; 2) to enable the timely identification of patients at high risk of developing OA, or with a poor prognosis; 3) to design and evaluate new technology for biomechanical assessments; 4) to develop personalized interventions.

Figure 1.7: KNEEMO Initial Training Network funded by the EU. (www.kneemo.eu)



1.4 Thesis Objectives

In line with the initial project proposal of the KNEEMO network, we defined two main objectives for this thesis:

Objective 1: Development of an ambulatory knee load estimation system, applicable in free-living environments, using input from inertial sensors.

In order to focus on specific aspects of the first objective, three related research questions were defined. Using only IMC input ...:

- ... can we estimate three-dimensional GRF&M during gait?
- ... can we assess net knee joint moment during knee load altering gait modifications?
- ... can we drive a detailed musculoskeletal model capable of assessing internal loads?

The focus of the first question is a major step towards joint load assessment. Following kinematics, GRF&M are the most important inputs for inverse dynamics and to date there is no highly practical and reliable solution to assess them in ambulatory conditions. Therefore assessing them indirectly through the kinematics of an ambulatory motion capture system would be of high value for such applications. Question two focused on what extent net knee joint moment measures can be assessed, during gait modifications commonly proposed for the target population of the KNEEMO project. Addressing this question is based on methods used to answer the first question using only IMC input. Finally, the third question is driven by the need for detailed musculoskeletal models in clinical practice. Such models have shown to be capable of estimating internal loads non-invasively, but they are not used extensively yet in clinical practice, due to the complex laboratory-based data collection setups required. Applying these existing detailed musculoskeletal models using inertial kinematic inputs would be a major step.

Objective 2: Development of an ambulatory real-time biofeedback system, driven by human body kinematics and/or kinetics, aiming at decreasing the knee load during gait, using input from inertial sensors.

- How accurate is an ambulatory system based on inertial sensors compared to conventional laboratory in assessing knee joint load-related biomechanical parameters in real-time?
- How effective is an ambulatory real-time biofeedback system compared to an established laboratory system?

Regarding the second objective, we focused on the application of gait retraining driven by inertial sensors. The scope of the proposed setup was to provide an ambulatory and easy to use solution that may facilitate the applicability of biomechanical interventions in clinical practice and potentially in daily life. The first question aimed at validating IMC versus optical motion capture to derive parameters related to the knee joint loading, such as the foot progression angle. The second question aimed at evaluating how effective a system based on inertial sensors and wearable

1.5. Thesis Outline

head-mounted displays could be, compared to laboratory visual feedback based on a virtual reality environment and optical motion capture.

1.5 Thesis Outline

Chapter 2 focuses on the assessment of the external GRF&M using only IMC input. This chapter addresses the first research question of the first objective. A whole-body inverse dynamic approach is used to derive the total external loads applied on the body. These forces and moments are subsequently distributed across left and right foot by adjusting an empirical function valid for gait, called smooth transition assumption. The analysis focused on the correlations and errors between the force-plate-derived GRF&M components and the ones assessed using either only OMC kinematics or only IMC kinematics. A sensitivity analysis is performed on the cut-off frequencies of the low-pass filters used to smoothen the kinematic input. This study comprises the first step to assess three-dimensional GRF&M, using solely input derived from inertial sensors.

Chapter 3 describes and evaluates the assessment of knee joint moments during various common gait modifications prescribed to patients of knee OA (objective 1, research question 2). This chapter utilizes the method described on Chapter 2, focusing on knee adduction and flexion moments. The investigated gait patterns typically aim at altering primarily the knee adduction moment, as a surrogate of medial compartment joint loading, but may also affect the knee flexion moment. We evaluate the agreement of the absolute moment values, as well as the intra-subject change from a comfortable walking baseline value. The proposed methods provide a solution to track the moment and its change as a result of an altered gait pattern, using only body-worn inertial sensors.

In Chapter 4, we propose and validate a method which integrates a musculoskeletal model with a commercial IMC system. In this chapter we present, the first ever (to our knowledge) validated approach to perform inverse dynamics via musculoskeletal modeling with kinematic input derived from ambulatory IMC system (objective 1, research question 3). Typically, musculoskeletal models function have different segment and joint definitions compared to IMC systems, such as the Xsens MVN function with more degrees of freedom. A way to map the motion of both kinematic models is presented, and subsequently a universally applicable muscle recruitment-based method is utilized to assess lower limb joint loads.

Chapter 5 focuses on closing the loop between estimates and user, by demonstrating a real-time biofeedback application, related to the second objective of this thesis. In this application, an augmented reality glass is utilized to project visual feedback based on parameters assessed using IMC. During the specific experiment the foot progression angle, a kinematic parameter affecting knee joint loading in knee OA has been used as a target of the feedback system. The proposed setup is fully wearable and potentially ambulatory and may decrease complexity of gait retraining interventions and boost clinical adoption.

Chapter 6 provides a general discussion of the findings of Chapters 2 to 5, as well as a conclusion of this thesis. Directions for future research are given regarding the necessary steps to achieve actual application of IMC technology in daily life and routine clinical practice.

Chapter 2

Estimation of Ground Reaction Forces and Moments During Gait Using Only Inertial Motion Capture

Published as:

Karatsidis, A., Bellusci, G., Schepers, H. M., de Zee, M., Andersen, M. S., & Veltink, P. H. (2016). Estimation of ground reaction forces and moments during gait using only inertial motion capture. Sensors, 17(1), 75. <http://dx.doi.org/10.3390/s17010075>

Abstract

Ground reaction forces and moments (GRF&M) are important measures used as input in biomechanical analysis to estimate joint kinetics, which often are used to infer information for many musculoskeletal diseases. Their assessment is conventionally achieved using laboratory-based equipment that cannot be applied in daily life monitoring. In this study, we propose a method to predict GRF&M during walking, using exclusively kinematic information from fully-ambulatory inertial motion capture (IMC). From the equations of motion, we derive the total external forces and moments. Then, we solve the indeterminacy problem during double stance using a distribution algorithm based on a smooth transition assumption. The agreement between the IMC-predicted and reference GRF&M was categorized over normal walking speed as excellent for the vertical ($\rho = 0.992$, rRMSE = 5.3%), anterior ($\rho = 0.965$, rRMSE = 9.4%) and sagittal ($\rho = 0.933$, rRMSE = 12.4%) GRF&M components and as strong for the lateral ($\rho = 0.862$, rRMSE = 13.1%), frontal ($\rho = 0.710$, rRMSE = 29.6%), and transverse GRF&M ($\rho = 0.826$, rRMSE = 18.2%). Sensitivity analysis was performed on the effect of the cut-off frequency used in the filtering of the input kinematics, as well as the threshold velocities for the gait event detection algorithm. This study was the first to use only inertial motion capture to estimate 3D GRF&M during gait, providing comparable accuracy with optical motion capture prediction. This approach enables applications that require estimation of the kinetics during walking outside the gait laboratory.

Keywords: Ground reaction force and moment; Inertial motion capture; Inverse dynamics; Gait analysis

2.1. Introduction

2.1 Introduction

Assessment of ground reaction forces and moments (GRF&M) is an important stage in the biomechanical analysis procedure. Conventionally, these measures are recorded using force plate (FP) systems, which, despite their high accuracy, have several significant limitations [37]. Firstly, the fixed position of the plates on the ground together with the requirement to step with the whole foot on the plate for a successful measurement may cause subjects to alter their natural gait pattern. Moreover, due to their high cost, most laboratories are equipped with one or a couple of FPs, which makes tracking many successive steps during overground walking impossible. In addition, the measurements are bounded by the laboratory space and cannot be performed outside this area, for example during daily life activities.

Towards ambulatory assessment of kinetics, previous studies have suggested the use of either pressure insoles [53, 93, 54] or instrumented force shoes [45, 94]. The main difference between these two systems is that the former measures only a pressure distribution in the shoe, whereas the latter measures directly three-dimensional forces applied beneath the shoe. Such devices have enabled ambulatory estimation of ankle kinetics [47] and knee kinetics [95], in combination with inertial measurement units (IMUs) and linked segment models. Although these methods are ambulatory and have estimated GRF&M with relative RMS errors of $(1.1 \pm 0.1)\%$ [96], they suffer from certain limitations. The low durability and repeatability of the pressure insoles result in a drop in the reliability of the results [56]. As for the instrumented force shoe, it has been suggested that optimization is needed to decrease the size and weight of its wearable instrumentation and make it practical for recording sessions of extended durations [49, 48].

Recent advances in biomechanical analysis techniques are allowing the estimation of GRF&M using only kinematic data [97, 40, 41, 42, 98, 43, 39]. When applied to gait analysis, a common problem that needs to be addressed is the distribution of the total external force and moment during periods of double foot support. Several methods have been previously proposed. Two studies proposed approaches based on artificial neural networks to determine the distribution of forces and moments [40, 41]. Recently, another approach used a musculoskeletal model-based technique in which a dynamic contact model is used to solve the indeterminacy problem, without using training data [42, 98, 43]. In another study, Ren et al. introduced a distribution function called the smooth transition assumption, which is based on the observation that the GRF&M on the trailing foot change smoothly towards zero during the double stance phase of gait [39]. The latter assumption was further validated and adjusted to decompose the right and left GRF&M measured from a single force plate [99]. That study pointed out a limitation of the original smooth transition assumption, in which the center of pressure remains constant during the double support due to the use of the same functions for both horizontal moments and vertical force.

To apply kinetics prediction methods to kinematic data, most of the existing research uses optical motion capture (OMC). However, the increased accuracy and reduced size, power and cost of IMUs have enabled the assessment of segment orientation [100] and later full-body motion capture in laboratory-free settings. This technique delivers good accuracy in estimating human body kinematics, such as joint

2. Estimation of Ground Reaction Forces and Moments

angles [24], and has been previously validated versus optical motion capture estimates [101]. Only a few studies have attempted to assess kinetics from kinematics using such inertial motion capture (IMC) systems. In a recent study, a top-down inverse dynamics approach was applied to estimate GRF&M and L5/S1 joint moments during trunk bending [102]. Another study used IMUs to estimate the joint forces and moments during ski jumping [103]. The common limitation of those studies is that they examined only the total external loads applied on both feet and are, therefore, inapplicable to gait analysis.

Therefore, the aim of this study was to develop a computational method to predict GRF&M, using only IMC-derived kinematics during gait. The method was evaluated for three walking speeds, by comparing the predicted GRF&M with the results of FP measurements. In addition, we performed two sensitivity analyses to investigate the effect of cut-off frequency on the estimated GRF&M, as well as to validate the choice of threshold velocities used in the gait event detection algorithm.

2.2 Methods

2.2.1 Experimental Protocol

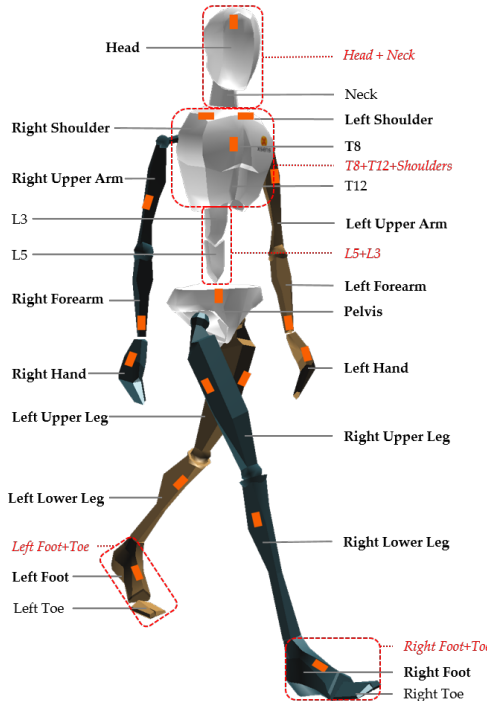
Eleven (11) healthy male volunteers (age: 30.97 ± 7.15 years; height: 1.81 ± 0.06 m; weight: 77.34 ± 9.22 kg; body mass index (BMI): 23.60 ± 2.41 kg/m²) participated in the measurements performed at the Human Performance Laboratory, at the Department of Health Science and Technology, Aalborg University, Aalborg, Denmark. The experiment was performed in accordance with the ethical guidelines of The North Denmark Region Committee on Health Research Ethics, and participants provided full written informed consent, prior to the experiment.

The core system used in this study is an IMC system (Xsens MVN Link, Xsens Technologies BV, Enschede, The Netherlands [104]) powered by the matching software (Xsens MVN Studio version 4.2.4), delivering data at 240 Hz. The 17 IMU modules were mounted on a tight-fitting Lycra suit on the following segments: head, sternum, pelvis, upper legs, lower legs, feet, shoulders, upper arms, forearms and hands [24, 105] (Figure 2.1). In addition, an OMC system, including eight infrared high-speed cameras (Oqus 300 series, Qualisys AB, Gothenburg, Sweden [106]), was used to capture 53 retro-reflective markers mounted on the body. The placement of the markers on the body is shown in Figure 2.8 and described in Table 2.12 in the Appendix section. Furthermore, three FPs (AMTI, Advanced Mechanical Technology, Inc., Watertown, MA, USA), embedded in the floor of the laboratory, recorded GRF&Ms (Figure 2.2). A combination of the OMC and FP systems (lab-based system) was used as a reference for comparison to the IMC-derived GRF&M predictions. To synchronize the IMC-based and lab-based systems, the Xsens sync station was used. The sampling frequency of the camera-based system was set to 240 Hz and that of FPs to 2400 Hz.

Before starting the recordings, the body dimensions of each subject were assessed and applied in the Xsens MVN software. Particularly, the heights of the ankle, knee, hip and top of head from the ground, the widths of the shoulder and pelvis, as well as the length of the foot were measured using a conventional tape with the subject in an upright posture [108]. These measurements were used to calibrate the IMC

2.2. Methods

Figure 2.1: The definition of the 23 segments in the kinematic model of Xsens MVN. An inertial measurement unit is mounted on each of the 17 segments indicated with bold text. The 5 new segments (red italic font) are formed by the combination of MVN segments (within dashed-lined boxes) to match the segment definitions of De Leva [107].



system using a steady upright posture, known as the neutral pose or n-pose [24]. The software classifies the quality of the calibration as “poor”, “fair”, “acceptable” or “good” based on the steadiness of the subject and the homogeneity of magnetic field around the IMUs at the time of the calibration. The calibration process was repeated before each set of walking speed trials and until the indication “good” was achieved in all cases, to maximize the quality of IMC.

Figure 2.2: The three AMTI force plate system used, denoting the coordinate system of the laboratory. The vertical axis (z) points upwards, perpendicular to the anterior (x) and lateral (y) axes.



2. Estimation of Ground Reaction Forces and Moments

Between the completion of the instrumentation setup and the start of the measurements, the subjects were given a five-minute acclimatisation period, to feel comfortable in the wearable equipment. Throughout the whole experiment, subjects remained barefoot, without wearing any type of footwear, apart from a thin strap wrapped around each foot to firmly mount the inertial measurement unit on these segments.

Gait at a self-selected normal (NW), fast (FW) and slow (SW) speed were measured. FW and SW speeds were instructed to the subjects as at least 20% higher or lower than their mean baseline NW speed, respectively. Particularly, the actual mean walking speeds performed were 1.28 ± 0.14 m/s for NW, 1.58 ± 0.09 m/s for FW (NW + 23%) and 0.86 ± 0.11 m/s for SW (NW – 33%). To prevent the generation of additional external forces, the use of handrails or contact with any other external objects was not allowed. Before each task was recorded, subjects were given oral instructions and practiced the respective movement patterns. At least five successful trials per walking speed were obtained. A trial was considered successful when the right (left) foot hit one of the FPs completely, followed by a complete hit of the left (right) foot on the next FP. This definition ensures that FPs capture both right and left feet successfully within a stride.

2.2.2 Data Processing: IMC System

Xsens MVN estimates the orientation of segments by combining the orientations of individual IMUs with a biomechanical model of the human body. The orientation of each IMU is obtained by fusing accelerometer, gyroscope and magnetometer signals using an extended Kalman filter [27]. To relate the sensor orientations to segment orientations, a sensor-to-segment calibration procedure is performed. In this procedure, called n-pose, the subject is asked to stand in a known n-pose for a few seconds. The estimated transformation is applied and considered constant during a recording session.

We developed a program in MATLAB to assess the kinetic values from IMC-derived kinematics. By default, Xsens MVN Studio uses 17 IMU sensors to derive the kinematics of 23 segments as shown in Figure 2.1. Due to lack of literature reporting inertial parameters and relative center of mass positions for these exact segments, the original kinematic model has been adjusted to match the definitions of the 16-segment model reported by De Leva, 1996. To achieve this adaptation, 5 new rigid body segments were defined by merging specific given segments:

- Head-neck segment, formed by constraining the relative movement between head and neck segments. Kinematics were derived from the orientation of the IMU mounted on the head.
- Upper trunk segment, formed by constraining the relative movement between T8 and T12, T8 and right shoulder and T8 and left shoulder segments. Kinematics were derived from the orientation of the IMU mounted on the sternum.
- Middle trunk segment, formed by constraining the relative movement between L3 and L5 segments. Kinematics were derived from interpolation between the upper trunk and pelvis segment.

2.2. Methods

- Foot-toe, formed by constraining the relative movement between foot and toe segments. Kinematics were derived from the orientation of the IMU mounted on the foot.

The segment definitions of the pelvis, upper legs, lower legs, hands, forearms and upper arms remained unchanged (Figure 2.1; Table 2.1).

For the analysis, two coordinate systems were defined:

- the global coordinate system of the IMC system (ψ_g), in which the anterior axis points to the magnetic north, the vertical axis matches the direction of the gravitational acceleration and the lateral axis perpendicular to these axes, such that a right-handed coordinate frame is formed
- the walking coordinate system (ψ_w), which is defined by the same vertical, but has the anterior axes pointing in the walking direction, which means the difference between the two systems is only a rotation around the vertical; the walking direction was derived from known initial and final positions of the pelvis segment and assuming that the subjects walked approximately in a straight line throughout the trial

Table 2.1: Segments used in the 16-segment body biomechanical model, as described by De Leva [107], and the corresponding segments derived from the kinematic model of Xsens MVN Studio. The table includes the segment mass ratios (m), the longitudinal position of the center of mass in each segment (CoM_z), as well as the radii of gyration ratios (r_x , r_y , r_z).

| De Leva 1996 Definition | Xsens MVN Equivalent | m (%) | CoM _z (%) | r _x (%) | r _y (%) | r _z (%) |
|-------------------------|----------------------|-------|----------------------|--------------------|--------------------|--------------------|
| Head | Head + Neck | 6.94 | 50.02 | 30.3 | 31.5 | 26.1 |
| Upper Trunk | T8 + T12 + Shoulders | 15.96 | 50.66 | 50.5 | 32 | 46.5 |
| Middle Trunk | L5 + L3 | 16.33 | 45.02 | 48.2 | 38.3 | 46.8 |
| Pelvis | Pelvis | 11.17 | 61.15 | 61.5 | 55.1 | 58.7 |
| Upper Arm | Upper Arm | 2.71 | 57.72 | 28.5 | 26.9 | 15.8 |
| Forearm | Forearm | 1.62 | 45.74 | 27.6 | 26.5 | 12.1 |
| Hand | Hand | 0.61 | 36.24 | 28.8 | 23.5 | 18.4 |
| Upper Leg | Upper Leg | 14.16 | 40.95 | 32.9 | 32.9 | 14.9 |
| Lower Leg | Lower Leg | 4.33 | 43.95 | 25.1 | 24.6 | 10.2 |
| Foot | Foot + Toe | 1.37 | 44.15 | 25.7 | 24.5 | 12.4 |

Knowing the kinematics and inertial properties of the segments of the biomechanical model, we estimated the total external force based on the Newton equations of motion:

$$\mathbf{F}_{ext} = \sum_{i=1}^N m_i(\mathbf{a}_i - \mathbf{g}) \quad (2.1)$$

where \mathbf{F}_{ext} denotes the total three-dimensional external force, N the total number of segments, m_i the mass of each segment, \mathbf{a}_i the linear acceleration in the center of mass of each segment and \mathbf{g} .

In a similar way, we calculated the total external moment from Euler's equation:

$$\mathbf{M}_{ext} = \sum_{i=1}^N [\mathbf{J}_i \dot{\boldsymbol{\omega}}_i + \boldsymbol{\omega}_i \times (\mathbf{J}_i \boldsymbol{\omega}_i)] - \sum_{i=1}^N \sum_{j=1}^{K_i} (\mathbf{r}_{ij} \times \mathbf{F}_{ij}) \quad (2.2)$$

where \mathbf{M}_{ext} denotes the total three-dimensional external moment, K_i the number of end points in each segment (joints and external contact points), $\boldsymbol{\omega}_i$ and $\dot{\boldsymbol{\omega}}_i$ the

2. Estimation of Ground Reaction Forces and Moments

angular velocities and angular accelerations of each segment, respectively. The inertia tensor around the center of mass of each segment is denoted by \mathbf{J}_i , the position vectors between the center of mass and the end points denoted by \mathbf{r}_{ij} and the resultant force in the end points of each segment described by \mathbf{F}_{ij} . All variables are expressed in the global coordinate system of the IMC system (ψ_g).

Segment linear accelerations exported from the Xsens MVN Studio software were expressed in the origin of each segment as described in detail in the manual of the IMC system [24]. To apply these variables in Equation (2.1), a translation to the segment's center of mass was required, defined as:

$$\mathbf{a}_i = \mathbf{a}_{i,o} + \dot{\boldsymbol{\omega}}_i \times \mathbf{r}_{oi} + \boldsymbol{\omega}_i \times (\boldsymbol{\omega}_i \times \mathbf{r}_{oi}) \quad (2.3)$$

The position vectors between the center of mass and the origin of each segment (\mathbf{r}_{oi}) and the inertial parameters of the body segments m_i and \mathbf{J}_i were calculated through scaled anthropometric data, based on adjustments to Zatsiorsky–Seluyanov's inertial parameters reported by De Leva [107]. The total body mass of the subjects includes their actual body mass plus the mass of the wearable instrumentation. The added mass of the inertial motion capture system was in total 390 g (seventeen IMUs of 10 g each, one wireless communication pack of 150 g and one battery of 70 g). These additional masses were initially subtracted from the total measured mass before calculating the net mass of each segment and then added individually to each of the corresponding body segments. The resulting mass was input to the calculation of the moment of inertia from the radii of gyration. The effect of the wearable equipment in the radii of gyration was assumed to be negligible.

Segment angular velocities ($\boldsymbol{\omega}_i$), angular accelerations ($\dot{\boldsymbol{\omega}}_i$) and linear accelerations of the origins ($\mathbf{a}_{i,o}$), provided by Xsens MVN software, were filtered using a second-order Butterworth zero-phase low-pass filter with a cut-off frequency of 6 Hz.

Our major assumption was that the GRF&Ms are the only significant external loads present. Thus, the total external force (moment) derived from Newton (Euler) equations of motion (Equations (2.1) and (2.2)) balances the sum of forces (moments) applied on both left and right lower limbs:

$$\mathbf{F}_L + \mathbf{F}_R = \mathbf{F}_{ext} \quad (2.4)$$

and

$$\mathbf{M}_L + \mathbf{M}_R = \mathbf{M}_{ext} \quad (2.5)$$

where \mathbf{F}_L (\mathbf{M}_L) and \mathbf{F}_R (\mathbf{M}_R) are the ground reaction forces (moments) applied on the left and right foot, respectively.

During the single support phase, the result of the computation is the GRF&M applied on the foot, which is in contact with the ground. The resulting GRM is expressed about the external contact point on that foot, which is chosen as the projection of the ankle joint on the ground. However, during the phase of double support, the system of equations is indeterminate. To overcome this, we applied a distribution algorithm based on a smooth transition assumption function (f_{STA}), which was constructed from empirical data similarly to previous studies [39, 99]. The curves of the measured GRF&M during the second double support phase were averaged for all steps. Subsequently, a cubic spline interpolation function was used to generate the f_{STA} . The generated function curves were compared to the ones

2.2. Methods

proposed by Ren et al. [39] and shown in Figure 2.3. A direct comparison to the function of Villeger et al. [99] was not possible, because that study calculated the GRM about a fixed point on the plate and not with respect to the body.

The distribution function f_{STA} was expressed in the coordinate system ψ_w . Since the input variables of the Newton–Euler equations were expressed in ψ_g , the same applied to the calculated vectors \mathbf{F}_{ext} and \mathbf{M}_{ext} . Therefore, before applying the distribution function, we rotated the force and moment vectors from the coordinate system ψ_g to ψ_w , resulting in two new vectors \mathbf{F}_{ext}^w and \mathbf{M}_{ext}^w . The GRF&Ms applied on the left and right lower limbs are shown in Table 2.2, where $\mathbf{f}_{F,STA}$ and $\mathbf{f}_{M,STA}$ are the components of \mathbf{f}_{STA} for the GRF and GRM, respectively. Both functions depend on time (t) relative to the timing of gait events denoted by t_{HSL} , t_{HSR} for heel-strike and t_{TOR} , t_{TOL} for toe-off events for the right or left lower limb, respectively. The behavior of the components of $\mathbf{f}_{F,STA}$ and $\mathbf{f}_{M,STA}$ that was used in this implementation is illustrated in Figure 2.3.

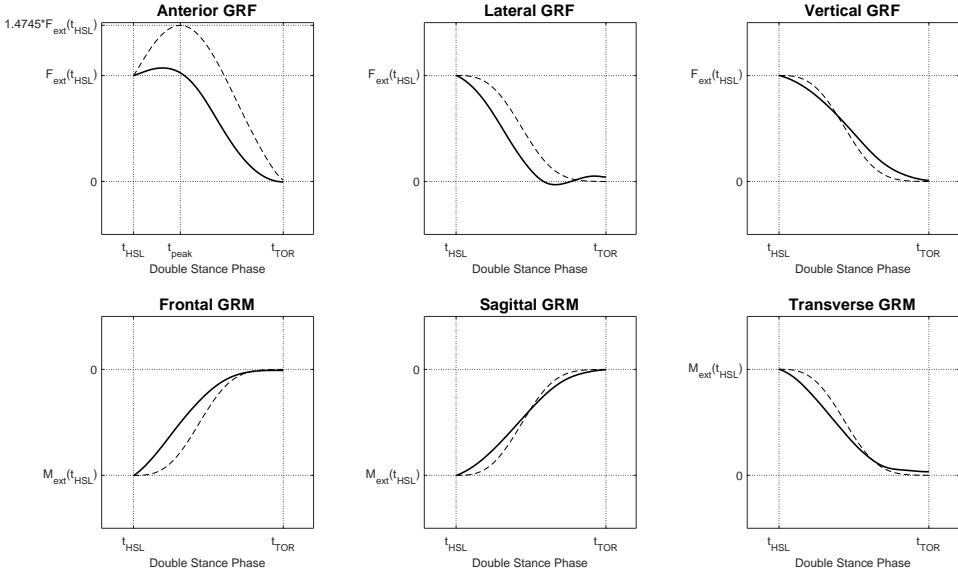


Figure 2.3: The curves of the smooth transition assumption function for the three GRF components ($f_{F,STA}$, three graphs on the top) and three GRM components ($f_{M,STA}$, three graphs on the bottom) used to distribute the total external force and moment among the two feet. Figure illustrates the curve of the GRF&Ms of the right foot between the events of left heel strike and right toe off (second double stance phase) expressed in the coordinate system defined by the walking direction. Continuous lines indicate the curves obtained from the average values across all subjects and trials of our dataset, whereas dashed lines indicate the curves proposed by Ren et al. [39].

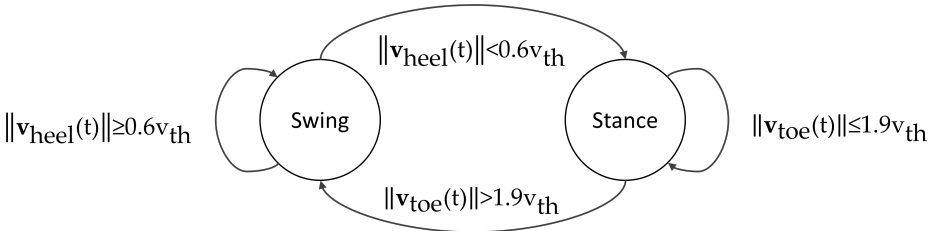
To distinguish between the phases of single and double stance, we used a gait event detection algorithm based on a threshold in the norm of the velocities of the heel ($\|\mathbf{v}_{heel}\|$) and the toe ($\|\mathbf{v}_{toe}\|$). The positions of the heel and toe points were provided by Xsens MVN Studio, and the velocity threshold (v_{th}) was set equal to the norm of the average velocity of the pelvis segment for each trial. The state of

2. Estimation of Ground Reaction Forces and Moments

Table 2.2: The calculation of the left and right GRF&Ms for each phase of the gait cycle. During single support, the GRF&M of the limb in contact with the ground is equal to the result of the Newton–Euler calculation ($\mathbf{F}_{ext}^w, \mathbf{M}_{ext}^w$), whereas during the double support phase, this result is distributed among legs based on the gait-event-dependent three-dimensional smooth transition assumption functions for the forces ($\mathbf{f}_{F,STA}(t)$) and moments ($\mathbf{f}_{M,STA}(t)$).

| Variable | First Double Stance $t_{HSL} \leq t < t_{TOL}$ | Right Single Stance $t_{TOL} \leq t < t_{HSL}$ | Second Double Stance $t_{HSL} \leq t < t_{TOR}$ | Left Single Stance $t_{TOR} \leq t < t_{HSL}$ |
|---------------------|--|---|--|--|
| $\mathbf{F}_L^w(t)$ | $\mathbf{F}_{ext}^w(t_{HSL})\mathbf{f}_{F,STA}(t)$ | 0 | $\mathbf{F}_{ext}^w(t) - \mathbf{F}_R^w(t)$ | $\mathbf{F}_{ext}^w(t)$ |
| $\mathbf{M}_L^w(t)$ | $\mathbf{M}_{ext}^w(t_{HSL})\mathbf{f}_{M,STA}(t)$ | 0 | $\mathbf{M}_{ext}^w(t) - \mathbf{M}_R^w(t)$ | $\mathbf{M}_{ext}^w(t)$ |
| $\mathbf{F}_R^w(t)$ | $\mathbf{F}_{ext}^w(t) - \mathbf{F}_L^w(t)$ | $\mathbf{F}_{ext}^w(t)$ | $\mathbf{F}_{ext}^w(t_{HSL})\mathbf{f}_{F,STA}(t)$ | 0 |
| $\mathbf{M}_R^w(t)$ | $\mathbf{M}_{ext}^w(t) - \mathbf{M}_L^w(t)$ | $\mathbf{M}_{ext}^w(t)$ | $\mathbf{M}_{ext}^w(t_{HSL})\mathbf{f}_{M,STA}(t)$ | 0 |

Figure 2.4: A state machine to detect the current state of the gait cycle, based on the previous state and a condition on the velocity of the heel or toe. The velocity v_{th} is equal to the norm of the average velocity of the pelvis segment for each trial.



the gait cycle at time t is shown in Figure 2.4.

An overview of the algorithmic steps used in our study is shown in Figure 2.5.

2.2.3 Data Analysis: Reference Lab System

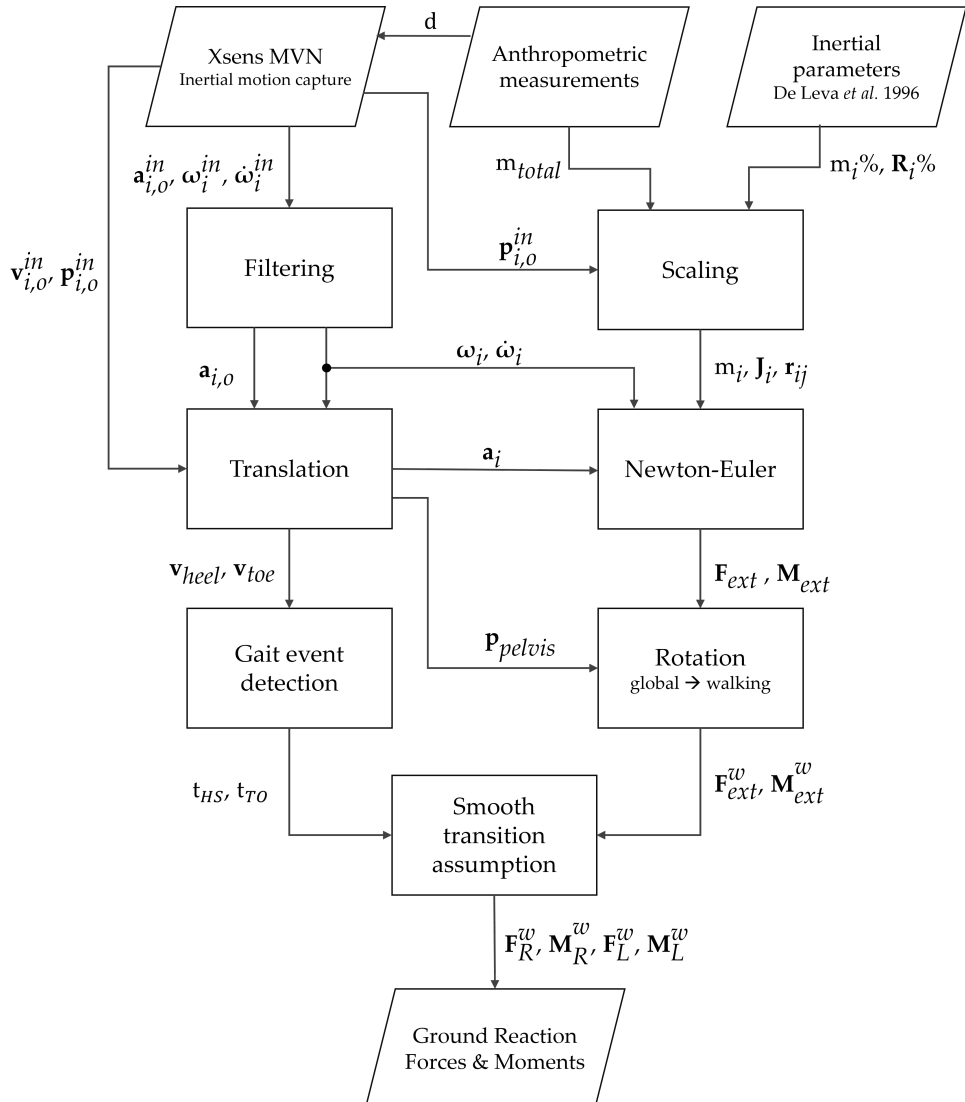
The Qualisys Track Manager 2.2 software package was used to process the three-dimensional positions of the markers and the GRF&Ms recorded using the FPs [106]. For each subject, a model for the automatic identification of markers was created, to assist the marker labeling across trials, and gaps were filled in the missing marker trajectories using a visual preview option. The marker trajectories were filtered using a second-order, zero-phase Butterworth low-pass filter with a cut-off frequency of 6 Hz, following the recommendations of the literature [37]. A biomechanical model composed of 16 segments, as described in Table 2.1, was constructed from the marker trajectories, with segment coordinate frames based on recommendations of the International Society of Biomechanics [109, 110]. A custom script was developed in MATLAB R2015a (The MathWorks Inc.; Natick, MA, USA) to downsample the measured GRF&Ms by a factor of 10 to match the sampling rate of the OMC system. Similarly to Ren et al. [39], no filtering was applied to the processed GRF&Ms.

To compare the OMC data with the IMC data, all quantities expressed in the OMC lab coordinate frame (ψ_{lab}) were rotated to the coordinate frame based on the walking direction (ψ_w). Similar to the transformation applied to the IMC, ψ_w is defined by a rotation around the vertical of ψ_{lab} , and the walking direction was derived from known initial and final positions of the pelvis segment.

In addition, the timing of the reference gait events (heel strike and toe-off) was identified and logged automatically, using a 5 N threshold on the vertical force

2.2. Methods

Figure 2.5: Block diagram of the algorithm used to estimate the GRF&M from anthropometry and inertial motion capture. \mathbf{p} = position, \mathbf{v} = velocity, \mathbf{a} = acceleration, $\boldsymbol{\omega}$ = angular velocity, $\dot{\boldsymbol{\omega}}$ = angular acceleration, \mathbf{F} = force, \mathbf{M} = moment, t = time, d = anthropometric dimensions, m = mass, \mathbf{R} = radius of gyration, \mathbf{J} = inertia tensor. Superscript “*in*” indicates quantities derived directly from the IMC system, and *w* denotes quantities expressed in the coordinate system defined by the walking direction. Subscript *i* indicates a variable of the *i*-th segment. Additional subscript *o* denotes that a linear variable is expressed in the origin of the segment, whereas no additional subscript denotes that it is expressed in the center of mass of the segment. Subscript *ext* = external, *R* = right, *L* = left.



measured by each FP. The steps that were only partially captured by the FPs were recognized and excluded based on the horizontal positions of the heel and toe markers

2. Estimation of Ground Reaction Forces and Moments

during gait events. Due to the limited number of FPs, heel strike events used to denote the end of the gait cycle were not always available directly from the force data. In such cases, a velocity-based gait event detection, driven by the marker data, was used, similarly to Figure 2.4. The method performed with an error of 12 ± 10 ms in heel strike detection across all walking speeds.

The ground reaction force (GRF) was normalized to body weight and the ground reaction moment (GRM) to body weight times body height. In addition, for each step, the time was normalized to 100% of the gait cycle, defined by two consecutive heel contacts of the same foot. Finally, the six components of the measured and predicted GRF&Ms were compared, per walking speed and in total. The GRM was calculated about the projection of the ankle joint on the ground.

To evaluate the accuracy of our method, we used absolute (RMSE) and relative (rRMSE) root mean square errors, as defined by Ren et al. [39]. The agreement between the measured and predicted data normalized to the gait cycle was derived from Pearson's correlation coefficients, which were categorized as weak ($\rho \leq 0.35$), moderate ($0.35 < \rho \leq 0.67$), strong ($0.67 < \rho \leq 0.9$) and excellent ($\rho > 0.9$), according to previous studies [42, 111].

Furthermore, we calculated the curve magnitude (M) and phase (P) percentage differences, based on the technique proposed by Sprague and Geers [112]. Out of 525 measured steps in total, 432 valid steps were included, and 93 steps were excluded due to incomplete stepping on the FPs.

In addition to the analysis over a whole gait cycle, we calculated the ρ , RMSE and rRMSE of the GRF&M throughout three sub-phases:

- DS1: first double stance phase of the ipsilateral foot, between a heel strike of the ipsilateral foot and a toe-off of the contralateral foot.
- DS2: second double stance phase of the ipsilateral foot, between a heel strike of the contralateral foot and a toe-off of the ipsilateral foot.
- SS: single stance phase of the ipsilateral foot, between a toe-off of the contralateral foot and heel strike of the contralateral foot.

Moreover, we analyzed the absolute and relative peak differences between the predicted and measured curves. The stance phase has been divided into three phases: early stance ($0\% < t/D_{stance} \leq 33\%$), middle stance ($33\% < t/D_{stance} \leq 66\%$) and late stance ($66\% < t/D_{stance} \leq 100\%$), where D_{stance} is the duration of the stance phase and t is the time initialized at the beginning of each stance phase. Within these phases, the following peaks have been sought for both predicted and measured values:

- In the early stance (ES) phase: the maximum values of lateral and vertical GRF and minimum value of anterior GRF.
- In the middle stance (MS) phase: the minimum value of the vertical GRF.
- In the late stance (LS) phase: the maximum values of the GRF components and transverse GRM and the minimum values of frontal and sagittal GRM components.

2.3. Results

Finally, we compared the center of pressure (COP) and frictional torque estimates to the FP measurements. To derive these values for the right foot, we used the following equations:

$$COP_{R,x}^w = -\frac{M_{R,y}^w}{F_{R,z}^w} \quad (2.6)$$

$$COP_{R,y}^w = \frac{M_{R,x}^w}{F_{R,z}^w} \quad (2.7)$$

$$COP_{R,z}^w = 0 \quad (2.8)$$

$$T_{R,F}^w = M_{R,z}^w - COP_{R,x}^w F_{R,y}^w + COP_{R,y}^w F_{R,x}^w \quad (2.9)$$

where $COP_{R,x}^w$ and $COP_{R,y}^w$ are the anterior and lateral positions of the center of pressure on the ground with respect to the projection of the right ankle joint on the ground. $T_{R,F}^w$ is the frictional torque, $F_{R,x}^w$, $F_{R,y}^w$ and $F_{R,z}^w$ the anterior, lateral and vertical GRF, respectively, and $M_{R,x}^w$, $M_{R,y}^w$ and $M_{R,z}^w$ the frontal, sagittal and transverse GRM, respectively, calculated about the projection of the right ankle joint on the ground. The COP was calculated and analyzed per foot during stance phase, when $F_{R,z}^w$ was greater than 5 N. In the same way, the calculations for the left foot were performed. All variables are used in the equations individually for both right and left foot and are expressed in the coordinate system ψ_w .

In our implementation, the estimates of GRF&M depend highly on the performance of the gait event detection. Particularly, during the double support phase, the GRF&Ms applied on the ipsilateral foot are driven by the smooth transition assumption function. This is represented by a curve, which is based on the magnitude of each GRF&M component during the last single support frame and assumes zero magnitude on the last frame of double support. Thus, we evaluated the sensitivity of the heel strike and toe-off detection while using the original thresholds, compared to 10% higher and 10% lower than that.

We additionally performed a sensitivity analysis to investigate the effect of the selection of the cut-off frequency used in the second-order Butterworth low-pass filter. The change in the root mean square errors of each component of the GRF&M was used to indicate the impact of the selection in the final estimates.

2.3 Results

2.3.1 Accuracy Analysis

The curves of the GRF&M throughout a whole gait cycle during normal walking, estimated via IMC and OMC, are depicted in Figures 2.6 and 2.7, respectively.

Table 2.3 shows the results of the GRF analyzed throughout a whole gait cycle for both the IMC and OMC solutions. Overall, a similar performance by both systems can be observed for all metrics. Small differences were found in the anterior GRF where OMC provided higher accuracy (OMC: rRMSE = 7.4%, IMC: rRMSE = 9.4%). In contrast, similarly small differences were found in the lateral GRF, where IMC performed better. Table 2.4 shows the GRF estimates during the first and second double stance phase, as well as during the single support. Since the analysis is performed over a smaller period, higher absolute and relative errors are

2. Estimation of Ground Reaction Forces and Moments

observed. Excellent correlations were found in all phases for both anterior and vertical GRF. The lateral GRF also presented excellent correlation during the second double support phase and strong correlations in the first double support phase. However, during the single support phase, the correlation is moderate and weak for IMC and OMC, respectively.

Similarly, the results for GRM are presented in Tables 2.5 and 2.6 for both IMC and OMC solutions. For all walking speeds, the performance of IMC was comparable to OMC, except for the frontal plane moment where the rRMSE for IMC was between 29.6% and 30.6% across walking speeds, whereas for OMC, that was between 22.7% and 23.5%. In contrast, IMC provided higher correlations for the frontal plane GRM (ρ ranging from 0.709 to 0.710), compared to OMC (ρ ranging from 0.652 to 0.684) in all walking speeds. Excellent correlations were observed in the sagittal plane GRM for both normal walking ($\rho = 0.933$, rRMSE = 12.4%) and slow walking trials ($\rho = 0.916$, rRMSE = 13.3%). The correlation and RMSE in the transverse plane moment were similar in both solutions (IMC: $\rho = 0.826$, rRMSE = 18.2%, OMC: $\rho = 0.825$, rRMSE = 16.3%, for normal walking speed).

The center of pressure and frictional torque estimates are compared in Table 2.7. RMSE values were similar in both IMC and OMC solutions. The average RMSE of the anterior COP position ranges from 4.5 cm to 6.6 cm for IMC and from 4.4 cm to 6.5 cm for OMC. The average RMSE of the lateral COP position was ranging from 2.9 cm to 3.6 cm for IMC and from 2.4 cm to 2.7 cm for OMC. The estimates of the frictional torque were comparable for both solutions with rRMSE ranging from 23.5 to 27.6 for IMC and from 25.8 to 29.8 for OMC.

Finally, Table 2.8 presents the differences in the peak values of the estimated and measured GRF&M. As shown in the table, low relative errors have been extracted for the peaks of the vertical component for both solutions. In contrast, the differences in peak values were higher for the horizontal components.

2.3.2 Sensitivity Analysis

The sensitivity analysis on threshold velocities for the gait event detection algorithm is shown in Table 2.9. The gait events were detected using the inertial motion capture system with an error of 14.02 ± 13.91 ms for heel strike and 16.09 ± 15.68 ms for toe-off. A 10% increase or decrease in the threshold velocity would only result in a small additional error on the detection of both gait events (16.09 ± 15.68 ms for 10% increase and 16.09 ± 15.68 ms for a 10% decrease).

Table 2.10 shows the results of the sensitivity analysis performed to evaluate the selection of the cut-off frequency used in the low-pass filtering. Particularly, it indicates the change in the RMSE per component for six different cut-off frequencies. A low cut-off frequency selection leads to a decrease in the errors in the components with a small magnitude, such as the lateral GRF and the frontal and transverse GRM. In contrast, in the components with larger magnitudes, such as the vertical GRF and sagittal GRM, the accuracy increases with a higher cut-off frequency selection. To solve this inconsistency, the norms of the RMSE changes of the GRF and GRM 3D vectors were also compared. The norm of GRF RMSE is minimized for approximately 7 Hz and the norm of GRM RMSE for 6 Hz.

2.3. Results

Figure 2.6: Ground reaction forces and moments (GRF&M) estimated using IMC (mean (thin grey line) ± 1 SD around mean (shaded area)), compared with measured FP data (mean (thick black line) (± 1 SD (thin black lines))) during normal walking. Curve magnitudes are normalized to body weight and body weight times body height for the GRF and GRM, respectively. Averaged over right and left steps of all 11 subjects.

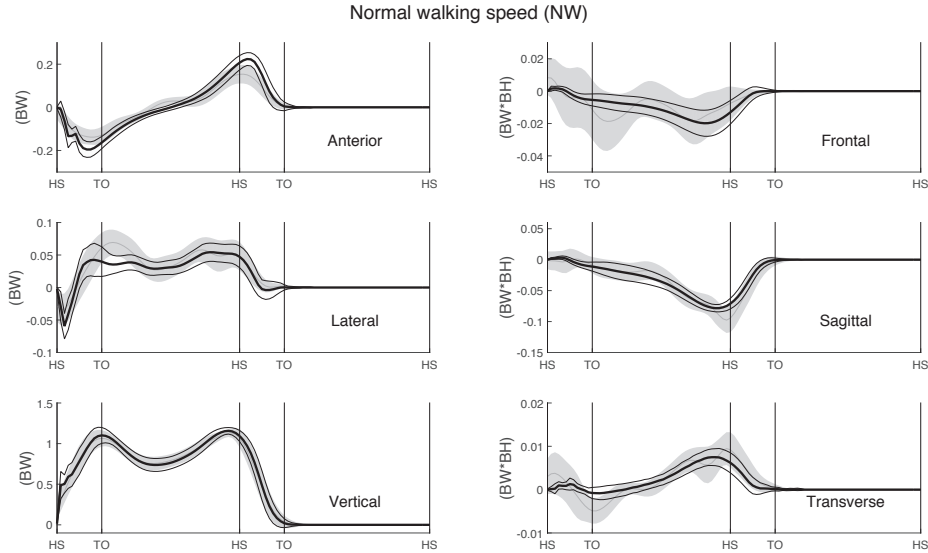
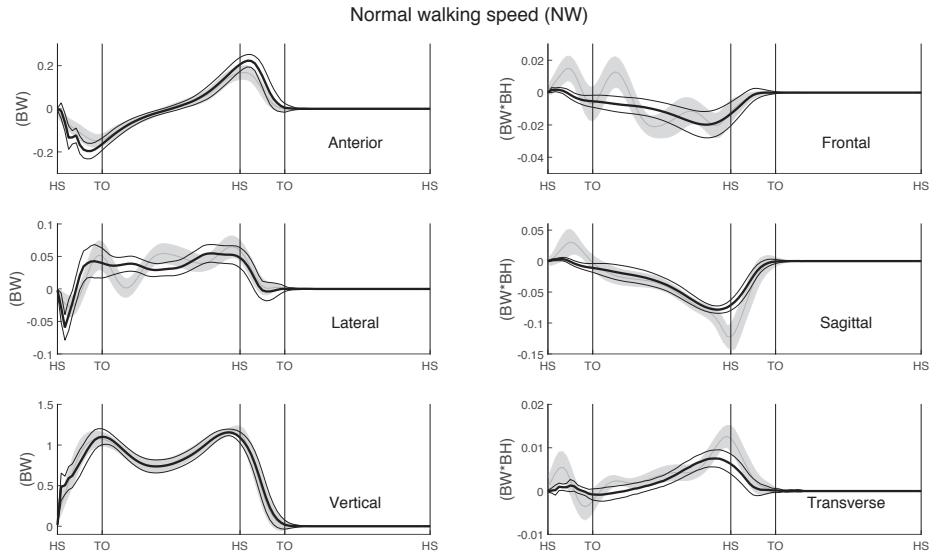


Figure 2.7: Ground reaction forces and moments (GRF&M) estimated using OMC (mean (thin grey line) ± 1 SD around mean (shaded area)), compared with measured FP data (mean (thick black line) (± 1 SD (thin black lines))) during normal walking. Curve magnitudes are normalized to body weight and body weight times body height for the GRF and GRM, respectively. Averaged over right and left steps of all 11 subjects.



2. Estimation of Ground Reaction Forces and Moments

Table 2.3: Comparison of ground reaction forces (GRF) estimated from inertial motion capture and optical motion capture versus force plate measurements. ρ = Pearson's correlation coefficient, RMS = root mean square error in N/BW, rRMSE = relative root mean square error (%), M = curve magnitude difference (%) and P = phase difference (%). Results are analyzed during normal (NW), slow (SW) and fast walking (FW) for the decomposed right and left GRF.

| | Inertial Motion Capture | | | Optical Motion Capture | | | |
|----------|-------------------------|---------------|---------------|------------------------|---------------|---------------|-------|
| | NW | SW | FW | NW | SW | FW | |
| Anterior | 0.965 | 0.955 | 0.950 | ρ | 0.977 | 0.974 | 0.977 |
| Lateral | 0.862 | 0.853 | 0.821 | | 0.814 | 0.814 | 0.757 |
| Vertical | 0.992 | 0.990 | 0.986 | | 0.993 | 0.991 | 0.987 |
| | | | | RMSE | | | |
| Anterior | 0.034 (0.007) | 0.036 (0.012) | 0.047 (0.011) | 0.028 (0.005) | 0.029 (0.007) | 0.034 (0.006) | |
| Lateral | 0.017 (0.003) | 0.018 (0.005) | 0.022 (0.004) | 0.017 (0.003) | 0.018 (0.005) | 0.022 (0.004) | |
| Vertical | 0.063 (0.035) | 0.075 (0.039) | 0.090 (0.040) | 0.058 (0.031) | 0.067 (0.027) | 0.081 (0.025) | |
| | | | | rRMSE | | | |
| Anterior | 9.4 (2.5) | 10.4 (3.2) | 10.9 (3.1) | 7.4 (1.5) | 8.0 (1.9) | 7.5 (1.3) | |
| Lateral | 13.1 (2.8) | 13.8 (3.3) | 14.6 (3.1) | 14.2 (2.9) | 14.2 (3.3) | 15.5 (4.0) | |
| Vertical | 5.3 (3.1) | 6.3 (3.3) | 6.9 (3.0) | 4.8 (2.7) | 5.5 (2.2) | 6.1 (1.8) | |
| | | | | M | | | |
| Anterior | -26.0 (10.5) | -28.8 (10.5) | -30.2 (9.9) | 9.5 (3.2) | 10.5 (3.5) | 11.0 (3.1) | |
| Lateral | 23.1 (10.7) | 24.6 (15.9) | 28.8 (13.2) | 14.1 (3.5) | 14.7 (4.3) | 16.1 (5.3) | |
| Vertical | -1.0 (2.4) | -1.2 (1.9) | -1.5 (1.6) | 3.1 (2.0) | 3.6 (2.0) | 4.2 (1.9) | |
| | | | | P | | | |
| Anterior | -22.0 (5.2) | -23.4 (5.9) | -22.5 (5.7) | 7.2 (2.0) | 7.7 (2.3) | 7.1 (1.3) | |
| Lateral | 8.5 (9.6) | 9.4 (11.0) | 12.7 (12.6) | 16.3 (3.7) | 16.5 (4.7) | 18.4 (5.7) | |
| Vertical | 0.3 (2.5) | 0.3 (1.9) | 0.6 (1.6) | 2.8 (1.8) | 3.2 (1.4) | 3.7 (1.2) | |

Table 2.4: Comparison of ground reaction forces (GRF) estimated from inertial motion capture and optical motion capture versus force plate measurements. ρ = Pearson's correlation coefficient, RMSE = root mean square error in N/BW, rRMSE = relative root mean square error (%). Results are analyzed for all walking speeds during the gait cycle phases of first double stance (DS1), second double stance (DS2) and single stance (SS) for the decomposed right and left GRF.

| | Inertial Motion Capture | | | Optical Motion Capture | | | |
|----------|-------------------------|---------------|---------------|------------------------|---------------|---------------|-------|
| | DS1 | DS2 | SS | DS1 | DS2 | SS | |
| Anterior | 0.918 | 0.976 | 0.975 | ρ | 0.921 | 0.983 | 0.993 |
| Lateral | 0.792 | 0.946 | 0.605 | | 0.791 | 0.959 | 0.325 |
| Vertical | 0.946 | 0.995 | 0.980 | | 0.936 | 0.997 | 0.984 |
| | | | | RMSE | | | |
| Anterior | 0.058 (0.023) | 0.066 (0.025) | 0.033 (0.013) | 0.056 (0.018) | 0.055 (0.014) | 0.018 (0.007) | |
| Lateral | 0.030 (0.012) | 0.013 (0.007) | 0.022 (0.007) | 0.029 (0.011) | 0.013 (0.009) | 0.022 (0.007) | |
| Vertical | 0.143 (0.077) | 0.118 (0.075) | 0.042 (0.030) | 0.149 (0.058) | 0.092 (0.060) | 0.033 (0.018) | |
| | | | | rRMSE | | | |
| Anterior | 33.3 (10.8) | 38.3 (16.5) | 10.0 (3.6) | 32.1 (8.6) | 29.3 (9.6) | 5.2 (1.6) | |
| Lateral | 30.9 (11.7) | 25.5 (16.3) | 35.4 (8.9) | 29.7 (9.7) | 22.9 (19.0) | 34.6 (7.5) | |
| Vertical | 14.4 (6.7) | 12.1 (8.6) | 9.0 (5.2) | 14.2 (4.7) | 8.9 (9.1) | 6.5 (2.4) | |

2.4 Discussion

In this study, we have developed a method to estimate 3D GRF&Ms during walking, using only kinematics from an IMC system. We evaluated the method for three different walking speeds performed by eleven healthy subjects. The accuracy of our estimates was assessed through comparison with force plate measurements, as well as with comparison to OMC-based estimates.

2.4.1 Comparison with Reported Optical-Based Estimation

In Table 2.11, we compare the performance of the IMC-based and OMC-based GRF&M estimation results during normal walking performed in the dataset of this

2.4. Discussion

Table 2.5: Comparison of ground reaction moments (GRM) estimated from inertial motion capture and optical motion capture versus force plate measurements. ρ = Pearson's correlation coefficient, RMSE = root mean square error in Nm/BW * BH, rRMSE = relative root mean square error (%), M = curve magnitude difference (%) and P = phase difference (%). Results are analyzed during normal (NW), slow (SW) and fast walking (FW) for the decomposed right and left GRM.

| Inertial Motion Capture | | | Optical Motion Capture | | | | |
|-------------------------|---------------|---------------|------------------------|---------------|---------------|---------------|-------|
| | NW | SW | FW | NW | SW | FW | |
| Frontal | 0.710 | 0.707 | 0.709 | ρ | 0.684 | 0.675 | 0.652 |
| Sagittal | 0.933 | 0.916 | 0.841 | | 0.942 | 0.932 | 0.880 |
| Transverse | 0.826 | 0.811 | 0.749 | | 0.825 | 0.817 | 0.768 |
| RMSE | | | | | | | |
| Frontal | 0.010 (0.004) | 0.010 (0.004) | 0.012 (0.004) | 0.008 (0.001) | 0.008 (0.002) | 0.009 (0.002) | |
| Sagittal | 0.013 (0.004) | 0.015 (0.006) | 0.020 (0.005) | 0.016 (0.006) | 0.019 (0.008) | 0.026 (0.006) | |
| Transverse | 0.003 (0.001) | 0.003 (0.001) | 0.004 (0.001) | 0.002 (0.001) | 0.003 (0.001) | 0.004 (0.001) | |
| rRMSE | | | | | | | |
| Frontal | 29.6 (9.3) | 30.2 (9.3) | 30.6 (8.0) | 22.7 (4.1) | 23.0 (4.6) | 23.5 (4.9) | |
| Sagittal | 12.4 (3.4) | 13.3 (3.8) | 16.1 (3.2) | 12.7 (3.5) | 13.7 (3.8) | 16.9 (2.7) | |
| Transverse | 18.2 (4.7) | 18.8 (4.8) | 21.6 (4.2) | 16.8 (4.5) | 17.6 (4.8) | 21.0 (4.3) | |
| M | | | | | | | |
| Frontal | 110.3 (146.3) | 116.6 (135.7) | 140.4 (116.1) | 63.0 (92.0) | 71.1 (94.9) | 77.0 (84.8) | |
| Sagittal | -0.7 (12.4) | 5.3 (19.0) | 22.5 (19.6) | 36.1 (14.6) | 41.2 (23.9) | 63.9 (22.6) | |
| Transverse | 49.6 (28.3) | 54.7 (33.7) | 75.9 (33.8) | 45.7 (27.5) | 54.1 (37.1) | 82.8 (40.9) | |
| P | | | | | | | |
| Frontal | 19.7 (8.5) | 21.5 (10.6) | 21.0 (9.0) | 23.8 (7.8) | 24.7 (8.5) | 25.2 (8.4) | |
| Sagittal | 13.1 (4.2) | 13.8 (4.9) | 16.9 (4.8) | 10.1 (2.8) | 11.2 (3.2) | 13.9 (2.4) | |
| Transverse | 18.0 (5.8) | 18.9 (6.2) | 21.0 (6.7) | 16.3 (3.9) | 17.1 (4.7) | 18.6 (5.0) | |

Table 2.6: Comparison of ground reaction moments (GRM) estimated from inertial motion capture and optical motion capture versus force plate measurements. ρ = Pearson's correlation coefficient, RMSE = root mean square error in Nm/BW * BH, rRMSE = relative root mean square error (%). Results are analyzed for all walking speeds during the gait cycle phases of first double stance (DS1), second double stance (DS2) and single stance (SS) for the decomposed right and left GRM.

| Inertial Motion Capture | | | Optical Motion Capture | | | | |
|-------------------------|---------------|---------------|------------------------|---------------|---------------|---------------|-------|
| | DS1 | DS2 | SS | DS1 | DS2 | SS | |
| Frontal | 0.556 | 0.803 | 0.431 | ρ | 0.515 | 0.951 | 0.472 |
| Sagittal | -0.262 | 0.994 | 0.940 | | -0.137 | 0.997 | 0.943 |
| Transverse | 0.379 | 0.958 | 0.913 | | 0.528 | 0.966 | 0.858 |
| RMSE | | | | | | | |
| Frontal | 0.010 (0.004) | 0.005 (0.004) | 0.014 (0.006) | 0.012 (0.005) | 0.004 (0.003) | 0.010 (0.003) | |
| Sagittal | 0.016 (0.007) | 0.019 (0.017) | 0.017 (0.006) | 0.027 (0.011) | 0.031 (0.023) | 0.017 (0.007) | |
| Transverse | 0.004 (0.002) | 0.003 (0.002) | 0.003 (0.001) | 0.005 (0.002) | 0.004 (0.003) | 0.003 (0.001) | |
| rRMSE | | | | | | | |
| Frontal | 60.3 (17.7) | 46.4 (28.4) | 54.8 (17.8) | 72.0 (30.7) | 37.2 (32.2) | 37.4 (7.4) | |
| Sagittal | 68.4 (16.2) | 22.2 (14.9) | 17.7 (5.2) | 95.4 (25.7) | 29.4 (22.1) | 15.1 (4.1) | |
| Transverse | 56.2 (16.7) | 31.3 (18.8) | 23.3 (7.1) | 61.8 (16.4) | 35.2 (30.8) | 19.8 (7.1) | |

study, with results previously reported in other optical-based studies using ρ and rRMSE.

In both the inertial and optical implementation of this study, we found higher correlation coefficients compared to the ones extracted from the 10-fold cross-validation method performed by Oh et al. [40] when they reimplemented the method of Ren et al. [39] for all components apart from the sagittal and transverse plane moments. Regarding rRMSE values, these followed a similar pattern, with the sagittal GRM providing slightly worse accuracy, whereas the transverse plane moment was better estimated in our method.

Compared to the dynamic contact model developed by Fluit et al. [42], we found

2. Estimation of Ground Reaction Forces and Moments

Table 2.7: Comparison of center of pressure (COP) and frictional torque estimated from inertial motion capture and optical motion capture versus force plate measurements. ρ = Pearson's correlation coefficient, RMSE = root mean square error in m for COP and Nm/BW * BH for frictional torque, rRMSE = relative root mean square error (%). Analysis performed over stance phase for normal (NW), slow (SW) and fast walking (FW) trials for the decomposed right and left quantities.

| | Inertial Motion Capture | | | Optical Motion Capture | | |
|-------------------|-------------------------|---------------|---------------|------------------------|---------------|---------------|
| | NW | SW | FW | NW | SW | FW |
| Anterior COP | 0.803 | 0.777 | 0.526 | 0.884 | 0.818 | 0.702 |
| Lateral COP | 0.559 | 0.546 | 0.522 | 0.619 | 0.596 | 0.574 |
| Frictional Torque | 0.776 | 0.775 | 0.677 | 0.764 | 0.746 | 0.676 |
| RMSE | | | | | | |
| Anterior COP | 0.045 (0.013) | 0.050 (0.018) | 0.066 (0.016) | 0.044 (0.010) | 0.054 (0.016) | 0.065 (0.012) |
| Lateral COP | 0.029 (0.012) | 0.031 (0.011) | 0.036 (0.011) | 0.024 (0.004) | 0.025 (0.006) | 0.027 (0.006) |
| Frictional Torque | 0.004 (0.001) | 0.004 (0.002) | 0.005 (0.002) | 0.005 (0.002) | 0.005 (0.002) | 0.006 (0.002) |
| rRMSE | | | | | | |
| Anterior COP | 21.3 (5.3) | 22.5 (6.9) | 28.5 (5.7) | 19.9 (3.4) | 22.2 (5.0) | 25.4 (4.0) |
| Lateral COP | 32.4 (10.9) | 34.5 (11.0) | 37.2 (9.8) | 28.3 (5.9) | 28.6 (5.4) | 29.2 (5.1) |
| Frictional Torque | 23.5 (5.1) | 23.9 (6.1) | 27.6 (5.5) | 25.8 (7.1) | 26.5 (7.4) | 29.8 (5.9) |

Table 2.8: Differences in the peak values of the ground reaction forces and moments estimated using inertial motion capture and optical motion capture versus measured using force plates. Analysis performed for normal (NW), slow (SW) and fast walking (FW) trials for the decomposed right and left quantities. The subscripts *ES*, *MS* and *LS* indicate the phase of stance where each peak was found (early, middle and late stance phase, respectively).

| | Inertial Motion Capture | | | Optical Motion Capture | | |
|--|-------------------------|----------------|----------------|------------------------|----------------|----------------|
| | NW | SW | FW | NW | SW | FW |
| Anterior GRF <i>Min_{ES}</i> | 0.051 (0.027) | 0.055 (0.032) | 0.086 (0.024) | 0.049 (0.019) | 0.051 (0.023) | 0.071 (0.017) |
| Anterior GRF <i>Max_{LS}</i> | -0.072 (0.024) | -0.073 (0.032) | -0.100 (0.027) | -0.057 (0.016) | -0.058 (0.020) | -0.073 (0.020) |
| Lateral GRF <i>Max_{ES}</i> | 0.026 (0.018) | 0.024 (0.016) | 0.023 (0.016) | 0.000 (0.018) | 0.001 (0.020) | 0.002 (0.026) |
| Lateral GRF <i>Max_{LS}</i> | 0.007 (0.014) | 0.012 (0.020) | 0.027 (0.024) | 0.010 (0.015) | 0.015 (0.022) | 0.035 (0.024) |
| Vertical GRF <i>Max_{ES}</i> | -0.031 (0.016) | -0.031 (0.024) | -0.047 (0.023) | -0.018 (0.021) | -0.019 (0.025) | -0.038 (0.026) |
| Vertical GRF <i>Min_{MS}</i> | 0.019 (0.011) | 0.018 (0.012) | 0.022 (0.012) | 0.008 (0.008) | 0.007 (0.007) | 0.005 (0.009) |
| Vertical GRF <i>Max_{LS}</i> | -0.003 (0.035) | 0.004 (0.046) | 0.003 (0.055) | 0.044 (0.047) | 0.053 (0.064) | 0.073 (0.078) |
| Frontal GRM <i>Min_{LS}</i> | -0.001 (0.013) | -0.005 (0.015) | -0.014 (0.016) | -0.002 (0.006) | -0.003 (0.008) | -0.007 (0.010) |
| Sagittal GRM <i>Min_{LS}</i> | -0.027 (0.020) | -0.033 (0.029) | -0.062 (0.025) | -0.053 (0.023) | -0.063 (0.035) | -0.098 (0.029) |
| Transverse GRM <i>Max_{LS}</i> | 0.003 (0.003) | 0.004 (0.004) | 0.006 (0.005) | 0.006 (0.003) | 0.007 (0.006) | 0.013 (0.005) |
| Relative (%) | | | | | | |
| Anterior GRF <i>Min_{ES}</i> | 25.1 (11.8) | 26.9 (15.8) | 34.5 (11.9) | 24.2 (7.7) | 25.3 (8.0) | 28.3 (7.1) |
| Anterior GRF <i>Max_{LS}</i> | -32.2 (12.6) | -32.5 (12.9) | -36.4 (9.4) | -25.5 (7.4) | -26.0 (7.6) | -26.5 (6.4) |
| Lateral GRF <i>Max_{ES}</i> | 65.9 (70.4) | 55.9 (59.4) | 50.7 (65.7) | 37.3 (38.4) | 8.5 (40.0) | 14.2 (54.2) |
| Lateral GRF <i>Max_{LS}</i> | 15.5 (36.9) | 32.5 (78.0) | 79.6 (124.5) | 19.8 (29.3) | 42.5 (104.6) | 111.2 (167.7) |
| Vertical GRF <i>Max_{ES}</i> | -2.8 (1.5) | -4.7 (3.0) | -4.0 (2.0) | -1.0 (0.0) | -1.0 (3.2) | -1.0 (0.0) |
| Vertical GRF <i>Min_{MS}</i> | 2.2 (1.6) | 2.8 (2.2) | 4.2 (2.6) | 1.1 (1.1) | 1.0 (1.9) | 1.0 (1.8) |
| Vertical GRF <i>Max_{LS}</i> | -0.2 (3.0) | 0.4 (4.1) | 0.4 (4.6) | 3.8 (4.1) | 4.7 (5.6) | 6.2 (6.7) |
| Frontal GRM <i>Min_{LS}</i> | -10.9 (71.0) | -42.5 (134.5) | -115.8 (195.8) | -22.3 (52.6) | -36.8 (120.2) | -82.1 (194.1) |
| Sagittal GRM <i>Min_{LS}</i> | -34.3 (25.0) | -41.8 (36.6) | -76.2 (33.3) | -66.8 (28.4) | -79.5 (44.1) | -120.8 (39.3) |
| Transverse GRM <i>Max_{LS}</i> | 46.2 (51.9) | 49.9 (57.2) | 72.5 (68.7) | 80.6 (60.2) | 102.3 (89.1) | 169.0 (109.2) |

Table 2.9: Sensitivity analysis on the threshold velocities used for the gait event detection.

| Heel Strike Detection | | | |
|------------------------------|--------------------|-------------------|--------------------|
| Threshold velocity | $0.6v_{th} - 10\%$ | $0.6v_{th}$ | $0.6v_{th} + 10\%$ |
| Mean error (ms) | 18.87 ± 15.44 | 14.02 ± 13.91 | 15.37 ± 14.35 |
| Toe Off Detection | | | |
| Threshold velocity | $1.9v_{th} - 10\%$ | $1.9v_{th}$ | $1.9v_{th} + 10\%$ |
| Mean error (ms) | 16.21 ± 17.22 | 16.09 ± 15.68 | 17.80 ± 14.60 |

similar correlation coefficients in all components, apart from the transverse plane, which was much higher in our case (IMC: $\rho = 0.826$; OMC: $\rho = 0.825$; Fluit et al.: $\rho = 0.704$). As for the rRMSE values, our technique performed similarly for

2.4. Discussion

Table 2.10: Percentage change in the root mean square error (RMSE) of the three components and norms of the ground reaction force and moment, versus selected cut-off frequency for the second-order, zero-phase Butterworth low-pass filter. Negative values indicate improvement in the accuracy (decreased RMSE). The selected cut-off frequency (6 Hz) was used as a baseline for the comparison.

| Frequency (Hz) | 3 | 4 | 5 | 6 | 7 | 8 | 9 |
|----------------|-----------------|--------|-------|------|-------|-------|-------|
| | RMSE change (%) | | | | | | |
| Anterior | 48.56 | 23.30 | 7.45 | 0.00 | -1.48 | 0.57 | 4.41 |
| Lateral | -13.78 | -10.59 | -5.39 | 0.00 | 7.72 | 18.07 | 29.89 |
| Vertical | 17.61 | 6.93 | 2.26 | 0.00 | -1.02 | -1.26 | -0.96 |
| Norm GRF | 43.56 | 20.34 | 6.23 | 0.00 | -0.52 | 2.45 | 7.23 |
| Frontal | -14.94 | -12.27 | -6.51 | 0.00 | 7.78 | 15.76 | 24.79 |
| Sagittal | 61.80 | 29.54 | 8.58 | 0.00 | -1.24 | 0.74 | 4.55 |
| Transverse | -19.04 | -11.35 | -6.62 | 0.00 | 8.71 | 18.37 | 29.22 |
| Norm GRM | 40.75 | 17.22 | 3.76 | 0.00 | 1.90 | 6.09 | 11.88 |

four components (anterior, lateral, vertical, sagittal). The rRMSE in the transverse plane was lower in our findings (IMC: rRMSE = 18.2%; OMC: rRMSE = 16.8%; Fluit et al.: rRMSE = 40.60%). Fluit et al. explained that the cause of the inaccuracy in the transverse plane was the one-degree-of-freedom knee joint used. In contrast, the IMC method provided lower accuracy in the frontal plane GRM (IMC: rRMSE = 29.6%; OMC: rRMSE = 22.7%; Fluit et al.: rRMSE = 22.9%).

In the comparison with the results reported by the machine-learning-based method of Oh et al. [40], we noted similar correlations for the anterior (IMC: $\rho = 0.965$; OMC: $\rho = 0.977$; Oh et al. $\rho = 0.985$) and vertical (IMC: $\rho = 0.992$; OMC: $\rho = 0.993$; Oh et al. $\rho = 0.991$). The remaining components provided lower correlations and higher rRMSE in our findings.

The number of subjects included in our study was 11, higher than the previous optical-based studies, which included 3 [39], 5 [40] and 9 subjects [42]. This factor may have contributed to the larger standard deviations found in our RMSE values in anterior and vertical GRF.

In all four studies, regardless of the distribution technique used, the anterior and vertical GRF, as well as the sagittal GRM estimates performed better than the lateral GRF and frontal and transverse GRM. This behavior can be explained by the smaller magnitude of the lateral measures, which causes small accumulated errors in the input to have a relatively large impact on the final estimates. The majority of our results were in good agreement with the OMC-based literature.

This performance comparison demonstrates that IMC can be used in applications such as GRF&M prediction, performing similarly to OMC while exempting the restrictions of OMC mentioned previously in the Introduction.

2.4.2 Limitations and Sources of Error

In this study, we solved the indeterminacy problem during the double support phases of the gait cycle by utilizing a concept known as the smooth transition assumption. A function was generated from the average values of the force plate data during the second double support phase, similarly to Ren et al. [39]. Since these curves were obtained from the gait of 11 healthy subjects of this study, they may not be suitable

2. Estimation of Ground Reaction Forces and Moments

Table 2.11: Pearson's correlation coefficients (ρ) and relative root mean square errors (rRMSE) found in our IMC-based and OMC-based results and reported by previous studies based on optical prediction for normal walking [42, 40, 39]. The values marked with (*) are sourced from the 10-fold cross-validation performed by Oh et al. [40]. The number of subjects used in each study is denoted by n .

| <i>n</i> | Ground Reaction Force | | | | Ground Reaction Moment | | |
|--------------------|-----------------------|------------|------------|-----------|------------------------|------------|-------------|
| | Anterior | Lateral | Vertical | Frontal | Sagittal | Transverse | |
| | ρ | | | | | | |
| This study (IMC) | 11 | 0.965 | 0.862 | 0.992 | 0.710 | 0.933 | 0.826 |
| This study (OMC) | 11 | 0.977 | 0.814 | 0.993 | 0.684 | 0.942 | 0.825 |
| Ren et al., 2008 * | 3 | 0.878 | 0.704 | 0.913 | 0.677 | 0.978 | 0.829 |
| Oh et al., 2013 | 5 | 0.985 | 0.918 | 0.991 | 0.841 | 0.987 | 0.868 |
| Fluit et al., 2014 | 9 | 0.957 | 0.818 | 0.957 | 0.684 | 0.922 | 0.704 |
| rRMSE | | | | | | | |
| This study (IMC) | 11 | 9.4 (2.5) | 13.1 (2.8) | 5.3 (3.1) | 29.6 (9.3) | 12.4 (3.4) | 18.2 (4.7) |
| This study (OMC) | 11 | 7.4 (1.5) | 14.2 (2.9) | 4.8 (2.7) | 22.7 (4.1) | 12.7 (3.5) | 16.8 (4.5) |
| Ren et al., 2008 | 3 | 10.9 (0.8) | 20.0 (2.7) | 5.6 (1.5) | 32.5 (4.3) | 12.2 (4.8) | 26.2 (9.4) |
| Oh et al., 2013 | 5 | 7.3 (0.8) | 10.9 (1.8) | 5.8 (1.0) | 22.8 (4.9) | 9.9 (1.1) | 25.5 (4.5) |
| Fluit et al., 2014 | 9 | 9.3 (2.0) | 14.9 (3.4) | 6.6 (1.1) | 22.9 (5.9) | 12.4 (3.5) | 40.6 (11.3) |

for other groups, especially for populations with movement disorders. In addition, the differences found for various walking speeds indicate that a more sophisticated force distribution model is required. Therefore, methods based on either machine learning or dynamic contact models could be incorporated to improve the accuracy, repeatability and range of movements to which the method can be applied.

Filtering the input kinematics was necessary to obtain the best fit and reduce the errors in the GRF&M estimates. We translated the linear accelerations expressed in the origin to the center of mass of each segment. However, these accelerations were already translated from the sensor to the origin of the segment in Xsens MVN and include assumptions about the sensor location on the segment [113]. Moreover, angular accelerations were calculated through differentiation of angular velocities. This differentiation introduced high frequency signals, which require filtering before being used to translate accelerations. Nevertheless, it was demonstrated in the sensitivity analysis (Table 2.10) that any cut-off frequency between 5 Hz and 7 Hz would result in minor differences in the RMSEs.

The sensitivity analysis on the gait event detection, using the kinematics of the IMC system, proved that the algorithm is valid for the walking speeds included in this study. The algorithm resulted in an error of 14.05 ± 13.91 ms, which for a sampling frequency of 240 Hz corresponds to 3.36 ± 3.33 samples. However, this algorithm may not be accurate for considerably slower or faster walking speeds or in cases of lower sampling frequencies. Gait misdetections could lead to considerable errors in the final estimates, so the method should be treated with caution.

In addition, mass ratios and radii of gyration of the body segments were estimated based on anthropometric tables found in the literature [107]. However, these parameters are averages and might not be suitable for all body types, for example for the elderly [114] or obese populations [115]. Therefore, inertia parameter approximations could have contributed to accumulative errors in the total external load estimation.

The IMC system uses a rigid-body linked-segment model in which the positions of the end points and joints were estimated through predefined measured lengths and IMU-derived segment orientations. The segment lengths were measured manually

2.4. Discussion

using a conventional measuring tape. Moreover, calibration limitations, such as a mismatch between the neutral pose practiced by the subject and the pose that the computational model is assuming, can cause errors. This limitation may explain the higher errors found in the frontal plane GRM in our solution, since it affects the estimates of the lever arms. Optical motion capture or photogrammetry could be used as an initial input to improve such offsets. Nevertheless, this implementation aimed to propose and investigate a completely laboratory-independent system.

Soft tissue artifacts are another common problem causing inaccuracies in both IMC and OMC kinematics [116, 23]. The IMUs measure acceleration and angular velocity on the soft tissue, which moves relative to the bone [24]. This motion may have negative influence on our final estimates, especially in the case of fast walking. On the other hand, the fact that eight of the participants had a normal BMI ($18.5 \leq \text{BMI} \leq 24.9$), three were overweight ($25 \leq \text{BMI} \leq 29.9$) and no obese participants were included in the experiment probably limits the soft tissue effects in our study.

Finally, the IMC is susceptible to magnetic interferences. Particularly, it has been shown that the magnetic field varies considerably inside gait laboratories [32]. This factor may have influenced the sensor orientations used to derive the segment kinematics in Xsens MVN Studio software. Any input errors in the segment orientations could lead to accumulated errors in the estimated joint positions and, therefore, in the distance vectors between the center of mass and the joint of each segment. The latter are used in important stages of the proposed method, firstly in the translation of each segment's linear kinematics from its origin to the center of mass (Equation (2.3)) and secondly in Euler's equation of motion (Equation (2.2)). A magnetometer-free approach to inertial motion capture could be adopted to reduce these sources of error [117].

2.4.3 Future Work

In our experiment, we only included male subjects without any musculoskeletal or neuromuscular disorders. However, we did not evaluate the applicability to patients with motor-related clinical conditions. Several challenges could be encountered in the clinical application of the system. For example, in the case of knee osteoarthritis, the increased static knee misalignment of the patients might lead to difficulty achieving a proper neutral pose to calibrate the IMC system [118]. Moreover, obesity, which is quite common in patients with musculoskeletal problems, could impose practical barriers in the optical and inertial motion capture.

The smooth transition assumption we incorporated can only be applied to gait movements. On top of this, the distribution algorithm allows the real-time estimation only during the single support phase. During double support, the algorithm needs information over the duration of this phase to estimate the kinetics. A real-time solution to distribute the forces could be explored in the future.

In this study, we assume that the GRF&Ms are the only significant external forces applied to the human body. This assumption could be valid for activities such as walking; however, in a wider spectrum of daily life activities, secondary external loads are introduced. Such activities include walking using a cane or stair climbing using handrails. In such cases, direct measurement or modeling of the additional forces and moments would be required. Future work could examine the types and biomechanical importance of forces and moments generated in free-living

2. Estimation of Ground Reaction Forces and Moments

environments, when performing daily life activities.

Finally, our proposed method is dependent on a full-body motion capture suit, which requires 17 IMUs. In future studies, minimizing the number of sensing modules [119] to make the system more practical for clinical and free-living applications could be investigated. Moreover, our system could be exploited in driving near real-time biofeedback, the popularity of which recently increased in gait training interventions [120].

2.5 Conclusions

In this paper, we have demonstrated that estimation of 3D GRF&Ms during walking using only kinematic information from inertial motion capture is achievable. Overall, strong and excellent correlations were found for all six estimated components compared to force plate measurements. The results were comparable to the ones reported by studies using OMC input.

The proposed system has high potential in monitoring critical biomechanical parameters in free-living conditions, outside the laboratory. Future work should validate and adapt the system to clinical and daily life applications.

2.A Appendix

2.A Appendix: Retroreflective Marker Protocol

Figure 2.8: A subject in the wearable instrumentation, indicating the placement of the 53 retroreflective markers on the human body segments.

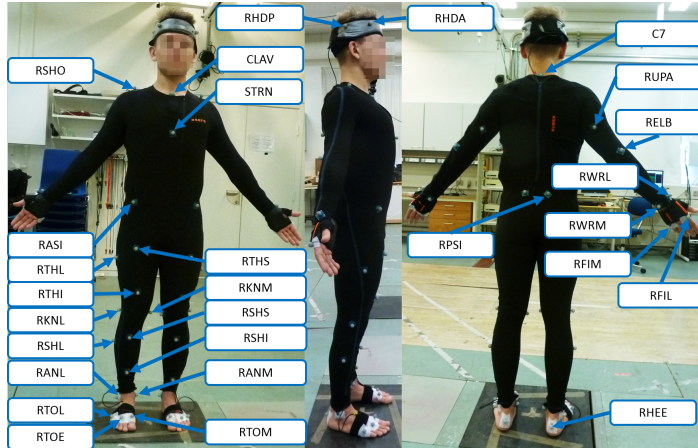


Table 2.12: Marker protocol, indicating marker labels and locations on the body.

| | Label | Placement |
|-------|-------|--------------------------------|
| Right | Left | Center |
| RHDA | LHDA | Head Anterior |
| RHDP | LHDP | Head Posterior |
| RSHO | LSHO | Acromio-clavicular Joint |
| RUPA | LUPA | Triceps Brachii |
| RELB | LELB | Elbow Lateral Epicondyle |
| RWRL | LWRL | Radial Styloid |
| RWRM | LWRM | Ulnar Styloid |
| RFIL | LFIL | Second Metacarpal Head |
| RFIM | LFIM | Fifth Metacarpal Head |
| RASI | LASI | Anterior Superior Iliac Spine |
| RPSI | LPSI | Posterior Superior Iliac Spine |
| RTHS | LTHS | Thigh Superior |
| RTHI | LTHI | Thigh Inferior |
| RTHL | LTHL | Thigh Lateral |
| RKNL | LKNL | Knee Lateral Epicondyle |
| RKNM | LKNM | Knee Medial Epicondyle |
| RSHS | LSHS | Shank Superior |
| RSHI | LSHI | Shank Inferior |
| RSHL | LSHL | Shank Lateral |
| RANL | LANL | Lateral Malleolus |
| RANM | LANM | Medial Malleolus |
| RTOM | LTOM | First Metatarsal |
| RTOE | LTOE | Third Metatarsal |
| RTOL | LTOL | Fifth Metatarsal |
| RHEE | LHEE | Calcaneus |
| C7 | | Seventh Cervical Vertebrae |
| CLAV | | Jugular Notch |
| STRN | | Xiphoid Process of the Sternum |

2. Estimation of Ground Reaction Forces and Moments

Chapter 3

Assessment of knee adduction and flexion moments using inertial sensors in knee unloading gait modifications

Submitted:

Karatsidis, A., Schepers, H. M., Bellusci, G., de Zee, M., Andersen, M. S., & Veltink, P. H. Assessment of knee adduction and flexion moments using inertial sensors in knee unloading gait modifications

3. Assessment of Knee Adduction and Flexion Moments

Abstract

The knee adduction moment (KAM) and knee flexion moment (KFM) have been related to medial compartment tibiofemoral contact forces, which play an important role in medial knee osteoarthritis. To date, conventional systems, such as optical motion capture (OMC) and force plates (FP), limit the application of biomechanical assessments to gait laboratories. These complex assessment systems impede the translation of these techniques towards clinical practice and daily life. Alternatively, inertial measurement units can be used to derive human body kinematics fairly accurately, while being applied in any environment. Kinematic input from a commercially available inertial motion capture (IMC) system was utilized to estimate the ground reaction forces and moments (GRF&M) using full-body inverse dynamics and a gait-specific external load distribution function. Subsequently, the net knee joint moments were calculated using the estimated GRF&M and the kinematics derived from the IMC system. Ten healthy subjects walked overground at a comfortable speed, as well as in four modified gait patterns suggested to reduce knee joint loading namely toe-in (TIW), toe-out (TOW), lateral trunk lean (LTLW), medialized knees (MKW). We evaluated the proposed method against knee joint moment estimates from a conventional setup including OMC and FP measurements. For the various gait patterns, the proposed ambulatory system presented moderate to strong Pearson correlation coefficients across the whole stance phase for the KAM ($\rho=0.64$ to 0.72) and strong ($\rho= 0.80$ to 0.84) for the KFM. An ANOVA test with Tukey's post hoc analysis on the discrete point value analysis of the first and second peak, and impulse values of KAM and KFM differences between conditions showed similar significance levels for most examined points. Paired t-test showed significant differences ($p < 0.05$) between the proposed and reference method for all gait conditions except for first peak and impulse KAM during MKW, first peak KFM during NW, second peak KFM during NW, TIW, and MKW. Similar analysis for the moment change from baseline NW showed no significant differences only in first peak KAM during TOW, second peak KAM and KFM during TOW and LTLW, impulse KAM during TIW and TOW, and first peak and impulse KFM during MKW. Peak KAM and KFM changes from baseline induced by gait modification were tracked with mean differences less than 0.2 % and 0.55 % of body weight times body height (BW*BH) between the proposed and reference approach in TIW, TOW, and LTLW patterns. A method to estimate net knee joint moments from human body kinematics assessed from inertial measurement units was presented. The evaluation showed that the system is performs better in estimating the change in KAM or KFM induced by a gait modification, rather than the absolute sizes of these moments. The proposed setup enables ambulatory applications, and could in the future be the basis for routine clinical assessments, where OMC and FP systems are complex and expensive to use.

Keywords: Knee adduction moment; Knee flexion moment; Inertial sensors; Gait modifications; Knee osteoarthritis; Ground reaction force

3.1. Introduction

3.1 Introduction

Gait modifications have been proposed as a non-invasive treatment for medial knee osteoarthritis (KOA) [84, 121, 122, 123, 124]. Typically, such modifications target the reduction of tibiofemoral joint loading, which has been associated with initiation and progression of the disease [125, 126, 127]. In particular, the knee adduction moment (KAM) and knee flexion moment (KFM) have been linked to the medial tibiofemoral contact forces [77, 78].

Mechanical torque is mathematically defined as the cross product between a distance vector and a force vector. Driven by this knowledge, gait modifications in KOA aim at manipulating either of these components, in such a way that the resultant knee moment decreases. For example, a slower walking speed can decrease the magnitude of the ground reaction force [128], whereas walking with a lateral trunk sway pattern can decrease the moment lever arm by shifting the GRF vector closer to the knee joint [88, 129, 130]. Similar decrease of the lever arm can be achieved either by altering the point of force application (center of pressure), through a more toe-in or toe-out gait pattern [83, 131, 81, 82, 132], or through a medial knee thrust gait pattern [80, 133, 134].

Research suggested that patient-specific treatments should be developed for optimal effect of the gait modifications [135, 136, 137, 138]. This tailored approach demands for accurate biomechanical analysis tools to assess the related clinical measures [139, 140]. Conventionally, gait laboratories are used, which make use of optical motion capture [13] and force plate systems [37]. However, these systems are limited by a small capture volume and are difficult to apply in situations of daily life or in large-scale clinical practice [141].

Recently, many studies attempted to assess lower limb joint moments with the use of ambulatory systems [44]. In these systems, the human body kinematics are typically tracked by inertial measurement units [100], whereas the external forces are obtained via pressure or force sensors, attached either above or beneath the sole of a shoe. Pressure insoles typically provide a foot pressure distribution, from which the complete ground reaction forces and moments (GRF&M) can be reconstructed [50, 51, 52, 53, 54, 55]. Despite their compact size and unobtrusive use, they suffer from repeatability and durability limitations [56]. As an alternative, instrumented force shoes, where force sensors are placed beneath the sole of a shoe to directly measure the GRF&M [45, 46]. In addition, research utilized such devices to ambulatorily assess ankle loads [47, 142], and knee loads in patients with KOA [143, 95], showcasing great potential for applications outside the lab. However, the height and weight of the force sensors, may influence the gait pattern and does not allow for applications in daily life or clinical practice [48, 49].

An alternative approach where the external forces and moments are estimated from human motion has been suggested in several studies [97, 39, 41, 40, 42, 43, 144]. The kinematics of the whole-body are used through the Newton-Euler equations of motion, to estimate the sum of forces and moments. These external loads can subsequently be distributed across the segments with external contacts, using methods based on empirical data about the gait cycle [39, 144], training database [41, 40], or dynamic contact models [42, 43]. Some of these studies reported performance of net knee moments, either on all three planes [39, 40], or only on the sagittal

3. Assessment of Knee Adduction and Flexion Moments

plane [42, 43], but none of them investigated conditions of gait variability or modifications. In addition, recent work of the authors towards ambulatory application of such motion-based techniques, demonstrated that the use of inertial sensor input performs similarly to optical motion capture in estimating the GRF&M [144]. At the same time, inertial motion capture input allows for use of the system outside the laboratory setting [24].

In this study, we extend this motion-driven method to estimate the KAM and KFM given only inertial motion capture input and evaluate it in ten healthy adults for various gait modifications that have been suggested to unload the knee joint loading. We initially construct the reference knee moment values, based on a bottom-up inverse dynamics approach driven by conventional camera-based motion capture and force plate systems. Subsequently, we compare the estimates of the proposed method with the reference values over the entire stance phase, as well as over the impulse, early stance peak and late stance peak values. Our hypothesis is that even if the absolute knee moment estimates differ from the reference, the relative change with respect to the subject's baseline when applying a gait modification, can be accurately assessed via the proposed approach.

3

3.2 Materials and methods

3.2.1 Subjects

Ten healthy male volunteers (age: 31.5 ± 7.3 years; height: 1.81 ± 0.06 m; weight: 77.16 ± 9.71 kg; body mass index (BMI): 23.60 ± 2.54 kg/m²) were recruited from the staff and students of Aalborg University. The data collection was performed at the Human Performance Laboratory, Aalborg University, Aalborg 9220, Denmark between 8th December 2015 and 21st April 2016. Prior to their participation, the subjects provided written informed consent, and the ethical guidelines of The North Denmark Region Committee on Health Research Ethics were followed.

3.2.2 Instrumentation

The inertial motion capture suit, Xsens MVN Link, was used in its full-body configuration, containing 17 MTx inertial measurement units. A lycra suit was utilized to mount the IMUs on the predefined body locations. Xsens MVN Studio 4.3.1 was used to acquire the inertial motion capture data at 240 Hz[145].

Qualisys Track Manager was used to control an eight-infrared-camera motion capture system sampling at 240 Hz (Oqus 300 series, Qualisys AB, Gothenburg, Sweden [146, 106]) and three overground force plates, sampling at 2400 Hz (AMTI OR6-7-1000, Advanced Mechanical 106 Technology, Inc., Watertown, MA, USA [147]). The marker protocol, contained 53 retroreflective markers is illustrated in the Appendix of [144].

Xsens MVN Sync Station was used to synchronously record in both MVN Studio and Qualisys Track Manager.

3.2. Materials and methods

3.2.3 Experimental procedures

Initially the required body measurements for the setup of Xsens MVN Studio were taken, using conventional tape measure [148]. Next, the subjects wore the tight-fitting Lycra suit, on which the Xsens MTx motion trackers were placed on the designated spots [149]. Subsequently, the reflective markers were placed on the body on top of the suit.

Following a few-minute-long acclimatization period, brief verbal instructions were given to the subjects regarding the movement pattern they should perform:

- Comfortable walking at self-selected speed (NW)
- Toe-in: walking with the toes pointing inwards (TIW)
- Toe-out: walking with the toes pointing outwards (TOW)
- Ipsilateral trunk lean: walking by moving the trunk to the side of the leg that hits the ground (LTLW)
- Medialized knees: walking by keeping the knees close to each other (MKW)

At least five trials were collected per gait pattern, with at least two strikes with the entire foot on the force plate, assessed via visual inspection during the data collection.

3.2.4 Computational procedures

The kinematic data recorded by Xsens MVN Studio were post-processed with the latest available version, Xsens MVN Analyze 2018.0. External GRF&M for right and left foot were estimated based on a previously proposed method utilizing solely inertial motion capture input and whole-body inverse dynamics [144]. In particular, a biomechanical model with 16 segments and 48 degrees-of-freedom was constructed, after adjusting the default 23-segment model of Xsens MVN Analyze by constraining the motion of the trunk joints (L5-L3, L3-T12, T12-T8, T8-Right Shoulder, T8-Left Shoulder, T8-Neck) and by neglecting the toe segments. Specifically, the model contained the following segments: head, upper trunk, middle trunk, and lower trunk, and a pair of upper arms, forearms, hands, thighs, shanks, and feet. Given the measured full-body mass and segment lengths, the individual segment masses, mass centers, and radii of gyration were computed from the anthropometric tables of De Leva [107].

A zero lag fourth order Butterworth low pass filter with a cut-off frequency of 6 Hz was applied to the kinematic data, based on sensitivity analysis performed in previous work [144]. Subsequently, the linear accelerations expressed by default in the proximal joint of each segment were translated to the center of mass of each segment.

The sum of external forces and moments was derived via the Newton-Euler equations of motion. Given the prior knowledge that the movement is gait, the only segments which can generate external non-gravitational forces are the ones in contact with the ground, namely the right and left foot. Therefore, to decompose the sum of external forces and moments between right and left feet, we applied a smooth

3. Assessment of Knee Adduction and Flexion Moments

transition assumption function [39], as adjusted in [144]. This assumption is based on gait events and defines the force on the trailing leg as a function of time with respect to the duration of the double stance phase and the total external force at the beginning of the double stance phase.

The system of equations is solved for any time t as follows:

$$\mathbf{F}_{sum}(t) = \sum_{i=1}^N m_i(\mathbf{a}_i(t) - \mathbf{g}) \quad (3.1a)$$

$$\mathbf{F}_{G,tr}(t) = \mathbf{f}_{F,STA}(t, t_{HS,ld}, t_{TO,tr}) \circ \mathbf{F}_{sum}(t_{HS,ld}) \quad (3.1b)$$

$$\mathbf{F}_{G,ld}(t) = \mathbf{F}_{sum}(t) - \mathbf{F}_{G,tr}(t) \quad (3.1c)$$

$$\mathbf{M}_{sum}(t) = \sum_{i=1}^N [\mathbf{J}_i(t)\dot{\boldsymbol{\omega}}_i(t) + \boldsymbol{\omega}_i(t) \times (\mathbf{J}_i(t)\boldsymbol{\omega}_i(t))] - \sum_{i=1}^N \sum_{j=1}^{K_i} (\mathbf{r}_{ij}(t) \times \mathbf{F}_{ij}(t)) \quad (3.2a)$$

$$\mathbf{M}_{G,tr}(t) = \mathbf{f}_{M,STA}(t, t_{HS,ld}, t_{TO,tr}) \circ \mathbf{M}_{sum}(t_{HS,ld}) \quad (3.2b)$$

$$\mathbf{M}_{G,ld}(t) = \mathbf{M}_{sum}(t) - \mathbf{M}_{G,tr}(t) \quad (3.2c)$$

where \mathbf{F} and \mathbf{M} denote a force and moment, respectively. Mass and moment of inertia are denoted with m and \mathbf{J} , respectively. N expresses the number of segments and K_i is the number of joints or external contact points on the i th segment. Variables \mathbf{a} , $\boldsymbol{\omega}$, $\dot{\boldsymbol{\omega}}$, and \mathbf{r} denote acceleration, angular velocity, angular acceleration and position vector, respectively. Constant gravity vector is indicated with \mathbf{g} . Index G indicates a ground related variable. $\mathbf{f}_{F,STA}$ and $\mathbf{f}_{M,STA}$ denote the smooth transition assumption functions corresponding to force and moment. Heel strike and toe-off events are indicated with HS and TO , respectively, while tr and ld indicate a variable of trailing and leading foot in the gait cycle.

Given the ground reaction forces and moment per foot, the net moments about all joints can be assessed, utilizing a conventional bottom-up inverse dynamic approach [150, 37]. In particular, to assess the net knee moment, we solve the free-body-diagram equations for the foot and shank segments:

$$\mathbf{F}_{ankle}^{foot}(t) = m_{foot}(\mathbf{a}_{foot}(t) - \mathbf{g}) - \mathbf{F}_G^{foot}(t) \quad (3.3a)$$

$$\mathbf{F}_{knee}^{shank}(t) = m_{shank}(\mathbf{a}_{shank}(t) - \mathbf{g}) - \mathbf{F}_{ankle}^{shank}(t) \quad (3.3b)$$

where

$$\mathbf{F}_G^{foot}(t) = -\mathbf{F}_G^{ground}(t) \quad (3.3c)$$

and

$$\mathbf{F}_{ankle}^{shank}(t) = -\mathbf{F}_{ankle}^{foot}(t) \quad (3.3d)$$

$$\begin{aligned} \mathbf{M}_{ankle}^{foot}(t) &= \mathbf{J}_{foot}(t)\dot{\boldsymbol{\omega}}_{foot}(t) + \boldsymbol{\omega}_{foot}(t) \times (\mathbf{J}_{foot}(t)\boldsymbol{\omega}_{foot}(t)) \\ &\quad - (\mathbf{r}_{ankle}^{foot}(t) \times \mathbf{F}_{ankle}^{foot}(t)) - (\mathbf{r}_G^{foot}(t) \times \mathbf{F}_G^{foot}(t)) - \mathbf{M}_G^{foot}(t) \end{aligned} \quad (3.3e)$$

3.3. Results

$$\begin{aligned} \mathbf{M}_{knee}^{shank}(t) &= \mathbf{J}_{shank}(t)\dot{\boldsymbol{\omega}}_{shank}(t) + \boldsymbol{\omega}_{shank}(t) \times (\mathbf{J}_{shank}(t)\boldsymbol{\omega}_{shank}(t)) \\ &\quad - (\mathbf{r}_{knee}^{shank}(t) \times \mathbf{F}_{knee}^{shank}(t)) - (\mathbf{r}_{ankle}^{shank}(t) \times \mathbf{F}_{ankle}^{shank}(t)) - \mathbf{M}_{ankle}^{shank}(t) \end{aligned} \quad (3.3f)$$

where

$$\mathbf{M}_G^{foot}(t) = -\mathbf{M}_G^{ground}(t) \quad (3.3g)$$

and

$$\mathbf{M}_{ankle}^{shank}(t) = -\mathbf{M}_{ankle}^{foot}(t) \quad (3.3h)$$

For convenience, the knee moments are projected on the plane of walking progression, due to the lack of direct measurement of anatomical landmarks in the inertial approach.

3.2.5 Data analysis

The reference knee moments were computed based on force plate data and marker trajectories, which were first low-pass filtered at 15 Hz and 12 Hz, respectively, using a fourth order zero-lag Butterworth filter [42]. The marker trajectories were used to construct a stick figure model of the lower body (pelvis, thighs, shanks, feet) with equal degrees of freedom to the model used in the inertial motion capture-based method, was constructed in AnyBody Modelling System [151]. Scaling was performed as in Lund *et al.* [152] and over-determinate kinematics were solved using the method of Andersen *et al.* [153].

To evaluate the performance of our KAM and KFM estimates, we evaluate their values using Pearson correlation coefficient (ρ), absolute and relative root mean square difference (RMSD and rRMSD, respectively) [154, 39], and magnitude and phase differences [112].

Commonly used variables in studies investigating clinical biomechanics of KOA are the first and second peak of the KAM (pKAM1 and pKAM2, respectively), the peak extension (pKEM) and peak flexion moment (pKFM). In addition, the impulse of the KAM and KFM are calculated (iKAM and iKFM, respectively). We compared the absolute values of these variables to the reference using the mean root mean square difference. In addition, we evaluate the accuracy of estimating the change from each subject's baseline by tracking the difference in the aforementioned peak values across the various gait patterns. To detect changes from the gait modifications with respect to the baseline walking, we used an analysis of variance (ANOVA) with Tukey's post-hoc analysis for both estimation methods (IMC and OMC + FP). We also performed a paired t-test between IMC and OMC+FP models for each gait condition to determine statistical differences between the estimation methods.

3.3 Results

The curves for the KAM and KFM averaged across all stance phases for the five different walking conditions are shown in Figure 3.1 and accuracy analysis in Table 3.1. Pearson correlation coefficients, individually estimated per walking condition, were found moderate to strong for KAM (range: 0.64-0.72), and strong for KFM (range: 0.80-0.84). Average absolute RMSD across whole stance phase for all 10 subjects ranged from 0.74 ± 0.25 for NW to 0.81 ± 0.35 for MKW for the KAM and

3. Assessment of Knee Adduction and Flexion Moments

from 1.12 ± 0.43 in NW to 1.44 ± 0.59 in MKW for the KFM. Similarly, rRMSD values were found between 23.55 ± 8.52 in TOW and 26.88 ± 9.53 in NW for the KAM and between 19.57 ± 7.67 in NW and 24.19 ± 10.19 in TOW for the KFM. Magnitude differences showed underestimation of the KAM, for all walking conditions except for MKW, and overestimation of KFM values for all walking conditions. hlPhase differences of the KAM ranged from 15.83 ± 8.67 in NW to 23.51 ± 16.00 in MKW and 13.31 ± 6.67 in MKW up to 23.33 ± 1.85 in TOW for the KFM.

Multivariate general linear model analysis across all conditions (five different gait patterns) showed significant differences for both KAM and KFM peak and impulse values in both ambulatory and laboratory approaches ($p < 0.001$). Tukey's post-hoc analysis across various walking conditions is shown in Table 3.2. In most cases, significant differences across walking conditions matched in both ambulatory and reference methods, even though p-values differed between systems.

In Table 3.3 and Figure 3.2, we compare the early and late stance peaks, and impulse values of KFM and KAM. This metric showed a similar underestimation behavior for the first and second peak of KAM in all conditions except MKW. KAM impulse values were consistently underestimated. In contrast, KFM peaks and impulse values were always overestimated, with only exception of the first KFM peak in normal walking. The paired t-test between discrete point values between the two assessment methods showed no statistically significant differences in iKAM in MKW, and pKAM1, and pKEM with p-values 0.136, 0.078, and 0.571, respectively. All other absolute discrete point values were significantly different.

Similar analysis was performed on KAM and KFM during the gait modifications in the change from baseline normal walking pattern (Table 3.4 and Figure 3.3). In TOW, no statistically significant differences were found in early stance KAM change ($p=0.066$), and pKAM2 and pKEM change ($p=0.926$ and $p=0.378$, respectively). Late stance pKAM2 and pKEM in LTLW condition followed a similar fashion with $p=0.202$ and 0.153 , respectively. Change in iKAM was estimated with no significant differences in TIW and TOW with p-values 0.836 and 0.549, respectively. In addition, change in pKFM in MKW condition was estimated with no statistically significant differences ($p=0.167$). The ambulatory solution, consistently overestimated the early stance peak changes from baseline in both KAM and KFM, whereas late stance peaks showed a mixed behavior. KAM impulse change was underestimated in all conditions apart from MKW, and KFM impulse change was consistently overestimated.

3.4 Discussion

In this paper we presented and evaluated an ambulatory technique to estimate knee joint moments commonly used to quantify knee joint loading, using only inertial sensor input. We validate the performance of our method in tracking absolute values and changes in knee joint moments as a result of modified gait mechanics, against a conventional laboratory approach with optical motion capture and force plate input.

3.4. Discussion

Figure 3.1: Knee adduction and flexion moment curves for normal, toe-in, toe-out, lateral trunk lean, and medialized knees walking patterns normalized to each subject's body weight times body height. Curves averaged across all subjects. Mean and standard deviation of the ambulatory estimates are indicated by dashed black thin grey line and the shaded area, and laboratory estimates indicated by the thick and thin black solid lines.

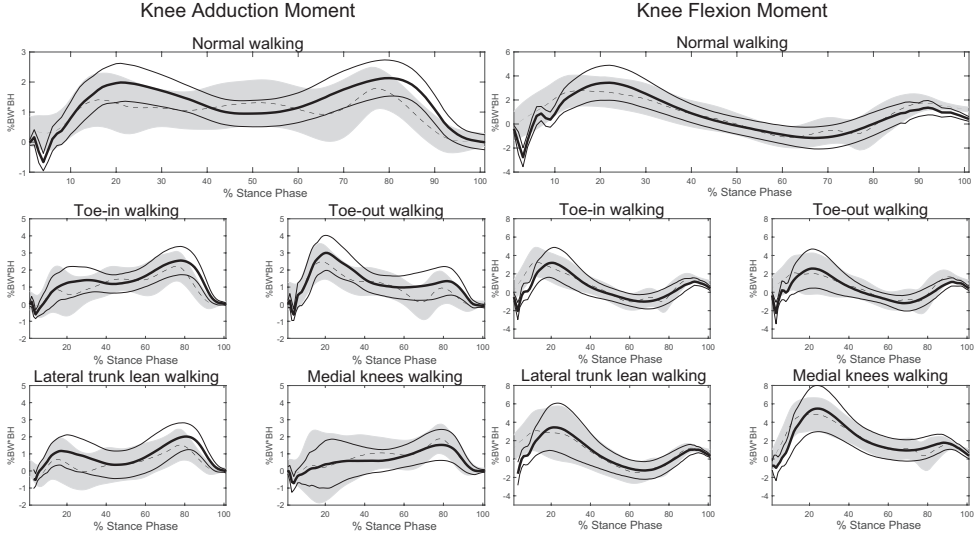


Table 3.1: Accuracy analysis for knee adduction and flexion moments averaged over all stance phases using Pearson correlation coefficient (ρ), root mean square error absolute and relative root mean square differences (RMSD in % body weight time body height and rRMSD in %, respectively) [154, 39], Sprague and Geers metrics for magnitude and phase differences (%) [112]. NW: normal walking, TIW: toe-in walking, TOW: toe-out walking, LTLW: lateral trunk lean walking, MKW: medialized knees walking.

| Knee Adduction Moment | | | | | | |
|-----------------------|--------|-----------------|-------------------|--------------------|-------------------|--|
| | ρ | RMSD | rRMSD | MD | PD | |
| NW | 0.64 | 0.74 ± 0.25 | 26.88 ± 9.54 | -36.50 ± 63.15 | 15.83 ± 8.67 | |
| TIW | 0.72 | 0.76 ± 0.25 | 24.38 ± 9.26 | -23.24 ± 43.19 | 16.50 ± 8.49 | |
| TOW | 0.68 | 0.80 ± 0.31 | 23.55 ± 8.52 | -31.24 ± 43.77 | 16.77 ± 8.03 | |
| LTLW | 0.69 | 0.80 ± 0.35 | 26.78 ± 10.96 | -21.25 ± 46.64 | 22.21 ± 11.48 | |
| MKW | 0.67 | 0.81 ± 0.34 | 25.57 ± 15.29 | 7.70 ± 53.77 | 23.51 ± 16.00 | |
| Knee Flexion Moment | | | | | | |
| | ρ | RMSD | rRMSD | MD | PD | |
| NW | 0.84 | 1.12 ± 0.43 | 19.57 ± 7.67 | 0.84 ± 22.29 | 19.84 ± 8.14 | |
| TIW | 0.80 | 1.22 ± 0.45 | 22.92 ± 10.19 | 10.15 ± 20.80 | 22.77 ± 11.45 | |
| TOW | 0.80 | 1.27 ± 0.45 | 24.19 ± 11.34 | 10.64 ± 24.89 | 23.33 ± 11.85 | |
| LTLW | 0.83 | 1.32 ± 0.45 | 22.75 ± 10.10 | 7.70 ± 22.76 | 20.51 ± 11.25 | |
| MKW | 0.84 | 1.44 ± 0.59 | 21.93 ± 9.83 | 6.27 ± 43.21 | 13.31 ± 6.67 | |

Interpretation of results

One of the main findings of this study is that the proposed method performed better in assessing the KAM and KFM change from a baseline value, rather than the abso-

3. Assessment of Knee Adduction and Flexion Moments

Table 3.2: For the two assessment methods, Tukey's post-hoc analysis performed on the discrete point values (curve peaks and impulses) of knee flexion and adduction moments per walking condition. Significance differences between conditions are observed for $p < 0.05$ colored in green, $0.05 \leq p < 0.50$ in yellow, and $p \geq 0.50$ in red.. Abbreviations: NW = normal walking, TIW = toe-in walking, TOW = toe-out walking, LTLW = lateral trunk lean walking, MKW = medialized knees walking, IMC = inertial motion capture input.

| | | Inertial Motion Capture | | | | Optical Motion Capture and Force Plate | | | |
|----------------|------|-------------------------|--------|---------------------|--------|--|--------|---------------------|--------|
| | | Knee Adduction Moment | | Knee Flexion Moment | | Knee Adduction Moment | | Knee Flexion Moment | |
| | | TIW | TOW | LTLW | MKW | TIW | TOW | LTLW | MKW |
| First Peak | NW | <0.001 | <0.001 | <0.001 | <0.001 | NW | <0.001 | <0.001 | <0.001 |
| | TIW | <0.001 | 0.468 | 0.954 | <0.001 | TIW | <0.001 | 0.451 | <0.001 |
| | TOW | <0.001 | <0.001 | <0.001 | <0.001 | TOW | <0.001 | <0.001 | <0.001 |
| | LTLW | <0.001 | <0.001 | <0.001 | 0.903 | LTLW | <0.001 | <0.001 | <0.001 |
| Second Peak | NW | 0.003 | <0.001 | 0.428 | 0.999 | NW | <0.001 | <0.001 | <0.001 |
| | TIW | <0.001 | <0.001 | 0.002 | <0.001 | TIW | <0.001 | <0.001 | <0.001 |
| | TOW | <0.001 | <0.001 | <0.001 | <0.001 | TOW | <0.001 | 0.038 | <0.001 |
| | LTLW | <0.001 | <0.001 | <0.001 | 0.664 | LTLW | <0.001 | <0.001 | <0.001 |
| Impulse | TIW | 0.999 | 0.988 | <0.001 | <0.001 | TIW | 0.984 | 0.985 | 0.001 |
| | TOW | 1.000 | <0.001 | <0.001 | <0.001 | TOW | 1.000 | <0.001 | <0.001 |
| | LTLW | <0.001 | 0.001 | <0.001 | 0.824 | LTLW | <0.001 | <0.001 | <0.001 |
| | | | | | | | | | |
| | | Knee Flexion Moment | | | | Knee Flexion Moment | | | |
| | | TIW | TOW | LTLW | MKW | TIW | TOW | LTLW | MKW |
| Peak Flexion | NW | 0.211 | 1.000 | <0.001 | <0.001 | NW | 0.978 | 0.207 | <0.001 |
| | TIW | 0.172 | <0.001 | 0.011 | <0.001 | TIW | 0.544 | 0.084 | <0.001 |
| | TOW | <0.001 | <0.001 | <0.001 | <0.001 | TOW | <0.001 | <0.001 | <0.001 |
| | LTLW | <0.001 | <0.001 | <0.001 | <0.001 | LTLW | <0.001 | <0.001 | <0.001 |
| Peak Extension | TIW | 0.629 | 0.709 | 0.668 | <0.001 | NW | 0.048 | 0.990 | 0.974 |
| | TOW | 1.000 | 1.000 | 1.000 | <0.001 | TIW | 0.181 | 0.236 | <0.001 |
| | LTLW | 1.000 | <0.001 | <0.001 | <0.001 | LTLW | 1.000 | <0.001 | <0.001 |
| | | | | | | | | | |
| Impulse | TIW | 0.820 | 0.933 | 0.002 | <0.001 | NW | 0.991 | 0.583 | 0.610 |
| | TOW | 0.999 | 0.078 | <0.001 | <0.001 | TIW | 0.858 | 0.351 | <0.001 |
| | LTLW | 0.042 | <0.001 | <0.001 | <0.001 | LTLW | 0.041 | <0.001 | <0.001 |
| | | | | | | | | | |

3.4. Discussion

Table 3.3: Knee adduction and flexion moments. Mean and standard deviation of the difference between ambulatory and laboratory system and p-values extracted from a paired t-test on early stance peak, late stance peak and impulse. Peak values are normalized to body weight (BW) times body height (BH) and impulses to BW*BH*s.

| Knee Adduction Moment | | | | | | |
|-----------------------|------------------|---------|------------------|---------|------------------|---------|
| | First Peak | | Second Peak | | Impulse | |
| | mean \pm std | p value | mean \pm std | p value | mean \pm std | p value |
| NW | -0.54 \pm 0.74 | <0.001* | -0.13 \pm 0.70 | 0.016* | -0.18 \pm 0.25 | <0.001* |
| TIW | -0.44 \pm 0.61 | <0.001* | -0.15 \pm 0.70 | 0.013* | -0.21 \pm 0.25 | <0.001* |
| TOW | -0.53 \pm 0.92 | <0.001* | -0.26 \pm 0.68 | <0.001* | -0.22 \pm 0.26 | <0.001* |
| LTLW | -0.47 \pm 0.69 | <0.001* | -0.25 \pm 0.81 | <0.001* | -0.31 \pm 0.32 | <0.001* |
| MKW | 0.13 \pm 0.84 | 0.078 | 0.30 \pm 0.98 | <0.001* | -0.05 \pm 0.38 | 0.136 |

| Knee Flexion Moment | | | | | | |
|---------------------|-----------------|---------|------------------|---------|-----------------|---------|
| | Peak Flexion | | Peak Extension | | Impulse | |
| | mean \pm std | p value | mean \pm std | p value | mean \pm std | p value |
| NW | 0.00 \pm 1.20 | 0.985 | 0.14 \pm 1.23 | 0.157 | 0.23 \pm 0.49 | <0.001* |
| TIW | 0.61 \pm 1.20 | <0.001* | 0.03 \pm 1.18 | 0.767 | 0.35 \pm 0.50 | <0.001* |
| TOW | 0.46 \pm 1.18 | <0.001* | 0.26 \pm 1.30 | 0.022* | 0.41 \pm 0.56 | <0.001* |
| LTLW | 0.73 \pm 1.37 | <0.001* | 0.23 \pm 1.06 | 0.010* | 0.41 \pm 0.65 | <0.001* |
| MKW | 0.33 \pm 1.85 | 0.049* | -0.06 \pm 1.27 | 0.571 | 0.32 \pm 0.71 | <0.001* |

Table 3.4: Change from baseline in knee adduction and flexion moments. Mean and standard deviation of the difference between ambulatory and laboratory system and p-values extracted from a paired t-test on early stance peak, late stance peak and impulse. Peak values are normalized to body weight (BW) times body height (BH) and impulses to BW*BH*s.

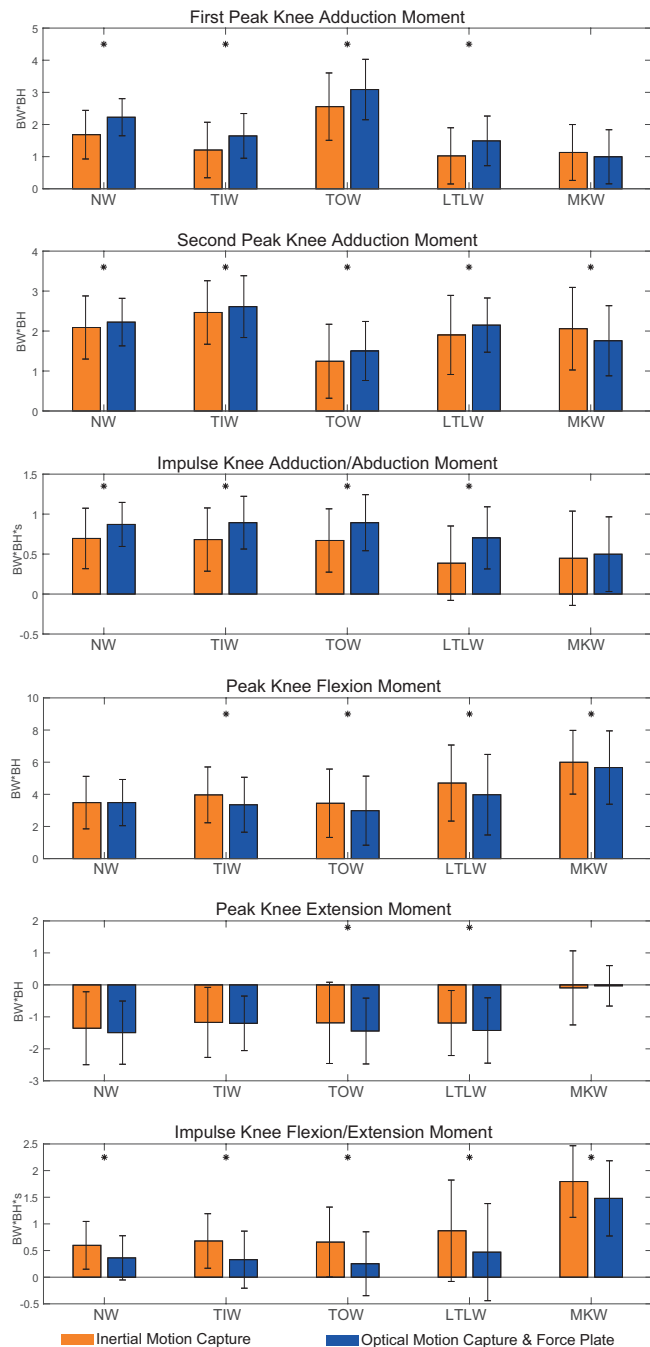
| Knee Adduction Moment | | | | | | |
|-----------------------|-----------------|---------|-----------------|---------|------------------|---------|
| | First Peak | | Second Peak | | Impulse | |
| | mean \pm std | p value | mean \pm std | p value | mean \pm std | p value |
| TIW | 0.17 \pm 0.49 | <0.001* | 0.09 \pm 0.41 | 0.014* | 0.00 \pm 0.13 | 0.836 |
| TOW | 0.11 \pm 0.68 | 0.066 | 0.00 \pm 0.46 | 0.926 | -0.01 \pm 0.14 | 0.549 |
| LTLW | 0.18 \pm 0.70 | 0.002* | 0.05 \pm 0.45 | 0.202 | -0.09 \pm 0.21 | <0.001* |
| MKW | 0.81 \pm 0.85 | <0.001* | 0.64 \pm 0.89 | <0.001* | 0.18 \pm 0.28 | <0.001* |

| Knee Flexion Moment | | | | | | |
|---------------------|-----------------|---------|------------------|---------|-----------------|---------|
| | Peak Flexion | | Peak Extension | | Impulse | |
| | mean \pm std | p value | mean \pm std | p value | mean \pm std | p value |
| TIW | 0.45 \pm 0.84 | <0.001* | -0.17 \pm 0.70 | 0.004* | 0.05 \pm 0.26 | 0.012* |
| TOW | 0.33 \pm 0.85 | <0.001* | 0.05 \pm 0.67 | 0.378 | 0.12 \pm 0.27 | <0.001* |
| LTLW | 0.55 \pm 1.09 | <0.001* | -0.08 \pm 0.64 | 0.153 | 0.10 \pm 0.33 | <0.001* |
| MKW | 0.16 \pm 1.29 | 0.167 | -0.29 \pm 0.90 | <0.001* | 0.03 \pm 0.36 | 0.320 |

lute value in, common gait modifications suggested for patients with medial KOA. KAM and KFM change was estimated with mean differences on the first and second peak ranging from 0.11 to 0.17 %BW*BH for TIW, TOW, and LTLW. Moreover, for the same gait conditions, we observe a match in the significance levels showed in both systems in the post-hoc analysis of Table 3.2. However, mean errors of about 0.8 %BW*BH were found during the MKW gait modification, which reveals a decreased and rather inconsistent performance of the method for this condition. In addition, accurately estimating the absolute knee joint moment values remains

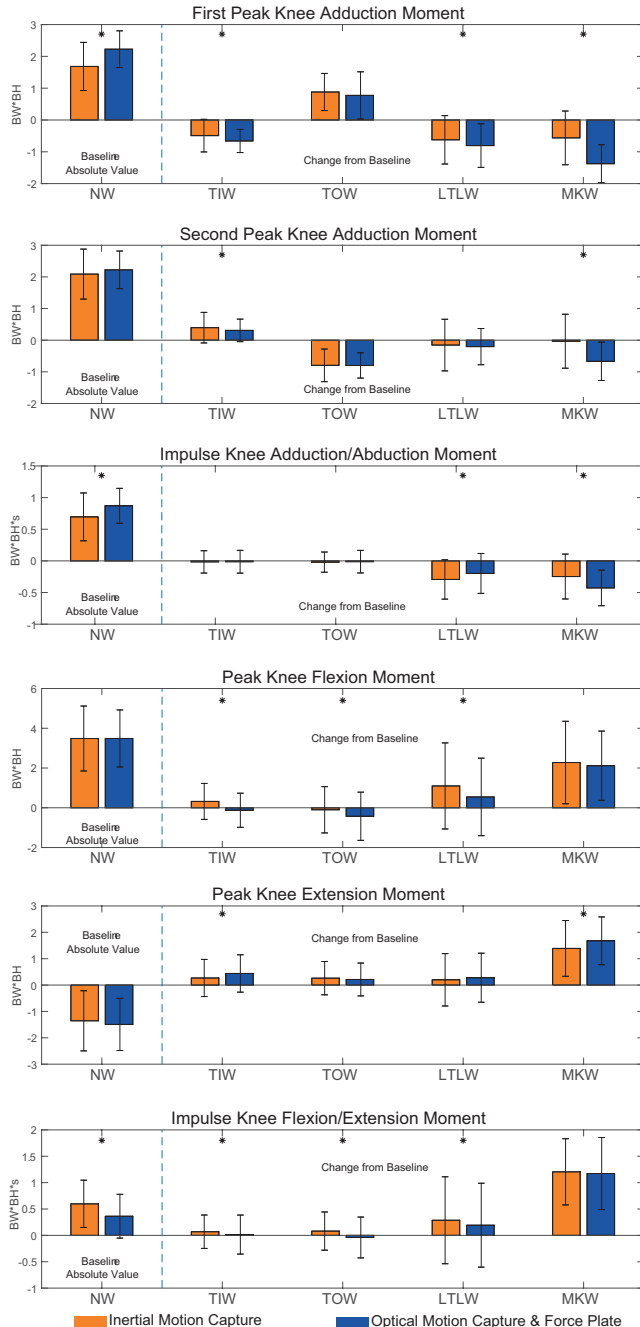
3. Assessment of Knee Adduction and Flexion Moments

Figure 3.2: Mean and standard deviations of the knee adduction and flexion moment first peak, second peak, and impulse values for ambulatory method (orange) and reference (blue). Significant differences between the proposed and reference method found from a paired t-test are indicated with an asterisk (*).



3.4. Discussion

Figure 3.3: Change from intra-subject baseline for knee adduction and flexion moment first peak, second peak, and impulse values for ambulatory method (orange) and reference (blue). Significant differences between the proposed and reference method found from a paired t-test are indicated with an asterisk (*).



3. Assessment of Knee Adduction and Flexion Moments

challenging due to lack of both measured force and absolute position estimates. Despite this fact, the intra-subject, intra-session change in knee moment induced by an altered gait pattern seems to be estimated more accurately and is still an important parameter for the clinical assessment of KOA and design of subject-specific gait modifications.

Comparison to literature

Van den Noort *et al.* investigated the knee moments assessed from an ambulatory system using measured force information from an instrumented force shoe and kinematic data of the shank and foot derived from inertial sensors [95]. RMS differences in that study were found 0.58 ± 0.14 and 1.07 ± 0.29 for KAM and KFM, respectively. For the same components, we found higher RMSD values of 0.74 ± 0.25 and 1.12 ± 0.43 for normal walking. Mean differences for early stance KAM peak were found $0.19 \pm 0.46\% \text{BW}^*\text{BH}$, whereas in our method that ranged from -0.54 ± 0.74 up to $0.13 \pm 0.84\% \text{BW}^*\text{BH}$ across the five gait patterns investigated. In contrast, late stance KAM peaks had reduced mean differences in our approach ranging from -0.26 ± 0.68 to $0.30 \pm 0.98\% \text{BW}^*\text{BH}$ versus $-0.78 \pm 0.43\% \text{BW}^*\text{BH}$, in the study with the force shoe input. However, that study did not investigate any gait modifications and examined a group of patients with KOA who typically have larger static knee varus angles and KAM magnitudes. Nevertheless, our approach provides a more lightweight setup without dependency on direct GRF&M measurements using instrumented force shoes that may impede the movement freedom of the application due to their increased height and weight.

Clinical applicability

Previous research investigated the test-retest reliability of the KAM using conventional laboratory systems [155]. The findings of that study reported mean differences of $0.1\% \text{BW}^*\text{BH}$, between sessions. In addition, the same study indicated measurement errors ranging from $0.24\% \text{BW}^*\text{BH}$ up to $0.70\% \text{BW}^*\text{BH}$ for 50% and 95% confidence levels, respectively. This indicates that even laboratory based systems may suffer from lower than expected inter-session repeatability, when examining absolute values of moments. Despite this fact they are widely used in clinical gait analysis.

Our method performed inconsistently for the assessment of absolute knee moment measures. However, the additional analysis showed lower mean and standard deviations of the errors in the change in moment with respect to a baseline, which for some gait conditions had no significant differences (Table 3.4). Therefore it could be cautiously used as a tool for the assessment of the induced KAM change due to a gait modification, enabling subject-specific gait modifications without the need for laboratory systems. Despite the similar performance observed during the first three gait modifications TIW, TOW, and LTLW, the knee moment estimates during MKW gait modification presented different behavior, with often higher differences to the reference. This inconsistency may be attributed to the joint constraints in the inertial motion capture model.

3.4. Discussion

Sources of error

The estimation of kinetics using a whole-body inverse dynamic approach relies on both anthropometric and kinematic input. Generic anthropometric tables from literature were used to estimate the mass, moment of inertia and the center of mass of each segment [107]. Sensitivity analysis performed by Ren *et al.* [39] showed that errors in the mass properties of the heavy segments, such as the thigh or torso contribute to high differences in the predicted GRF&M. Recent methods for subject specific segment parameters can be incorporated to decrease the effect of the assumptions of the generic models [156, 157].

Regarding kinematics of the inertial motion capture system, errors may come from two sources; sensor-to-segment calibration and sensor/segment motion tracking. Regarding the former, errors may stem from a mismatch between the practiced and modelled neutral N-pose of Xsens MVN. In addition, errors in joint position estimation can be introduced from discrepancies in the segment lengths required in the forward kinematics approach to derive position from orientation. Regarding the latter, soft tissue artifacts or slight movement of the sensors or markers with respect to the bone, may also compromise the quality of both inertial, but also optical motion capture systems. Due to the use of the Xsens MVN Analyze 2018.0 software in this study, which has demonstrated immunity to magnetic disturbances, the orientations of the segments will be affected minimally by non-homogeneous magnetic field in the laboratory.

Overall, the performance of the proposed system was higher when analyzing the knee adduction or flexion moment change from baseline as a result of modified gait. In general, KAM was underestimated and KFM was overestimated in the inertial approach. The afore-mentioned sources of error in the kinematics and anthropometrics explain most of these variations. For instance, lack of positional data and N-pose calibration assumptions in the Xsens MVN system may introduce offsets in segment orientations and positions that may result in discrepancies in the estimated moments. By nature accelerometer and gyroscope sensors measure relative quantities (accelerations and angular rates) and therefore have an advantage in quantifying related relative measures such as forces ($F=ma$). However, in the case of torques lever arms derived from absolute positional data which are highly influenced by the sensor-to-segment calibration procedures.

Limitations and future work:

Despite the wide acceptance of the KAM in the past years as a measure reflecting the medial knee contact force, the exact relation is still ambiguous [79]. Research stressed the important role of KFM in the knee joint loading [158]. Alternatively, recent methods based on musculoskeletal models [151, 159], have enabled the non-invasive estimation of internal knee contact forces [160, 161]. Further research is necessary to thoroughly investigate the effect of such gait modifications on in-vivo knee contact forces, and secondly develop methods to assess these quantities with ambulatory instrumentation.

To date there is no consensus regarding the choice of an ideal coordinate system to express the knee moments. Only a limited number of studies examined the effect of the reference frame selection on KAM, including orthogonal tibia, femur, and lab-

3. Assessment of Knee Adduction and Flexion Moments

oratory coordinate systems, as well as a non-orthogonal knee joint coordinate system [85, 162]. Schache *et al.* [85] showed that the change in peak KAM values follows the same sign regardless of coordinate frame, even though the size of the change varied per frame. In addition, another work demonstrated that regardless of frame selection KOA patients exhibit higher moment values compared to controls [163]. In our study, knee moments were projected on the body progression coordinate frame, which is referred to as laboratory frame in the aforementioned studies. This frame was selected to avoid biasing the results for joint moments due to known incompetence of conventional skin marker and possibly also sensor systems to accurately quantify transverse plane kinematics [22]. In this way, the progression coordinate frame ensures that the moments are expressed in a consistent manner across subjects, sessions and computational methods. Ideally, a frame on which the KAM and KFM correlate best with the medial contact forces should be chosen, however until today there is not much evidence on this topic.

A limitation of the setup used in this study is its dependence on a high number of 17 IMU sensors that are required to reconstruct the full-body motion, and subsequently estimate the external and joint loads. Future work is necessary to investigate kinematic reconstruction from sparse sensor sets [164, 165].

Finally, a natural future step would be to evaluate the proposed method in a group of patients with medial KOA. In that case, considerably high knee varus angles typically observed in such patients [166], could influence more the shank and thigh segment orientations and joint position estimates. More accurate assessment of the static knee malalignment on the frontal plane could be performed using inclinometer [87] or camera-based data.

3.5 Conclusion

In this study, we have investigated the estimation of net knee adduction and flexion moments across various gait patterns recommended to reduce knee loading. Our results indicate that the change from baseline in the knee joint moments can be estimated more accurately than the absolute moment values and for several gait modifications present no significant differences with the reference system. These findings enable the application of knee joint loading estimation outside laboratory setting, with less complex instrumentation. The decrease in complexity and costs-featured by the proposed system may boost clinical adoption of gait modifications in the future.

Chapter 4

Musculoskeletal model-based inverse dynamic analysis under ambulatory conditions using inertial motion capture

Submitted:

Karatsidis, A., Jung, M., Schepers, H. M., Bellusci, G., de Zee, M., Veltink, P. H., & Andersen, M. S. Musculoskeletal model-based inverse dynamic analysis under ambulatory conditions using inertial motion capture

4. Ambulatory Musculoskeletal Inverse Dynamic Analysis

Abstract

Inverse dynamic analysis using musculoskeletal modeling is a powerful tool, which is utilized in a range of applications to estimate forces in ligaments, muscles, and joints, non-invasively. To date, the conventional input used in this analysis is derived from optical motion capture (OMC) and force plate (FP) systems, which restrict the application of musculoskeletal models to gait laboratories. To address this problem, we propose the use of inertial motion capture to perform musculoskeletal model-based inverse dynamics by utilizing a universally applicable ground reaction force and moment (GRF&M) prediction method. We validated the joint angle and kinetic estimates of the lower limbs against an equally constructed musculoskeletal model driven by OMC and FP system. The sagittal plane joint angles of ankle, knee, and hip presented excellent Pearson correlations ($\rho = 0.95, 0.99$, and 0.99 , respectively) and root-mean-squared-differences (RMSD) of $4.1 \pm 1.3^\circ$, $4.4 \pm 2.0^\circ$, and $5.7 \pm 2.1^\circ$, respectively. The GRF&M predicted using IMC input were found to have excellent correlations for three components (vertical: $\rho = 0.97$, RMSD= $9.3 \pm 3.0\text{ \%BW}$, anteroposterior: $\rho = 0.91$, RMSD= $5.5 \pm 1.2\text{ \%BW}$, sagittal: $\rho = 0.91$, RMSD= $1.6 \pm 0.6\text{ \%BW}\text{*BH}$), and strong correlations for mediolateral ($\rho = 0.80$, RMSD= $2.1 \pm 0.6\text{ \%BW}$) and transverse ($\rho = 0.82$, RMSD= $0.2 \pm 0.1\text{ \%BW}\text{*BH}$). The proposed IMC-based method removes the complexity and space-restrictions of OMC and FP systems and could enable applications of musculoskeletal models in either monitoring patients during their daily lives or in wider clinical practice.

Keywords: Musculoskeletal modeling; Inertial motion capture; Inverse dynamics; Ground reaction forces and moments; Gait analysis

4.1. Introduction

4.1 Introduction

Assessment of muscle, joint, and ligament forces is important to understand the mechanical and physiological mechanisms of human movement. To date, the measurement of such in-vivo forces is a challenging task. For this reason, computer-based musculoskeletal models have been widely used to estimate the variables of interest non-invasively [167, 159].

The most common approach used in musculoskeletal modeling is the method of the inverse dynamics [168]. This analysis utilizes the equations of motion with input from human body kinematics in conjunction with kinetics obtained from external forces [37], to estimate joint reaction and muscle forces, as well as net joint moments using muscle recruitment methods [169]. Measurements of the external forces are typically required and measured using force plates (FPs), however, the use of FPs has several limitations. First, subjects tend to alter their natural gait patterns in order to hit the small and fixed measurement area of a plate [38]. In addition, this static and limited measurement area, impedes the assessment of several consecutive steps, when only a couple of FPs are available. Finally, the combined use of FP with motion input introduces a dynamic inconsistency, which results to residual forces and moments in the inverse dynamics. [170, 171].

Several studies have proposed replacing the FP input with wearable devices such as shoes with three-dimensional force and torque sensors beneath the sole [45, 47, 94]. In a similar fashion, pressure insoles were proposed to reconstruct the complete ground reaction forces and moments (GRF&M) from pressure distributions [93, 53, 54]. Although these wearable devices are suitable for the assessment of external forces, the increased height and weight of the shoes equipped with force/torque sensors [49, 48], as well as the repeatability of the pressure sensors [56] are considered important limitations.

Recent research has suggested the replacement of the force input with predictions derived solely from motion input [97, 39, 40, 41, 42, 43]. In these studies, human body kinematics are combined with the inertial properties of the body segments, from which Newton-Euler equations are utilized to compute the external forces and moments. Since the system of equations becomes indeterminate during the double stance of gait, each of the aforementioned studies focused on methods to solve this issue. Ren *et al.* [39] suggested a gait event-based function which is only applicable in gait, while Oh *et al.* [40] and Choi *et al.* [41] suggested methods based on a machine learning that require a training database and thus are not applicable for movements not included in that database. A last approach enables the universal application of these methods using a muscle recruitment approach has shown promising performance for various activities of daily living [42] and sports [43].

The majority of the existing research which studied the prediction of GRF&M, used conventional optical motion capture (OMC) input. Despite the high accuracy of this method in tracking marker trajectories, its dependence on laboratory equipment restricts possible applications during daily life activities or in wider clinical practice. In the previous decade, ambulatory motion tracking systems based on inertial measurement units (IMUs), have been proposed as a suitable alternative for estimating 3D segment kinematics [100, 27, 24, 172]. A key benefit of such systems is that they can be applied in virtually any environment without depending on

4. Ambulatory Musculoskeletal Inverse Dynamic Analysis

external infrastructure, such as cameras. Driven by these advances in inertial motion capture (IMC), recent work of the authors demonstrated its ability to estimate three-dimensional GRF&M [144], which were distributed between the feet using a smooth transition assumption concept [39]. However, limitations of that approach is that it is only valid for gait and has no muscle, bone or ligament force estimate capabilities.

To date, the use of detailed musculoskeletal modeling with kinematic inputs from IMUs has only received limited attention. Koning *et al.* [173] previously demonstrated the feasibility of kinematically driving a musculoskeletal model using only orientations from IMUs. However, that study only compared the kinematics of the musculoskeletal model, without any inverse dynamic calculations.

The aim of this study was to develop a workflow to perform musculoskeletal model-based inverse dynamics using exclusively IMC input, applicable in ambulatory environments and validate it against a conventional laboratory-based approach. To achieve this, we utilize a virtual-marker based technique to map the kinematics of the IMC model to the musculoskeletal model, and subsequently a ground reaction force and moment prediction method to enable inverse dynamics computations. We validate the kinematics as well as the predicted GRF&M, joint reaction forces and net moments (JRF&M) compared against an OMC and FP-driven musculoskeletal model.

4.1.1 Subjects

The experimental data was collected at the Human Performance Laboratory, at the Department of Health Science and Technology, Aalborg University, Aalborg, Denmark following the ethical guidelines of The Scientific Ethical Committee for the Region of North Jutland (Den Videnskabsetiske Komité for Region Nordjylland). Eleven healthy male individuals with no present musculoskeletal or neuromuscular disorders volunteered for the study (age: 31.0 ± 7.2 years; height: 1.81 ± 0.06 m; weight: 77.3 ± 9.2 kg; body mass index (BMI): 23.6 ± 2.4 kg/m²). All participants provided written informed consent, prior to data collection.

4.1.2 Instrumentation

Full-body IMC data were collected using the Xsens MVN Link (Xsens Technologies B.V., Enschede, the Netherlands), in which 17 IMUs were mounted on the head, sternum, pelvis, upper legs, lower legs, feet, shoulders, upper arms, forearms and hands using the dedicated clothing. The exact location of each sensor on the respective segment followed the manufacturer guidelines described in the manual of Xsens MVN [174]. The affiliated software Xsens MVN Studio 4.2.4 was used to track the IMU orientations with respect to an earth-based coordinate frame[100, 27]. Segment orientations were obtained by applying the IMU-to-segment alignment, found using a known upright pose (N-pose) performed by the subject at a known moment in time, while taking specific care to minimize the effect of magnetic disturbances. In addition, this information is fused with updates regarding the joints and external contacts to limit the position drift [24].

For validation purposes, an OMC system utilizing 8 infrared high speed cameras (Oqus 300 series, Qualisys AB, Gothenburg, Sweden) and the software Qual-

4.1. Introduction

isys Track Manager 2.12 (QTM) were used to track the trajectories of 53 reflective markers mounted on the human body, as described in the Appendix of [144]. In addition, three FP systems (AMTI OR6-7-1000, Advanced Mechanical Technology, Inc., Watertown, MA, USA) embedded in the floor of the laboratory, were utilized using QTM to record the GRF&Ms. Both IMC and OMC systems sampled data at a frequency of 240 Hz, while the FP system sampled data at 2400 Hz. A second-order forward-backward low-pass Butterworth filter was applied to the reflective marker trajectories and measured GRF&M, with cut-off frequencies of 6 Hz and 15 Hz, respectively.

4.1.3 Experimental protocol

For each participant, the body dimensions were extracted using a conventional tape following the guidelines of Xsens. During the data collection, the subjects were instructed to walk barefoot in three different walking speeds (comfortable; CW, fast; FW, and slow; SW). The walking speeds performed experimentally were quantified as 1.28 ± 0.14 m/s (mean \pm standard deviation) for CW, 1.58 ± 0.09 m/s for FW (CW + 23%) and 0.86 ± 0.11 m/s for SW (CW–33%). For every walking speed, five successful trials were assessed. A successful trial was obtained when a single foot hit one of the FPs entirely, followed by an entire hit of the other foot on the successive FP.

4.1.4 Overall description of the components in the musculoskeletal models

Three musculoskeletal models have been constructed in AnyBodyTM Modeling System (AMS) v.6.0.7 (AnyBodyTM Technology A/S, Aalborg, Denmark) [167]:

- a model in which the kinematics are driven by IMC and the GRF&M are predicted from the kinematics (IMC-PGRF).
- a model in which the kinematics are driven by OMC and the GRF&M are predicted from the kinematics (OMC-PGRF).
- a model in which the kinematics are driven by OMC and the GRF&M are measured from FPs (OMC-MGRF).

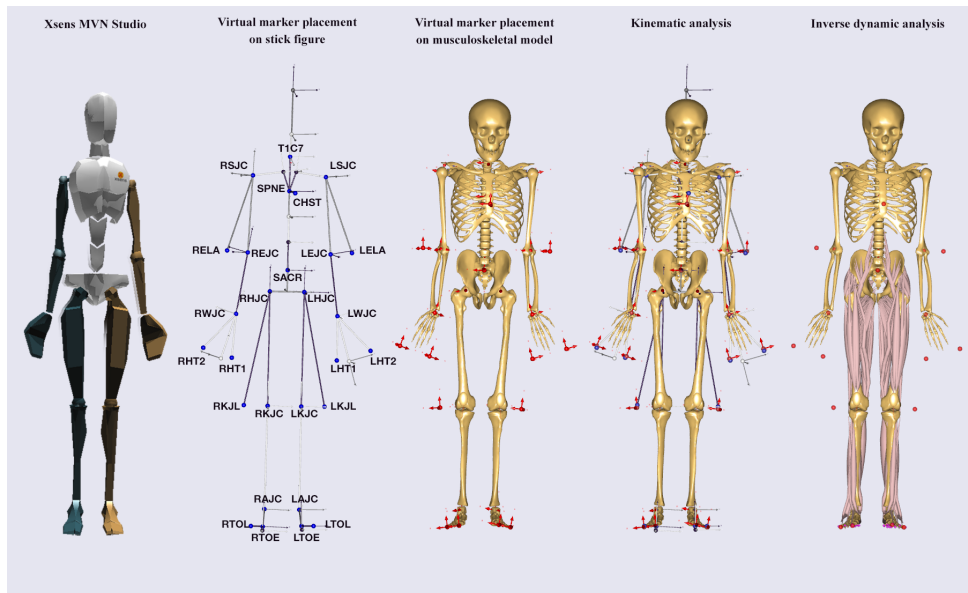
In the IMC-PGRF model, a Biovision Hierarchy (BVH) file is exported from Xsens MVN Studio and imported in AMS, in which a stick figure model is initially reconstructed. The BVH file contains a hierarchy part with a description of the linked segment model in a static pose, as well as a motion part that contains, for each time frame, the absolute position and orientation of the root pelvis segment, and the joint angles between the segments described in the hierarchy. The generated stick figure model contains 72 degrees-of-freedom (DOF). In order to match the stick figure model with the musculoskeletal model, we utilize a concept of virtual markers (VMs) demonstrated in a previous Kinect-based study [175]. The VMs are mapped to particular points of each model that are well defined in both models, such as joint centers and segment end points. The VM placement is illustrated in Figure 4.1 and described in more detail in the supplementary material. Following this step,

4. Ambulatory Musculoskeletal Inverse Dynamic Analysis

the VMs are treated as actual experimental markers, as if they were derived from an OMC system and they are assigned weights in three directions in the segment frame. Contrary to OMC, no filtering was applied to the VM trajectories.

In all models, the GaitFullBody template of the AnyBodyTM Managed Model Repository (AMMR) 1.6.2 was used to reconstruct the musculoskeletal models in AMS. The lumbar spine model was derived from the study of de Zee *et al.* [176], the lower limb model was derived from the Twente Lower Extremity Model Klein-Horsman *et al.* [177], and the shoulder and upper limb models were based on the model of the Delft Shoulder Group [178, 179, 180]. The full-body kinematic model contained 39 DOF in total. Specifically, a pelvis segment with three rotational and three translational DOF, two spherical hip joints, two revolute knee joints, two universal ankle joints, a spherical pelvic-lumbar joint, two glenohumeral joints with five DOF each, two universal elbow joints, and two universal wrist joints. The motion of the neck joint was locked to a neutral position.

Figure 4.1: Illustration of the pipeline used in the IMC-PGRF approach. A recording from Xsens MVN Studio (a) is exported to a BVH file to generate a stick figure model (b), in which virtual markers (blue) are placed. Virtual markers (red) are also placed on points of the musculoskeletal model (c), and by projecting b on c the kinematics of the musculoskeletal model are solved. Finally, inverse dynamic analysis using prediction of ground reaction forces and moments is performed to estimate the kinetics.



4.1.5 Scaling and kinematics analysis of the musculoskeletal models

For each subject, a standing reference trial with an anatomical pose was utilized to identify the parameters of segment lengths and the (virtual) marker positions, using a least-square minimization between the model and input (virtual or skin-mounted) marker positions [181]. In the IMC-PGRF musculoskeletal model, the lengths of the

4.1. Introduction

shanks, thighs, head, upper arm and forearms were derived directly from the stick figure, as generated from Xsens MVN studio using the measured body dimensions. In contrast, the pelvis width, foot length, and trunk height were optimized based on the above-mentioned least-square minimization method. The estimated segment lengths were used in all subsequent dynamic trials to perform the kinematic analysis based on the method of Andersen *et al.* [153].

4.1.6 Inertial and geometric scaling of the musculoskeletal models

The mass of each segment was linearly scaled based on the total body mass and the segment mass ratio values reported by Winter [37]. The inertial parameters were calculated by considering the segments as cylinders with uniform density. In addition, geometric scaling of each segment, where the longitudinal axis was defined as the second entry, was achieved using the following matrix:

$$S = \begin{bmatrix} \sqrt{\frac{m_s}{l_s}} & 0 & 0 \\ 0 & l_s & 0 \\ 0 & 0 & \sqrt{\frac{m_s}{l_s}} \end{bmatrix} \quad (4.1)$$

where S is the scaling matrix, l_s is the ratio between the unscaled and scaled lengths of the segment, m_s is the mass ratio of the segment.

4.1.7 Muscle recruitment

The muscle recruitment problem was solved by defining an optimization problem:

$$G(\mathbf{f}^{(M)}) = \sum_{i=1}^{n^{(M)}} A_i \left(\frac{f_i^{(M)}}{N_i} \right)^3 \quad (4.2a)$$

$$\mathbf{C}\mathbf{f} = \mathbf{d} \quad (4.2b)$$

$$0 \leq f_i^{(M)} \leq N_i, i = 1, \dots, n^{(M)} \quad (4.2c)$$

This system of equations minimizes the cost function G (4.2a), subject to the dynamic equilibrium equations (4.2b) and non-negativity constraints, so that each muscle can only pull, but not push, while its force ($f_i^{(M)}$) remains below its strength (N_i) (4.2c). The vector \mathbf{f} contains all the unknown muscle and joint reaction forces, $\mathbf{f}^{(M)}$ denotes the muscle forces, and $n^{(M)}$ denotes the number of muscles. The physiological cross-sectional area of the i th muscle is denoted by A_i . The coefficient matrix \mathbf{C} contains the equations of dynamic equilibrium and \mathbf{d} the external loads and inertia forces [167, 175, 160].

The strengths of the muscles were derived from previous studies which described the models of the body parts, and were considered constant for different lengths and contraction velocities [176, 177, 178, 179, 180]. To scale the muscle strengths, fat percentage was used as in Veeger *et al.* [179], calculated from the body mass index [182]. The model of the lower body contained 110 muscles, distributed into 318

4. Ambulatory Musculoskeletal Inverse Dynamic Analysis

individual muscle paths. In contrast, in the upper body model, ideal joint torque generators were utilized. Actuators for residual forces and moments with capacity up to 10 N and Nm, respectively, were placed at the origin of the pelvis and included in the muscle recruitment problem previously described.

4.1.8 Ground reaction force and moment prediction

The GRF&M were predicted by adjusting a method of Skals *et al.* [43]. A set of eighteen dynamic contact points were overlaid 1 mm beneath the inferior surface of each foot. Each dynamic contact point consisted of five unilateral force actuators, which could generate a positive vertical force perpendicular to the ground, and static friction forces in the anterior, posterior, medial, and lateral directions using a friction coefficient of 0.5. In addition, the height and velocity activation thresholds were set to 0.03 m and 1.2 m/s, respectively.

4.1.9 Data Analysis

Lower limb joint angles calculated in the IMC-PGRF model were compared to the OMC-PGRF/OMC-MGRF. In addition, GRF&M and JRF&M of the IMC-PGRF and OMC-PGRF were compared to OMC-MGRF.

Forces were normalized to body weight (BW) and moments to body weight times body height (BW*BH). The time axis of the curves was normalized to 100% of the gait cycle for the kinematics (time between two consecutive heel-strike events of the analyzed limb) and 100% of the stance phase (time between heel-strike and toe-off events of the analyzed limb) for the kinetics.

The above-mentioned comparisons of kinematic and kinetic variables to their respective references were performed using absolute and relative root-mean-square-differences (RMSD and rRMSD, respectively) as described by Ren *et al.* [39]. In addition, for every curve, the magnitude (M) and phase (P) difference metrics [112] have been utilized. Pearson correlation coefficient (ρ) were calculated, averaged using Fisher's z transformation method [183], and categorized similarly to Taylor *et al.* [111], as "weak" ($\rho \leq 0.35$), "moderate" ($0.35 < \rho \leq 0.67$), "strong" ($0.67 < \rho \leq 0.90$), and "excellent" ($\rho > 0.90$).

4.2 Results

4.2.1 Estimated kinematics of the musculoskeletal model

Table 4.1 presents the results for the accuracy analysis for the joint angles of the IMC-driven model versus the OMC-driven model. Similarly, Figure 4.2 illustrates the curves for the joint angles of the lower extremities averaged across all gait cycles performed by the eleven subjects. Excellent Pearson correlation coefficients have been found in all sagittal plane angles for ankle, knee, and hip (0.95, 0.99, and 0.99, respectively). For the same variables, the RMSDs across a gait cycle were found as $4.1 \pm 1.3^\circ$, $4.4 \pm 2.0^\circ$ and $5.7 \pm 2.1^\circ$, respectively (mean \pm standard deviation). Hip flexion angles were overall underestimated ($M = -4.0 \pm 13.9\%$), whereas knee and ankle magnitude differences showed an average overestimation ($0.7 \pm 6.2\%$ and

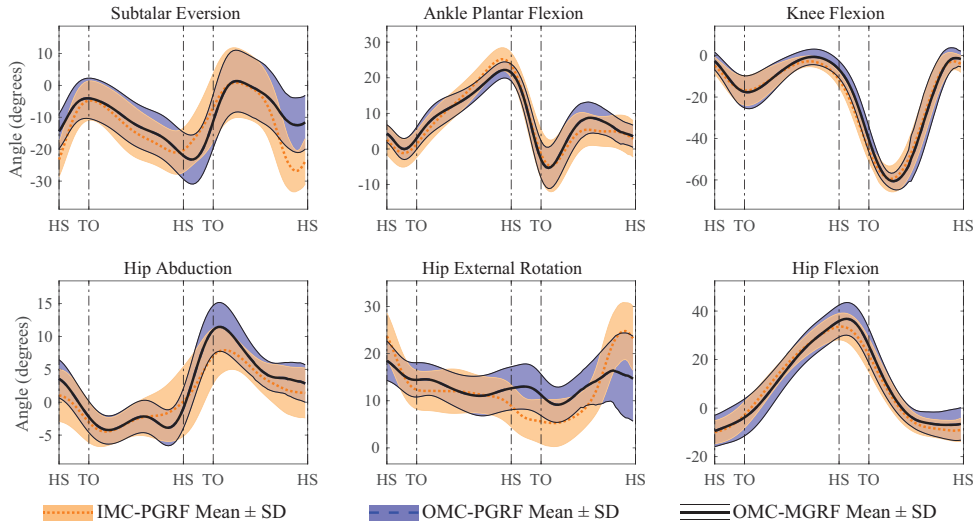
4.2. Results

Table 4.1: Comparison of lower limb joint angles between musculoskeletal model driven by the inertial (IMC-PGRF) and optical motion capture (OMC-PGRF/OMC-MGRF), using Pearson correlation coefficient (ρ), absolute and relative root-mean-squared-differences ($RMSD$ in degrees and $rRMSD$ in %, respectively). M and P denote the % magnitude and phase differences .

| | ρ | RMSD | rRMSD | M | P |
|-----------------------|--------|-----------|-------------|--------------|-------------|
| Subtalar Eversion | 0.81 | 9.7 (3.2) | 32.6 (10.3) | 24.0 (34.7) | 19.3 (10.2) |
| Ankle Plantarflexion | 0.95 | 4.1 (1.3) | 14.0 (4.8) | 8.6 (16.4) | 9.8 (3.9) |
| Knee Flexion | 0.99 | 4.4 (2.0) | 7.2 (3.4) | 0.7 (6.2) | 4.8 (2.7) |
| Hip Abduction | 0.91 | 4.1 (2.0) | 25.9 (10.7) | -12.2 (34.7) | 21.2 (9.3) |
| Hip External Rotation | 0.68 | 6.5 (2.8) | 36.9 (15.2) | 5.5 (39.0) | 12.6 (6.2) |
| Hip Flexion | 0.99 | 5.7 (2.1) | 12.7 (5.3) | -4.0 (13.9) | 8.8 (4.2) |

$8.6 \pm 16.4\%$). The hip abduction showed excellent correlations ($\rho = 0.91$) with an RMSD of $4.1 \pm 2.0^\circ$ and a mean underestimation with a magnitude difference $M = -12.2 \pm 34.7\%$. Strong correlation values ($\rho = 0.68$) were observed in the hip internal-external rotation angle with an RMSD of $6.5 \pm 2.8^\circ$ and an underestimation of magnitude difference $M = 5.5 \pm 39.0\%$. Finally, the subtalar eversion angle showed strong correlation ($\rho = 0.82$), RMSD of $9.66 \pm 3.07^\circ$ and $M = 24.0 \pm 34.7\%$.

Figure 4.2: Ankle, knee, and hip joint angle estimates (standard deviation around mean) of the IMC-PGRF (orange shaded area around orange dotted line) and OMC-PGRF models (blue shaded area around blue dashed line) versus OMC-MGRF model (thin black solid lines around thick black solid line).



4.2.2 Predicted kinetics using inertial and optical motion capture

The results of the accuracy analysis for GRF&M and JRF&M are presented in Table 4.2 and 4.3, for IMC-PGRF and OMC-PGRF, respectively. The mean values

4. Ambulatory Musculoskeletal Inverse Dynamic Analysis

and standard deviations of the curves from IMC-PGRF, OMC-PGRF, and OMC-MGRF models, are illustrated in Figures 4.3 and 4.4, for the forces and moments, respectively.

The Pearson correlation coefficients of the IMC-PGRF model were excellent for vertical ($\rho = 0.97$) and anteroposterior GRF&M ($\rho = 0.91$) and strong for mediolateral GRF&M ($\rho = 0.80$). For the same components, RMSD values observed were of 9.3 ± 3.0 , 5.5 ± 1.2 and 2.1 ± 0.6 %BW, respectively (mean \pm standard deviation). The OMC-PGRF model performed better in the anteroposterior GRF&M components ($\rho = 0.96$, RMSD = 3.7 ± 1.1 %BW), and similarly to IMC-PGRF for the other two GRF&M components (mediolateral: $\rho = 0.79$, RMSD = 1.9 ± 0.5 BW, vertical: $\rho = 0.99$, RMSD = 5.9 ± 1.9 BW).

Concerning GRM, the sagittal plane was predicted with similar excellent correlations in both IMC-PGRF ($\rho = 0.91$) and OMC-PGRF ($\rho = 0.94$) driven models. The correlation coefficients for frontal and transverse GRM components found in the IMC-PGRF model were $\rho = 0.64$, $\rho = 0.82$, respectively, whereas in the OMC-PGRF model ($\rho = 0.66$, $\rho = 0.81$, respectively). The RMSDs found in the IMC-PGRF approach were 0.9 ± 0.6 , 1.6 ± 0.6 , and 0.2 ± 0.001 %BW*BH for frontal, sagittal and transverse GR&M, respectively, which were either slightly higher or similar to the RMSDs of the OMC-PGRF approach (0.7 ± 0.2 , 1.2 ± 0.4 , and 0.2 ± 0.1 %BW*BH, respectively).

4.3 Discussion

We have presented a method to perform musculoskeletal model-based inverse dynamics using exclusively IMC input (IMC-PGRF). First, we compared the kinematic joint angle estimates of the lower limbs against those assessed through a conventional, laboratory-based OMC input. In addition, we tested the performance of the approach in calculating the JRF&M, while predicting the GRF&M from the kinematics, against a similarly constructed model (OMC-MGRF) which uses input from both FP and OMC. Finally, we performed a similar comparison to evaluate the predicted kinetics of a model driven exclusively by OMC input (OMC-PGRF).

Regarding the IMC-based joint angles in the musculoskeletal model, all three sagittal plane angles provided excellent correlations (range: 0.95-0.99) and average RMSD values remained below 6° . Slightly lower correlations were observed in the frontal and transverse plane angles, which can be explained due to the smaller range of motion within these planes. For instance, even though the hip abduction and external rotation joint angles present absolute RMSD values similar to the flexion component, their rRMSDs which take into account the range of motion are two and three times higher, respectively.

Both GRF&M and JRF&M of the vertical axis presented higher correlations and lower RMSDs than the ones in the anteroposterior and mediolateral axes. Similarly, sagittal plane moments were found in most cases to be more accurate than frontal and transverse plane moments. By visual inspection of the curves, we observe that the magnitude of the IMC-PGRF anteroposterior GRF&M seems to be underestimated both in the negative early stance and positive late stance peak, which can be confirmed by the magnitude difference for that curve ($M = -28.3\%$). However, this behavior is not observed in the OMC-PGRF, nor during the single stance of the

4.3. Discussion

Table 4.2: IMC-PGRF-based ground and joint reaction forces (first three quantities) and net moments (second three quantities) versus OMC-MGRF. Pearson correlation coefficient is denoted with ρ . Absolute per body weight (or body weight times height) and relative root-mean-squared-difference are denoted with *RMSD* (%BW or %BW*BH) and *rRMSD* (%), respectively. *M* and *P* indicate the magnitude and phase differences (%).

| | ρ | RMSD | rRMSD | M | P |
|-------------------|--------|--------------|-------------|---------------|-------------|
| Ground | | | | | |
| Anteroposterior | 0.91 | 5.5 (1.2) | 15.0 (2.4) | -25.4 (7.3) | 14.4 (3.2) |
| Mediolateral | 0.80 | 2.1 (0.6) | 18.5 (3.2) | 7.3 (19.3) | 15.4 (3.8) |
| Vertical | 0.97 | 9.3 (3.0) | 7.7 (2.1) | -1.5 (1.5) | 3.4 (1.0) |
| Frontal | 0.64 | 0.9 (0.6) | 38.0 (23.1) | 125.5 (319.9) | 30.6 (17.3) |
| Sagittal | 0.91 | 1.6 (0.6) | 17.5 (6.8) | 14.3 (18.2) | 12.1 (4.5) |
| Transverse | 0.82 | 0.2 (0.1) | 23.3 (7.2) | -8.5 (41.9) | 17.8 (5.3) |
| Ankle | | | | | |
| Anteroposterior | 0.84 | 22.2 (10.3) | 26.1 (10.2) | 49.0 (45.8) | 10.8 (2.1) |
| Mediolateral | 0.93 | 24.3 (8.9) | 15.2 (5.3) | 14.3 (17.1) | 7.9 (2.7) |
| Proximodistal | 0.93 | 88.5 (30.6) | 13.6 (4.6) | 9.8 (14.1) | 7.2 (2.3) |
| Eversion | 0.76 | 0.6 (0.2) | 33.3 (20.2) | 107.7 (220.3) | 18.9 (10.7) |
| Plantar Flexion | 0.93 | 1.6 (0.6) | 15.1 (6.6) | 10.6 (18.1) | 9.9 (3.6) |
| Axial | 0.67 | 0.5 (0.2) | 30.4 (12.2) | 46.5 (49.1) | 27.2 (13.5) |
| Knee | | | | | |
| Anteroposterior | 0.82 | 30.6 (10.3) | 25.8 (9.7) | 43.7 (53.5) | 13.0 (4.5) |
| Mediolateral | 0.91 | 12.0 (3.5) | 14.1 (3.8) | 6.6 (8.6) | 7.0 (2.0) |
| Proximodistal | 0.90 | 63.1 (26.9) | 14.3 (6.6) | 5.1 (9.1) | 7.2 (2.8) |
| Abduction | 0.81 | 1.1 (0.4) | 18.9 (6.8) | -2.7 (16.1) | 10.7 (3.8) |
| Flexion | 0.58 | 1.9 (0.5) | 29.8 (7.6) | 17.9 (45.0) | 32.8 (9.6) |
| Axial | 0.73 | 0.3 (0.1) | 25.4 (10.3) | 2.3 (30.5) | 27.9 (13.8) |
| Hip | | | | | |
| Anteroposterior | 0.71 | 17.6 (7.6) | 27.2 (9.6) | 6.8 (24.4) | 27.6 (10.9) |
| Mediolateral | 0.73 | 27.0 (12.5) | 23.0 (7.4) | 7.7 (14.6) | 10.6 (4.1) |
| Proximodistal | 0.78 | 102.8 (30.6) | 21.7 (4.5) | 20.2 (10.0) | 9.0 (2.5) |
| Abduction | 0.83 | 1.4 (0.7) | 19.7 (5.8) | 6.3 (16.9) | 13.7 (7.9) |
| Flexion | 0.92 | 2.2 (0.6) | 19.4 (4.2) | 73.2 (26.3) | 14.8 (4.2) |
| External Rotation | 0.50 | 0.5 (0.2) | 31.6 (6.6) | -3.9 (36.4) | 25.6 (10.1) |

IMC-PGRF curve. Despite the higher rRMSD found in the non-sagittal joint angles, the performance of the IMC-PGRF in the mediolateral, frontal and transverse plane GRF&M components matched closely the OMC-PGRF approach. This observation reveals that OMC-based kinematics suffer from errors of similar size, when capturing the typically small movements of the frontal and transverse planes, given the fact that both IMC-PGRF and OMC-PGRF had the same model characteristics. Therefore, OMC-MGRF should also be used with caution, when comparing either kinematic or JRF&M quantities of the non-sagittal planes.

A number of error sources contribute to discrepancies in the OMC kinematics. First, soft tissue artefacts can create a relative movement of the marker with respect to the bone [23, 184]. In addition, mismatches between the experimental and modelled marker positions can lead to errors in segment orientations calculated during inverse kinematics. Both error sources would have a relatively larger impact on the kinematics of the frontal and transverse plane, than on the sagittal plane. Finally,

4. Ambulatory Musculoskeletal Inverse Dynamic Analysis

Table 4.3: OMC-PGRF-based ground and joint reaction forces (first three quantities) and net moments (second three quantities) versus OMC-MGRF. Pearson correlation coefficient is denoted with ρ . Absolute per body weight (or body weight times height) and relative root-mean-squared-difference are denoted with $RMSD$ (%BW or %BW*BH) and $rRMSD$ (%), respectively. M and P indicate the magnitude and phase differences (%).

| | ρ | RMSD | rRMSD | M | P |
|-------------------|--------|-------------|------------|--------------|-------------|
| Ground | | | | | |
| Anteroposterior | 0.96 | 3.7 (1.1) | 8.3 (2.0) | 7.7 (12.0) | 8.8 (1.8) |
| Mediolateral | 0.79 | 1.9 (0.5) | 18.6 (4.1) | 2.4 (10.8) | 15.2 (4.9) |
| Vertical | 0.99 | 5.9 (1.9) | 4.9 (1.4) | -1.2 (1.1) | 2.1 (0.7) |
| Frontal | 0.66 | 0.7 (0.2) | 30.3 (9.3) | 71.0 (122.2) | 24.5 (9.1) |
| Sagittal | 0.94 | 1.2 (0.4) | 13.1 (3.8) | 15.9 (15.3) | 9.2 (3.2) |
| Transverse | 0.81 | 0.2 (0.1) | 20.7 (7.5) | 7.1 (22.9) | 17.5 (7.5) |
| Ankle | | | | | |
| Anteroposterior | 0.83 | 18.9 (6.9) | 23.0 (6.1) | 37.3 (28.6) | 10.8 (2.3) |
| Mediolateral | 0.96 | 16.1 (4.2) | 10.7 (2.6) | 6.8 (9.6) | 5.8 (2.1) |
| Proximodistal | 0.96 | 62.2 (17.6) | 9.8 (2.7) | 7.1 (9.0) | 5.2 (1.8) |
| Eversion | 0.76 | 0.5 (0.1) | 25.5 (7.0) | 45.3 (64.1) | 18.7 (10.2) |
| Plantar Flexion | 0.96 | 1.0 (0.3) | 10.1 (3.3) | 5.9 (10.0) | 7.0 (2.6) |
| Axial | 0.64 | 0.5 (0.1) | 27.2 (7.3) | 33.3 (36.9) | 27.5 (11.5) |
| Knee | | | | | |
| Anteroposterior | 0.93 | 11.9 (4.5) | 12.3 (4.3) | -7.3 (8.7) | 7.4 (2.0) |
| Mediolateral | 0.96 | 7.2 (2.0) | 8.8 (2.6) | -4.2 (5.6) | 4.4 (1.0) |
| Proximodistal | 0.95 | 41.7 (12.0) | 9.3 (2.6) | -2.7 (5.8) | 4.9 (1.2) |
| Abduction | 0.91 | 0.8 (0.2) | 12.6 (2.6) | -0.1 (10.5) | 7.7 (1.6) |
| Flexion | 0.86 | 0.9 (0.3) | 16.7 (4.8) | -1.7 (14.3) | 16.9 (5.2) |
| Axial | 0.82 | 0.2 (0.1) | 18.5 (6.6) | -3.4 (17.7) | 20.6 (8.0) |
| Hip | | | | | |
| Anteroposterior | 0.89 | 9.9 (3.6) | 16.0 (6.7) | -10.4 (10.6) | 16.6 (7.6) |
| Mediolateral | 0.92 | 14.7 (4.0) | 12.7 (3.1) | -1.9 (6.9) | 6.2 (1.5) |
| Proximodistal | 0.92 | 50.0 (15.9) | 11.5 (2.6) | -4.6 (6.1) | 5.5 (1.2) |
| Abduction | 0.91 | 0.8 (0.2) | 13.3 (2.6) | -3.2 (6.3) | 8.7 (2.4) |
| Flexion | 0.86 | 1.3 (0.4) | 16.4 (3.4) | -9.3 (12.3) | 18.0 (4.1) |
| External Rotation | 0.68 | 0.3 (0.1) | 22.5 (3.7) | 6.5 (15.8) | 18.8 (4.8) |

the JRF&M of the OMC-PGRF were compared against a non-independent OMC-MGRF reference, which could have contributed to underestimation of the actual errors.

The IMC-PGRF approach has a number of possible sources of errors which would influence the performance. Similarly to OMC models, soft-tissue artifacts may compromise the kinematic estimates. Further errors in segment kinematics may stem due to the N-pose calibration assumptions. In particular, mismatches between the practiced and modelled N-pose could result in offsets in the estimated positions. Other common error sources in IMC include manual measurements of segment lengths as well as IMU inaccuracies. In addition, the stick figure model, which was utilized to recreate the VMs, has a higher number of DOF, compared to the musculoskeletal model used.

A possible source of error in all inverse dynamic approaches concerns the inertial parameters (masses and moments of inertia), as well as the center of mass (CoM)

4.3. Discussion

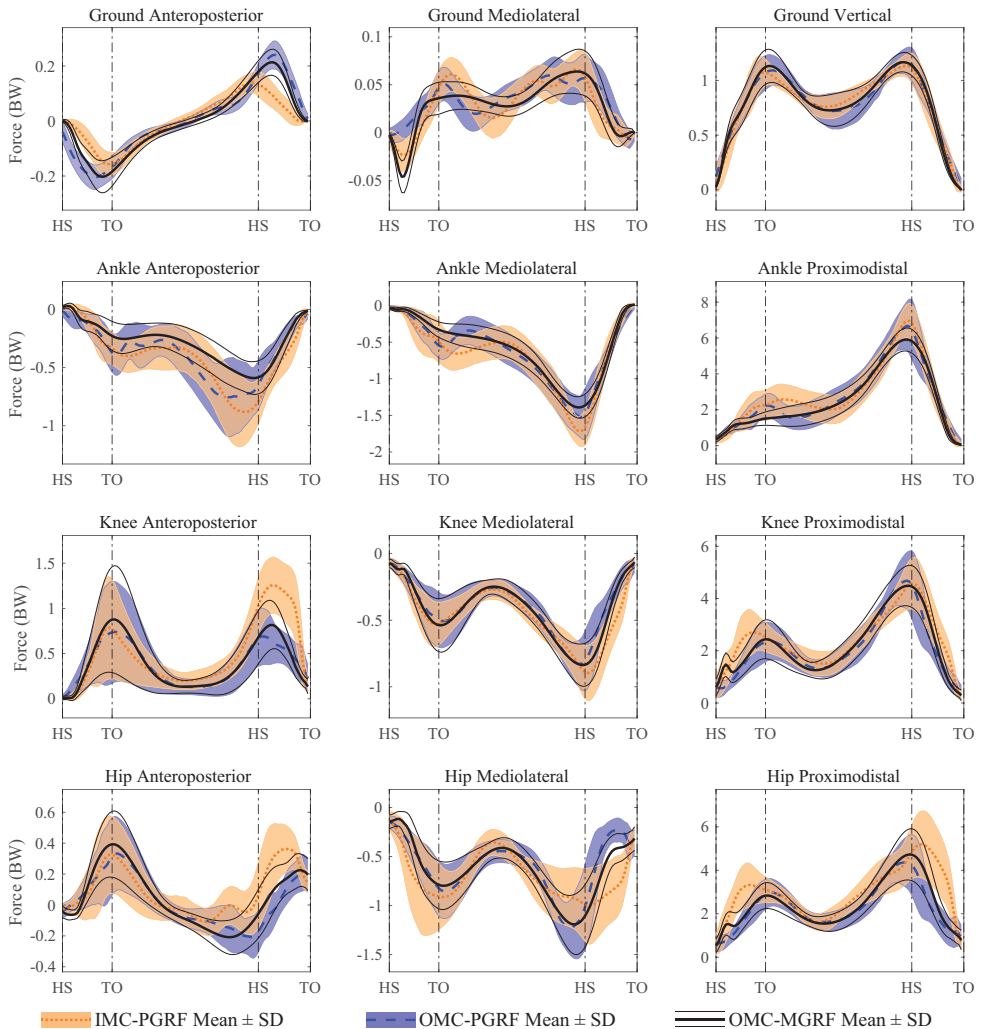


Figure 4.3: Ground and lower limb joint reaction force estimates (standard deviation around mean) of the IMC-PGRF (orange shaded area around orange dotted line) and OMC-PGRF models (blue shaded area around blue dashed line) versus OMC-MGRF model (thin black solid lines around thick black solid line).

locations of each human body segment, which were calculated based on anthropometric tables found in the literature.

This study focused on presenting and evaluating a general workflow for musculoskeletal model-based inverse dynamic simulations using ambulatory IMC systems. The presentation of results in this study was performed on the level of ground and joint reaction forces and moments. These measures are calculated from muscle force estimates derived from a muscle recruitment optimization technique. Given the high number of muscles in the model (110) and without a clear medical research question, it is challenging to choose which muscles are more important to present and analyze. Future studies could examine specific applications and pathologies in order

4. Ambulatory Musculoskeletal Inverse Dynamic Analysis

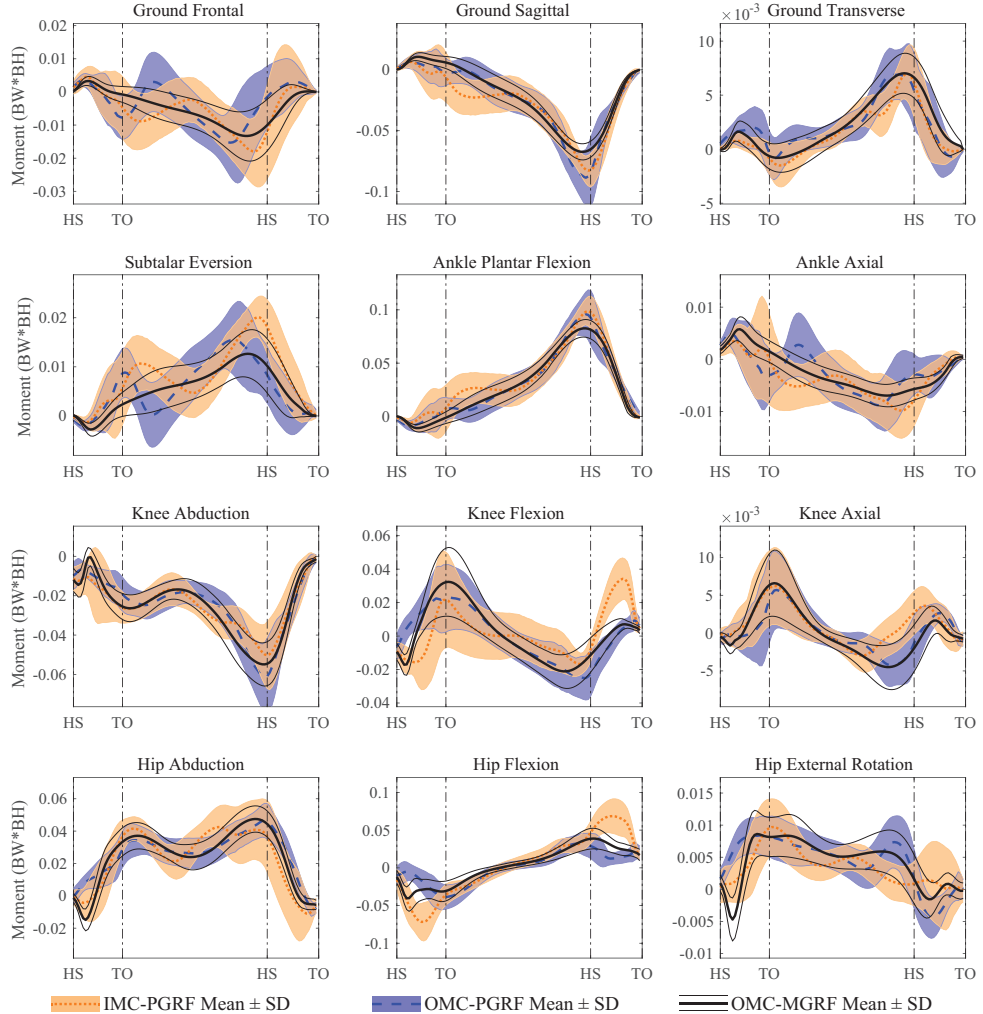


Figure 4.4: Ground reaction and lower limb net joint moment estimates (standard deviation around mean) of the IMC-PGRF (orange shaded area around orange dotted line) and OMC-PGRF models (blue shaded area around blue dashed line) versus OMC-MGRF model (thin black solid lines around thick black solid line).

to identify the most important muscles and evaluate their respective force estimates.

A limitation of this study is that, even though the method has been previously shown to be universally applicable in OMC-based studies [42, 43], we only evaluated its performance in gait of three different speeds. Moreover, our experiments included only healthy subjects, but the underlying methods have been recently shown to be applicable in Parkinson's patients [185]. Future studies could investigate the application of IMC systems combined with musculoskeletal modeling in patient groups.

4.4. Conclusion

4.4 Conclusion

In this study, we have demonstrated a workflow to perform musculoskeletal model-based inverse dynamics using input from a commercially available IMC system. Our validation findings indicate that the prediction of GRF&M as well as JRF&M using musculoskeletal model-based inverse dynamics based on only IMC data provides comparable performance to both OMC-PGRF and OMC-MGRF methods. The proposed method allows assessment of kinetic variables outside the laboratory.

4. Ambulatory Musculoskeletal Inverse Dynamic Analysis

Chapter 5

Validation of wearable visual feedback for retraining foot progression angle using inertial sensors and an augmented reality headset

Published as:

Karatidis, A., Richards, R. E., Konrath, J. M., van den Noort, J. C., Schepers, H. M., Bellusci, G., Harlaar, J., Veltink, P. H. (2018). Validation of wearable visual feedback for retraining foot progression angle using inertial sensors and an augmented reality headset. *Journal of NeuroEngineering and Rehabilitation*, 15(1), 78. <http://dx.doi.org/10.1186/s12984-018-0419-2>

5. Wearable Visual Feedback on Foot Progression Angle

Abstract

Gait retraining interventions using real-time biofeedback have been proposed to alter the loading across the knee joint in patients with knee osteoarthritis. Despite the demonstrated benefits of these conservative treatments, their clinical adoption is currently obstructed by the high complexity, spatial demands, and cost of optical motion capture systems. In this study we propose and evaluate a wearable visual feedback system for gait retraining of the foot progression angle (FPA). The primary components of the system are inertial measurement units, which track the human movement without spatial limitations, and an augmented reality headset used to project the visual feedback in the visual field. The adapted gait protocol contained five different target angles ranging from 15 degrees toe-out to 5 degrees toe-in. Eleven healthy participants walked on an instrumented treadmill, and the protocol was performed using both an established laboratory visual feedback driven by optical motion capture, and the proposed wearable system. The wearable system tracked FPA with an accuracy of 2.4 degrees RMS and ICC=0.94 across all target angles and subjects, when compared to an optical motion capture reference. In addition, the effectiveness of the biofeedback, reflected by the number of steps with FPA value ± 2 degrees from the target, was found to be around 50% in both wearable and laboratory approaches. These findings demonstrate that retraining of the FPA using wearable inertial sensing and visual feedback is feasible with effectiveness matching closely an established laboratory method. The proposed wearable setup may reduce the complexity of gait retraining applications and facilitate their transfer to routine clinical practice.

Keywords: Foot progression angle; Inertial sensors; Real-time biofeedback; Augmented reality headset; Gait retraining; Knee osteoarthritis

5.1. Background

5.1 Background

Knee osteoarthritis (KOA) is a leading cause of disability in the elderly population [186]. To date, there is no cure available for the disease and treatment options are of pharmacological, surgical or biomechanical nature [187, 74, 188]. Pharmacological treatments alleviate only the symptoms (pain, discomfort and swelling), while surgical treatments usually involve total knee replacement and are only considered in severe stages of the disease [189]. Biomechanical interventions are conservative non-pharmacological treatments, which aim at decreasing or distributing the loading across the knee joint. This mechanical joint loading has been related to cartilage degeneration, pain, and disease progression [190].

A common biomechanical treatment is gait retraining. Through these treatments patients learn and gradually adopt a modified gait pattern that results in decreased loading across the knee joint. [133, 84]. The training is typically achieved by tracking the body biomechanics and using this information to drive a real-time feedback modality, such as a vibration, an audio sound or a visualization pattern [191]. An advantage of gait retraining compared to other biomechanical treatments, such as use of wedge insoles, knee braces or canes, is that it does not require any additional devices to alter gait mechanics.

Knee joint loading can be quantified through the medial and lateral tibiofemoral contact forces [127]. Due to practical difficulties in measuring the internal knee contact forces in a non-invasive manner, the net knee joint moment has been considered a convenient surrogate measure [77]. However, instructing patients to decrease a complex kinetic parameter, such as the knee joint moment, in real-time, has been shown to be less effective than explicitly instructing the correct movement that achieves the decrease in the loading [132]. These findings are in line with previous studies which showed that higher reduction in the knee adduction moment can be achieved by altering related kinematic parameters, such as the foot progression angle (FPA) [131, 128, 192, 83, 124, 193, 81, 82].

Despite the demonstrated benefits of gait retraining, it is currently not used in clinical practice [194]. One of the primary reasons impeding clinical adoption is the expensive, complex, time-consuming, and space-bound instrumentation that is required to accurately assess the biomechanical parameters. Conventionally, a gait laboratory is utilized, in which multiple cameras track the three-dimensional positions of skin-mounted passive or active markers. Next, the segment positions and orientations are assessed through computational techniques such as direct or inverse kinematics [195, 153].

An ambulatory alternative to the lab-bounded measurement systems is composed of inertial measurement units (IMUs) that can derive orientation of a sensor in space [100]. Specifically, fusion of the accelerometer, gyroscope, and magnetometer signals and incorporation of a biomechanical model and external contact updates enable consistent drift-free motion capture [24, 33]. In addition, IMU-based systems are typically low cost, low power, highly portable, minimally obstructive, easily wearable, acceptable by older adults and therefore comprise an ideal alternative to facilitate the clinical translation of movement analysis systems. Despite their potential, to date, the use of IMUs in gait retraining applications for KOA has only received limited attention [196, 197]. Exploiting the advantages of IMUs, featuring high per-

5. Wearable Visual Feedback on Foot Progression Angle

formance and applicability, may remove the complexity of the current laboratory approaches, decrease the costs, and make treatments available to a larger number of patients.

Besides motion tracking, the second component required in gait retraining is the biofeedback. In a recent systematic review, studies using laboratory-based biofeedback to target knee joint loading either directly or indirectly were analyzed [198]. Most studies used visual feedback modes [133, 87, 120, 130, 82, 199, 200, 132, 161, 201] or multi-modal visual-tactile [137, 136], and less often solely tactile [202, 81, 203, 204] or auditory feedback [205]. Another review focusing on wearable sensing and feedback techniques reported that until recently, most studies utilizing wearable feedback incorporated primarily tactile modalities [191]. These devices are typically unobtrusive, but they act as on/off switches that can only convey binary information to the user. In addition, tactile feedback was reported to require longer training times for patients to converge to a target pattern, compared to visual feedback. [137] Wearable visual feedback was until recently challenging due to practical limitations. The conceptual and technical feasibility of wearable visual feedback for knee joint angle using two IMUs and a small screen on a smart-glass was demonstrated by Steuner *et al.* [206]. Recent advances in augmented reality (AR) headsets, such as the Microsoft HoloLens [207], allow the projection of virtual objects on the user's field of view, via head-worn screens. As a result, the wearable biofeedback setups can be enriched with quantitative information, which can not only convey whether the user is achieving the desired target range, but also quantify the difference from the target.

The overarching objective of this study was to develop and evaluate a wearable biofeedback system for gait retraining purposes, as an alternative to currently existing lab-bound setups. In order to achieve this, the first objective was to develop a wearable real-time visual feedback driven by FPAs calculated using input from a commercially available inertial motion capture system; utilizing accelerometers, gyroscopes, and magnetometers. We hypothesized that the proposed wearable system would provide accurate assessments in timing and magnitudes of the FPA when compared to a conventional optical motion capture laboratory setup. The second objective was to evaluate the feedback effectiveness of the wearable system reflected by the number of steps with FPA within a defined target range. We hypothesized that participants would perform equally well in achieving the desired FPAs using the wearable system, when compared to the established laboratory setup. It is envisioned that the proposed wearable setup may reduce the complexity of gait retraining and facilitate their transfer into routine clinical practice.

5.2 Methods

5.2.1 Subjects

Eleven (11) healthy volunteers (4 males, 7 females, age: 28.26 ± 4.55 years; height: 1.78 ± 0.10 m; weight: 77.91 ± 15.01 kg; body mass index (BMI): 24.50 ± 2.52 kg/m²) participated in the data collection performed at the Virtual Reality Laboratory of the VUmc Amsterdam. Subjects provided written informed consent prior to their voluntary participation in the study and after receiving detailed information

5.2. Methods

about the study. Ethical approval was provided by the Scientific and Ethical Review Board (Dutch: Vaste Commissie Wetenschap en Ethisiek - VCWE) of the Faculty of Behavior & Movement Sciences, VU University Amsterdam.

5.2.2 Instrumentation

Human movement analysis was performed in a Gait Real-time Analysis Interactive Lab (GRAIL, MOTEK BV, Amsterdam, NL) depicted in Figure 5.1. The GRAIL system is composed of a dual-belt instrumented treadmill with two full 6D force plates beneath each belt capturing at 1000 Hz. In addition, the system features a ten-camera system tracking 22 passive reflective markers at 100 Hz (Vicon, Oxford Metrics Group, Oxford, UK). Markers were placed on the following body locations according to the lower body configuration of Human Body Model 2: anterior and posterior superior iliac spine, medial and lateral femoral epicondyle, medial and lateral malleolus, second metatarsal, fifth metatarsal, calcaneus, lateral mid-shank, and lateral mid-thigh. To enable the laboratory feedback, a semi-cylindrical screen located anterior to the treadmill was utilized that projected an immersive virtual reality environment. Integration and control of the GRAIL components is enabled by the D-Flow software package [208], and real-time biomechanical modeling was performed through the Human Body Model (HBM) software package [120, 209].

Concurrently with the GRAIL measurements, Xsens MVN Awinda inertial motion capture system (Xsens Technologies BV, Enschede, NL)[210] was used with the lower body configuration. Seven Xsens MTw IMUs with dimensions 47 x 30 x 13 mm and orientation dynamic accuracy 0.75 deg RMS for roll/pitch and 1.5 deg for heading components were used. The full scales of the measurement units are $\pm 160m/s^2$ for the accelerometer, $\pm 2000deg/s$ for the gyroscope, and $\pm 1.9Gauss$ for the magnetometer [211]. Five IMUs were mounted on pelvis, thighs, and shanks using the accompanying Velcro straps and two IMUs were placed on feet by firmly tying them with the laces on each participant's own shoes. The software version of Xsens MVN Analyze 2018.0 was used to reconstruct the lower body kinematics at 60 Hz [33]. The software features consistent behavior, even at the presence of magnetic disturbances, making it suitable for use on a treadmill and any other environment regardless of its magnetic field homogeneity. Segment orientations were obtained through the software by applying the IMU-to-segment alignment, found using an a-priori-known upright pose (N-pose) performed by the subject during the calibration [149]. The second part of the calibration of Xsens MVN consisted of comfortable walking in a straight line for approximately 5 meters. The output of the Xsens MVN Analyze is three-dimensional positions and orientations of the modeled body segments, expressed in an external coordinate frame defined during the calibration [33].

To enable the wearable biofeedback, Microsoft HoloLens was used (Microsoft Corp., Redmond, WA, USA) [207]. This wearable augmented reality headset device is capable of projecting holograms (three-dimensional visualizations) in the environment of use. The biofeedback was developed as a Universal Windows Platform (UWP) application built in Unity 3D Game Engine version 5.6.2 (Unity Technologies SF, San Francisco, CA, USA), and receives kinematic input (packet size = 760 bytes) from Xsens MVN Analyze, in real-time, via User Datagram Protocol (UDP) at 30 Hz. Networking of the devices was configured via an access point (TP-Link

5. Wearable Visual Feedback on Foot Progression Angle

TL-WR802N, 300MBit/s, 2.4GHz), which was connected to the computer running Xsens MVN Analyze via Ethernet and to the Microsoft HoloLens via Wi-Fi. The components comprising the wearable biofeedback system are illustrated in Figure 5.2.

The biofeedback was visualized similarly on both laboratory and wearable screen, in accordance with a previous gait retraining study involving patients of KOA [132]. Figure 5.2 illustrates the wearable biofeedback setup, in which the feedback object is a blue cone with 2D orientation updated based on the FPA per step. The target object is an arrow placed behind the feedback cone, the color of which is updated depending on the agreement between the estimated and target FPA. More specifically, the color changes were based on the absolute difference between target and performed FPA: green when $|FPA\text{-target}| \leq 2^\circ$, yellow when $2^\circ < |FPA\text{-target}| \leq 5^\circ$, and red when $|FPA\text{-target}| > 5^\circ$. These are arbitrary chosen values, with the green range matching targets used in previous studies [204, 132, 201].

In the Microsoft HoloLens visualizations, billboarding and tag along features were added to the holograms to update their position, such that they would always face the user and only translate when they were entirely outside the user's field of view. These techniques ensure availability of the content at all times while minimizing the unpleasant effects of visualizations that are tightly coupled to the motion of the headset (head-locked content) [212].

For practical reasons, the Microsoft HoloLens application featured speech command capabilities to enable the initialization of the training protocol. Thus, right after the initialization of the treadmill belt, the researcher performing the experiment approached the subject who was already walking on the treadmill to provide the triggering key-phrase "go to mode zero" close to the microphone of the Microsoft HoloLens.

5.2.3 Experimental procedures

Subsequently, placement of the reflective markers and IMUs was performed, followed by calibration of Xsens MVN system. As a last preparation step, participants performed a T-pose and walked a few steps on the treadmill to anatomically calibrate the optical motion capture system.

The first series of experiments comprised treadmill walking at a preselected constant speed of 1.2 m/s for 13.5 minutes. An acclimatization period with no target was provided for one minute. Next, the following five target angles were projected in a random order, for two minutes each: 15, 10, 5 degrees toe-out, 0 degrees straight toes, and 5 degrees toe-in. Visual feedback on the performed FPA was provided on each performed step on the laboratory screen. Before any new target, a 30-second active rest period was provided, during which subjects kept walking without receiving any target.

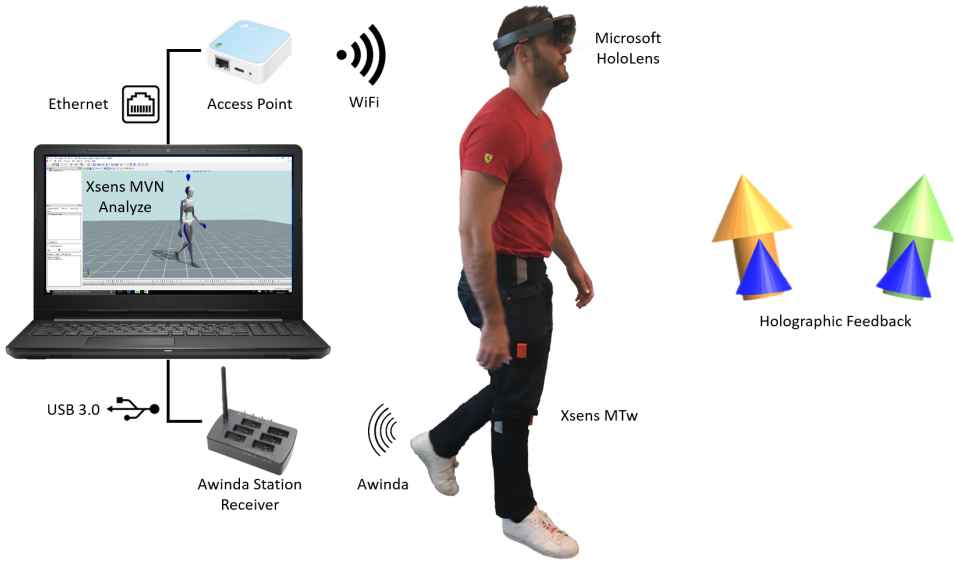
During the second series of experiments, participants wore the Microsoft HoloLens for a brief period to familiarize with the device. The complete protocol was repeated for another 13.5 minutes, by projecting the targets and IMU-driven feedback only on the wearable screen of the Microsoft HoloLens. An additional calibration step was introduced, where participants were asked to walk with their toes pointing straight for one minute to detect and reduce any heading offsets introduced by the inertial motion capture system. The average FPA estimated by the wearable system during

5.2. Methods

Figure 5.1: Virtual reality laboratory equipped with a GRAIL system. The subject receives a target foot progression angle (FPA) through an arrow, which changes color, from red to green, depending on the performed angle.



Figure 5.2: Wearable biofeedback setup. Xsens MVN Analyze receives the MTw sensor data via the Xsens Awinda Station, reconstructs the lower body kinematics, and streams via UDP. Microsoft HoloLens receives the kinematic input via Wi-Fi, calculates the foot progression angle, and updates the holographic feedback visualization.



this period was subtracted from the FPA values estimated in the rest of the trial. An example of the feedback protocol with the targeted and performed FPA values,

5. Wearable Visual Feedback on Foot Progression Angle

and the various modes across the full duration of the protocol is illustrated in Figure 5.4.

5.2.4 Computational procedures

The inertial motion capture system outputs global positions and orientations of the tracked body segments. The toe and heel positions are used to calculate the FPA of the i th step, when the foot is placed approximately horizontally on the treadmill belt. Assuming heel strike at initial foot contact, entire contact of a foot is identified at the timepoint when the magnitude of heel and toe velocities is close to zero, empirically found as the magnitude of the first derivative of toe position ($\dot{\mathbf{p}}_t$) and heel position ($\dot{\mathbf{p}}_h$), $|\dot{\mathbf{p}}_t| < 0.2 \text{ m/s}$ and $|\dot{\mathbf{p}}_h| < 0.2 \text{ m/s}$, respectively.

We define the foot vector for the i th step ($\mathbf{r}_{f,i}$) as the line from heel ($\mathbf{p}_{h,i}$) to toe ($\mathbf{p}_{t,i}$) during phase of entire foot contact:

$$\mathbf{r}_{f,i} = \mathbf{p}_{t,i} - \mathbf{p}_{h,i} \quad (5.1)$$

Similarly, the heading vector of the i th step ($\mathbf{r}_{w,i}$) is defined as the displacement vector between the position of the heel in two successive steps:

$$\mathbf{r}_{w,i} = \mathbf{p}_{h,i} - \mathbf{p}_{h,i-1} \quad (5.2)$$

FPA is calculated as the difference between the foot and the heading vectors projected on the transverse plane (Figure 5.3), defined by anterior (x) and lateral (y) axes:

$$\theta_{FP,i} = \arctan2\left(\frac{r_{w,i,x}}{r_{w,i,y}}\right) - \arctan2\left(\frac{r_{f,i,x}}{r_{f,i,y}}\right) \quad (5.3)$$

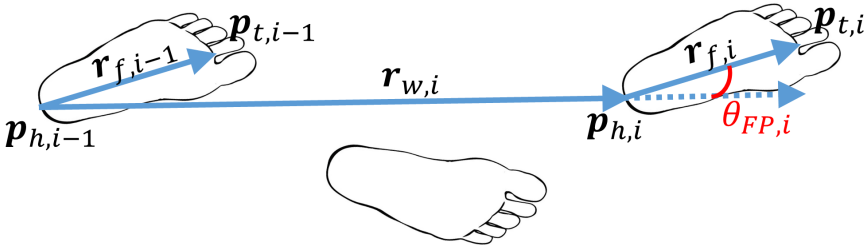
In the laboratory system, FPA is calculated and averaged within a time interval, when the vertical ground reaction force recorded by the respective plate, is greater than a threshold of 10N. Toe and heel positions correspond to the markers placed on the second metatarsal and calcaneus, respectively and the foot vector is calculated based on equation 5.1. Differently to the wearable system, the heading vector is constant and defined as the anterior axes of the lab coordinate system aligned with the belt of the treadmill.

5.2.5 Data Processing and Statistical Analysis

Data analysis focused on evaluating the performance of the wearable system in estimating FPA, in real-time versus the laboratory system, and to quantify the effectiveness of the two feedback modalities. Firstly, we compared the calculated FPA using the inertial motion capture system versus the optical motion capture system during the second series of experiments with the wearable feedback. The root-mean-squared differences were computed per target angle. Pearson's r^2 correlation and two-way random single measures intraclass correlation (ICC) were used to quantify the agreement and consistency between the two estimation systems. Secondly, we examined the effectiveness of the wearable biofeedback system versus the established laboratory solution in altering the user's FPA. To quantify the effectiveness, we analyzed the number and percentage of good steps, defined as the steps with FPA within the ± 2 degrees tolerance range as suggested in the literature [204, 136]. An

5.3. Results

Figure 5.3: Transverse caudal view of the feet, illustrating the calculation of the foot progression angle for the right foot. The foot progression angle (θ_{FP}) of the i th step is derived from the difference of foot vector (r_f) and heading vector (r_w). The latter two vectors are computed based on the positions of the heel (p_h) and toe (p_t) as illustrated in the figure.



analysis of variance (ANOVA) across all target conditions and systems, with Tukey's post-hoc analysis was performed to test whether the performed FPAs differ significantly across target conditions. Significance level was set to 0.05 and confidence interval at 95%. Data analysis was performed in MATLAB 2017a.

5.3 Results

Correlation and Bland-Altman plots are shown in Figure 5.5. Correlation coefficients were found of 0.9 for r^2 and of 0.94 for ICC. Accuracy analysis across all data points showed RMS difference of 2.38 degrees and level of agreement (LOA) about 4.7° between the wearable and laboratory estimates. Per target mode, RMS difference (average across subjects \pm standard deviation) was found to be 2.25 ± 1.10 , 2.18 ± 0.90 , 2.02 ± 0.90 , 2.62 ± 1.22 , 1.86 ± 0.73 degrees for target FPAs of -15, -10, -5, -0, and 5 degrees, respectively.

During the first minute of the wearable feedback session, when subjects were instructed to walk with straight toes, mean FPA values equaled $-1.61 \pm 2.47^\circ$ as recorded by the laboratory system, and $-1.96 \pm 2.91^\circ$ as recorded by the wearable system.

Figure 5.6 shows the box plots per target mode and per feedback scheme. The mean \pm standard deviations of the differences from the targets for the wearable feedback were $0.48 \pm 3.75^\circ$, $0.07 \pm 2.86^\circ$, $-0.46 \pm 2.57^\circ$, $-0.78 \pm 3.01^\circ$, $-0.83 \pm 3.97^\circ$ and for the laboratory feedback $1.04 \pm 3.44^\circ$, $0.28 \pm 3.13^\circ$, $-0.91 \pm 3.03^\circ$, $-1.20 \pm 3.07^\circ$, $-1.49 \pm 3.50^\circ$ for -15°, -10°, -5°, 0°, and 5° target FPA, respectively. In both systems multivariate ANOVA test showed significant differences between the FPAs of each target mode regardless of system used for the feedback, while post-hoc analysis across the five different modes showed that the FPAs during each target mode differed significantly to other target modes ($p < 0.001$).

Feedback effectiveness based on the percentage of good steps with FPA within the $\pm 2^\circ$ range is illustrated in Figure 5.7. Percentage of good steps in the laboratory

5. Wearable Visual Feedback on Foot Progression Angle

feedback was $51\pm15\%$ across 12033 steps over all subjects and targets. Per target percentage of good steps was found to be $42.7\pm13.2\%$, $52.7\pm12.2\%$, $58.6\pm15.5\%$, $54.5\pm18.7\%$, $46.3\pm15.7\%$ for FPAs of -15, -10, -5, 0, and 5 degrees, respectively. In the case of FPA feedback provided and calculated in the wearable setup, an overall percentage of good steps $48.3\pm12.8\%$ across 12075 steps was found. For the aforementioned ascending order of targets, effectiveness per mode was observed to be of $39.4\pm9.2\%$, $54.4\pm14.9\%$, $54.3\pm11.0\%$, $51.4\pm15.1\%$, $42.1\pm13.9\%$. When the FPAs of the wearable feedback were calculated from the optical motion capture system, the percentage of good steps was found overall $51.3 \pm 13.4\%$, with individual per mode effectiveness of $45.3\pm7.4\%$, $56.5\pm17.0\%$, $56.1\pm10.3\%$, $53.3\pm19.7\%$, $45.1\pm12.7\%$.

5.4 Discussion

In this study we proposed a method to perform gait retraining of the FPA using real-time biofeedback based entirely on wearable sensing and feedback modules. To our knowledge, this is the first study investigating a fully wearable visual feedback system for the purpose of retraining the FPA. Our findings demonstrated that FPA estimates derived from the inertial motion tracking input matched closely the ones from optical motion capture, with an overall RMS difference of 2.38 degrees. In addition, when incorporating a wearable augmented reality headset, the biofeedback effectiveness, based on steps within a $\pm 2^\circ$ target range, matched closely the laboratory approach.

Our accuracy analysis depends on an optical motion capture system reference. However, previous studies have indicated that orientations of the transverse plane may also suffer from inter-trial, inter-session, and inter-observer differences. In particular, for the foot heading angle, median within-assessor reliability across four studies [213, 214, 215, 216] was reported to provide multiple correlation coefficient of 0.55 [22]. In addition, the same systematic review discussed five other studies that reported inter-assessor standard deviation of the foot progression that ranged from 2 to 5 degrees [217, 218, 219, 220, 221]. These literature findings suggest that error magnitudes of around 2 degrees, as found in our study, are typically found in conventional optical motion capture systems, as a result of marker placement, computational method, measurement system accuracy and resolution, or observer's experience and skills. Therefore, given that these measurement errors are considered clinically acceptable, our method is sufficiently accurate in tracking FPA for the specific application.

In our study we used a sensor set of seven IMUs required by Xsens MVN software to track both positions and orientations of the feet and other lower body segments. A question arises whether fewer IMUs would suffice for this task. Related studies have proposed a set of one sensor per foot combined with a magneto-inertial sensor fusion algorithm to derive the FPA [222, 196]. Even though those studies noted no effect of magnetic disturbances in the estimates, it has been previously shown that inertial-magnetic motion tracking is affected by the homogeneity of the magnetic field [32]. In addition, the use on a treadmill, which typically contain several electromagnetic components beneath the belt, would create a non-homogeneous magnetic field. As a result, an approach heavily relying on magnetometers would suffer from orientation drift over time. The present study used the latest version of Xsens MVN software, which provides a consistent pose of the body regardless of magnetic disturbances

5.4. Discussion

Figure 5.4: Illustration of the right and left foot progression angles across the whole protocol, estimated at each entire foot contact via inertial (blue lines) or optical (red lines) motion capture input. An offset correction is calculated during the first 60 seconds when participants are instructed to walk with straight toes and applied after that. A unique random target is provided for 120 seconds (mid-point of green dashed lines indicating the $\pm 2^\circ$ good step range), after 30 seconds of no target (rest) period.

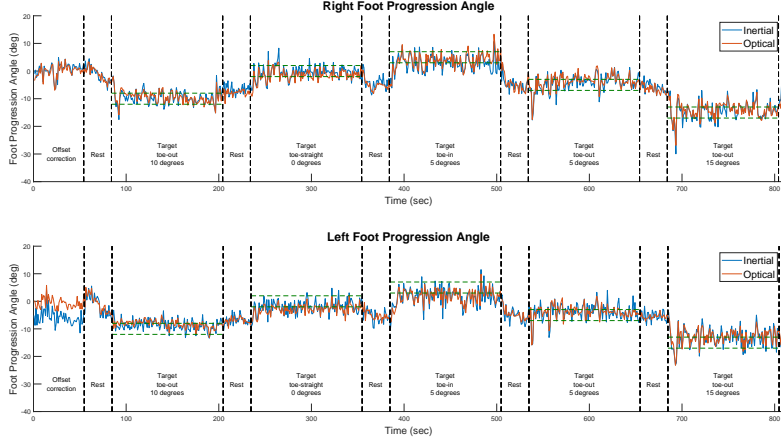
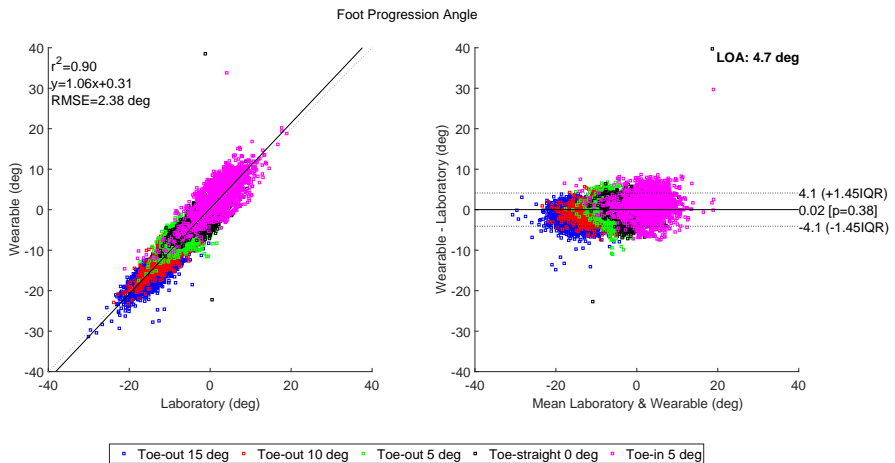


Figure 5.5: Correlation and Bland-Altman plots for the foot progression angle estimates based on the wearable and laboratory setup.



in the environment of use [33].

Calculation of the foot vector angle using both inertial and optical motion capture solutions may suffer from offsets of approximately 1-3 degrees, due to measurement and modeling error in both approaches. In inertial motion capture, offsets in the foot vector may be introduced as a result of a mismatch between the modeled and prac-

5. Wearable Visual Feedback on Foot Progression Angle

Figure 5.6: Box plot of all steps per target mode in the wearable and laboratory feedback. Green lines are the target limits of each mode.

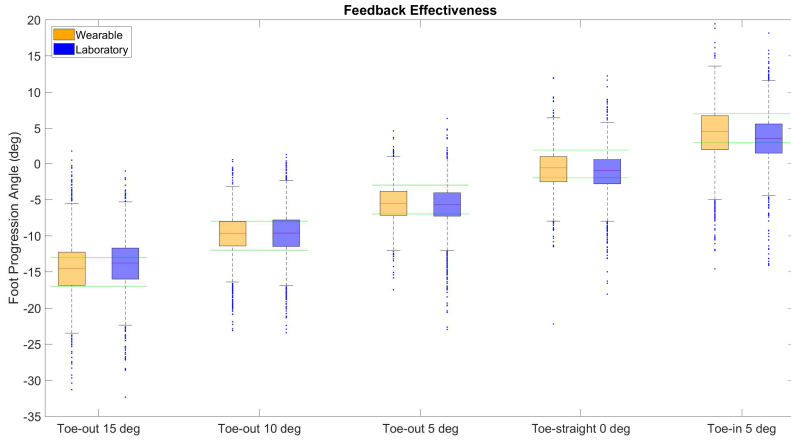
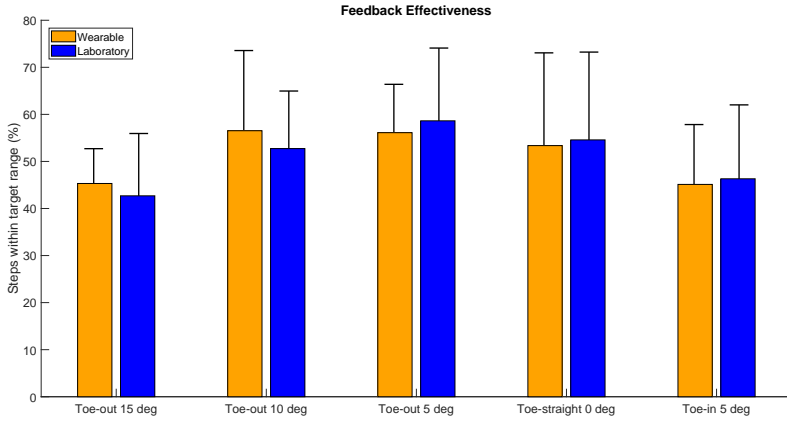


Figure 5.7: Bar plot illustrating the mean and standard deviation of the percentage of good steps (± 2 degrees from the target), across 11 subjects, for wearable (orange) and laboratory (blue) feedback setups.



ticed N-pose used to calibrate the system. Similarly, optical motion capture may be susceptible to sub-centimeter misplacement of the markers on the second metatarsal and calcaneus. For instance, misplacements of markers on the foot may result in erratic estimation of the foot vector. In the accuracy analysis we subtracted these offsets, based on the median FPA during the first one minute of the trial. Moreover, gait event detection methods differ between both systems and may introduce differences. The wearable system relies on detection of near-zero velocity to detect contact with the ground which may be sensitive to the walking speed and style.

5.4. Discussion

In contrast, the laboratory system is based on force plate detection, which may be erratic in real-time in case the subject steps on the contra-lateral force plate. In the offline analysis we have corrected for these cases, by calculating the gait events based on marker velocity. Another source of difference in the laboratory system is that for convenience, the heading vector was set constant, aligned with the anterior axis of the global coordinate system matching the movement direction of the belt. In other words, contrary to the wearable system, differences in walking direction are not taken into account in the FPA calculation of the laboratory system.

A major advantage of the proposed wearable system compared to laboratory-based setups is its significantly lower cost. Fully functional virtual reality laboratories typically cost between tens to hundreds thousand dollars, depending on the type of optical motion capture systems, instrumented treadmills, and immersive environment systems. The setup proposed in this study is composed of an augmented reality headset and inertial sensors. Current price of the development version of Microsoft HoloLens is around 3,000 dollars, while the cost of goods for inertial sensor components (accelerometer, gyroscope, and magnetometer) has nowadays dropped to a few tens of dollars per module. Additional costs may include the cost for networking devices, computers and software. Costs for software vary considerably and are therefore difficult to quantify, since they usually depend on development efforts, number of users and other market-driven factors [223].

Besides costs, the proposed method based on a set of IMUs and an AR headset reduces the complexity and increases the flexibility of gait retraining methods significantly compared to conventional laboratory techniques. Alternative approaches with lower cost and complexity have been previously proposed, even without the necessity for electronic equipment. For instance, mirror-based biofeedback for FPA retraining of patients with knee osteoarthritis has been investigated by Hunt *et al.* [199]. That study reported significantly lower performance of the mirror feedback compared to real-time visual biofeedback, with mean differences of approximately 2 degrees. However, despite the significantly lower performance of the mirror and given the high costs of laboratory-based biofeedback setups, the former was favored as an acceptable solution for clinical practice. Our work provides a method that matches closely the performance of laboratory feedback systems in terms of both tracking accuracy and feedback effectiveness, while reducing the costs and increasing the portability and potential of performing gait retraining in any environment. In addition, recent studies reported that subject-specific gait modifications decrease knee joint loading significantly more, compared to generalized targets [224]. Therefore, performance of motion tracking and biofeedback are both important factors in decreasing the loading of the joint, effectively in each individual patient.

The feedback effectiveness of both wearable and laboratory systems is affected by the arbitrary chosen value of $\pm 2^\circ$. This has been a point of discussion also by Chen *et al.* [204] when applying a vibrotactile feedback setup driven by marker-based motion capture. Further research is required to identify optimal thresholds for the green, yellow and red zones of the visualization. Moreover, in this study we have used visualization of the target and feedback values as arrows and cones able to rotate. Alternative visualizations such as in [120] should be examined to find the ideal visualization method for gait retraining of the FPA with visual biofeedback.

Inertial sensing and augmented reality technologies have both advanced vastly in the last years. Their unique combination enables not only applications of reha-

5. Wearable Visual Feedback on Foot Progression Angle

bilitation, such as gait retraining, but could potentially be expanded to other fields, such as live entertainment and gaming using input from a user's own body motion to drive graphics in a mixed reality environment. Devices such as the Microsoft HoloLens utilize a number of sensors to derive its own position and orientation in space. All heavy computations needed for self-localization and visualization of the holograms in space are executed standalone in real-time. In addition, these kinematic estimates can be fused with inertial motion capture to correct any position drift introduced by the latter, for instance due to errors in the measured segment lengths. The downsides of the first commercially available and latest to date version of the headset are that it is rather heavy (approx. 0.5 kg), bulky, and impractical for use in daily life. Moreover, the field of view is currently narrow. Upcoming developments in augmented reality headsets are expected to improve the functionality for potentially unobtrusive daily life use in the future.

We evaluated the method on a treadmill, however, the wearable setup enables the application of gait retraining in overground walking that differs in terms of gait mechanics and metabolic energy cost [225]. As discussed previously the use of more sensors may reduce the drift over time, however, the system may not be comfortable for uses of long duration during daily living. Further research towards magnetically immune motion tracking systems that require fewer sensors is necessary, to achieve reliable orientation estimates regardless the environmental conditions or movement performed. Leveraging the increased practicality of fewer sensors and consistent performance over time could enable daily life applications, requiring continuous monitoring of important kinematic parameters.

In our study, awareness of the distance from the FPA target was considered an important advantage of visual feedback with respect to alternative modalities, such as tactile and auditory. Wheeler *et al.* compared both visual and tactile feedback, reporting that despite both being equally effective, visual feedback required less time from subjects to converge to the targeted gait pattern. However, whether quantitative information can actually boost the feedback effectiveness remains unknown. Another advantage of visual feedback compared to other modes are the gamification prospects, which could motivate subjects to perform the training in a game-like fashion. Nevertheless, further comparison studies between various feedback modalities should be performed to assess the most effective and most engaging type of biofeedback.

In our study we examined the wearable sensing and feedback in a group of young healthy adults, similarly to previous studies evaluating experimental technology for gait retraining [133, 197, 120, 130, 161, 137, 136, 202, 204, 205, 226]. However, the eventual application is targeted to patients of KOA who are generally older and less familiar with technology. Further studies to evaluate the applicability of the system in patients with KOA is required. Potential issues that may be met with the current setup is the inability of patients to perform the N-pose due to increased static knee varus/valgus type malalignment with an unknown effect to the FPA estimate. Manual input of the joint angles performed during the static calibration trial may be an appropriate solution for this. Nevertheless, the portability of the system could facilitate applications initially in clinical environments with the help of a medical specialist, and subsequently for home use. In particular, such setup allows for increased number of training sessions, which may result in enhanced training retention over time. Moreover, combining such home retraining system with

5.5. Conclusion

telemedicine techniques could enable objective data for remote monitoring of the gait pattern of patients and identifying changes over time.

5.5 Conclusion

This study investigated the feasibility, accuracy, and effectiveness of combining a commercially available inertial motion capture system and an augmented reality headset to perform gait retraining to alter the FPA. The findings proved sufficient accuracy of the FPA estimates with the ones obtained from optical motion capture. At the same time, average feedback effectiveness based on number of steps within a $\pm 2^\circ$ range from the target was found around 50% for both setups. The proposed setup is completely wearable and enables gait retraining applications in clinical settings without the need for a complex gait motion analysis laboratory. For daily monitoring of FPA, further developments towards reduced sensor setups with immunity to magnetic disturbances are recommended.

5. Wearable Visual Feedback on Foot Progression Angle

Chapter 6

General Discussion

6.1 Overall Insights and Conclusions

In this thesis we have developed and evaluated a number of methodologies for gait analysis with a focus on kinetics, using inertial motion capture technology. The first three studies focused on estimation of kinetic quantities as a product of inertial motion capture input with biomechanical modeling. The fourth study examined a wearable feedback solution for gait retraining on the foot progression angle using an augmented reality headset, in order to alter the moments about the knee joint.

The first main objective of this thesis was to develop an ambulatory knee load estimation system, applicable in free-living environments, using input from inertial sensors. This objective was divided into three sub-questions. Firstly we asked whether we can estimate three-dimensional GRF&M during gait using only inertial sensor input. This question has been investigated in Chapter 2, where a solution based on inertial motion capture has been presented to derive the external loads. The performance of the technique was assessed using force plate measurements as a reference, and comparison of the same technique using optical motion capture was performed. For the vertical, anterior, and sagittal GRF&M components excellent correlation coefficients have been found, which showcased the potential of the technique for use in biomechanical analysis. Further development and investigation of the technique was performed in Chapter 3, focusing on the second question about knee joint moment assessment for variable gait patterns. We demonstrated that for several gait patterns it is possible to estimate knee moments and observe the variability induced by the gait patterns. In particular, we found that the uncertainty decreases when we look into the change in the moment values with respect to a baseline value, as a result of an altered gait pattern. The inertial-based knee moment estimation method is therefore adequately sensitive for distinguishing knee moments for these different gait patterns that are relevant in clinical practice. Chapter 4 looked into answering the third question of the first objective. The capabilities of inertial motion capture systems to estimate the movement, which serves as input to the existing highly-detailed musculoskeletal models was demonstrated. A solution to map the motion of the kinematic models of the inertial motion capture system and the musculoskeletal model using a virtual marker approach was validated. Given the motion, kinetics were predicted based on a physiologically inspired muscle-recruitment approach. Good agreement between three different models was demonstrated, one with solely inertial-derived kinematics and predicted ground reaction forces and moments, while the other two with optical-derived kinematics and either measured or predicted ground reaction forces and moments. Finally, Chapter 5 investigated the second objective of the thesis and the research questions related to it about the accuracy of motion tracking and effectiveness of a biofeedback solution. The kinematic estimates related to knee joint loading were fed in a real-time biofeedback application using a promising augmented reality headset. Visual feedback may convey more information than other modes, but so far its ambulatory application could not be realized due to the lack of suitable hardware. Recent advances in augmented reality headsets may solve this problem. Such devices can process input data from inertial sensors in real-time in order to translate them into a visual or audial feedback message to the user. In the study, we found that the effect of an established laboratory-based feedback solution is similar to our novel ambulatory

6.2. Sensors

solution, in momentarily changing the foot progression angle of 11 healthy subjects.

The studies described in this thesis showcase the large potential of ambulatory inertial motion capture in assessing both kinematic and kinetic estimates. The findings of each individual study are promising for future applications of the technology in daily life and clinical practice. Without any doubt, this research created many insights about not only the potential of inertial sensors, but also limitations of the approaches. In the next section, we discuss directions for future research, such as the number, type, and size of sensors as well as the required modelling and algorithms. Addressing these topics is essential to further improve the performance and applicability of the techniques for kinetics estimation and biofeedback, based on wearable inertial sensors.

6.2 Sensors

6.2.1 Number of Sensors

The methods presented in Chapters 2,3, and 4 of this thesis require full-body motion capture input derived from a relatively high number of 17 IMUs. Even though this setup is already more convenient than a marker-based setup, the number of sensors can make the application in continuous daily life use impractical. Intelligent computational algorithms based on optimization or machine learning show promising results for reducing the number of sensing models to derive full-body motion [165, 164, 227]. In general, full-body kinematics is necessary to estimate the external forces, but anthropometric parameters can play a major role in the contribution of each segment in the final external load estimates. For instance, segments with generally low weight (e.g. hands) or low range of motion with respect to the main segment (e.g. head or scapula segments with respect to the trunk) could be omitted in an attempt to reduce the number of required sensors. Further research should examine the minimum number of sensors required and what techniques can still maintain high performance, while facilitating the use of the system.

Similarly, the biofeedback application presented in Chapter 5 could benefit from using fewer sensors. The current lower-body setup of 7 sensors used is primarily due to the Xsens MVN software. In particular the real-time and drift-free use on a treadmill is made possible thanks to the recent advances of the Xsens MVN software, where motion data is used to compensate for the homogeneous magnetic field assumptions [33]. Other groups demonstrated the use of one sensor per foot to perform tracking of the foot progression angle [196], however heavy reliance on magnetometers may result in highly erratic measurements in a space with non-homogeneous magnetic field. Therefore, we recommend that future studies look further into modeling methods to derive the heading components of orientation from other sources rather than magnetic measurements [117]. Finally, incorporating the inertial sensors in a smart shoe is a promising next step for the clinical application of the technology [222].

Towards minimal sensing the question arises, whether we can derive full-body kinematics and kinetics from inertial sensors contained in devices that are already widely used, such as mobile phones and wrist-worn devices (smartwatches and fitness trackers). In a recent publication, Mousas demonstrated the use of one wrist- or

ankle-worn inertial sensor to reconstruct the full-body motion [228]. In another study, Holden *et al.* proposed a deep learning framework for synthesis of realistic human motion [229]. Such studies show promising findings for the use of a single conveniently worn sensor for reconstruction of the full-body movement. Besides the synthesis of realistically-looking motion, further work is necessary for the analysis of the variability in gait, which is important when examining pathological movement.

6.2.2 Types of Sensors

In Chapters 2, 3, and 4 of this thesis, we focused on estimating kinetic quantities using exclusively inertial sensor input using computational techniques and models. Incorporating data from other sensing sources may contribute to improved performance of both kinematic and kinetic estimates.

In terms of kinematics, lack of positional information in inertial measurements is a considerable drawback. For that reason, other types of sensors could be incorporated in order to assess more accurate estimates of position. Several examples of multi-sensor fusion for human movement analysis can be found in the literature. Weenk *et al* demonstrated an Extended Kalman Filter (EKF) to fuse measurements from foot-worn inertial and ultrasound sensors to assess relative positions of the feet [230]. Kortier *et al* proposed a setup with permanent magnets, in which magnetic and inertial measurements are fused to derive position and orientation of the hand segment with respect to the trunk [231]. Similarly, fusion methods based on an EKF were proposed for vision-aided inertial navigation [232]. In another study, a Global Navigation Satellite System (GNSS) was proposed to derive the trajectory of a skier, while the pose was derived from an inertial motion capture system [233]. In a non-ambulatory, but potentially convenient setup for clinical applications, Microsoft Kinect was integrated with inertial sensors to improve the joint angle estimates [234]. Alternatively, photodiode-based tracking was recently proposed for virtual reality applications [235]. Hybrid motion tracking systems could exploit the plurality of sensing information to improve kinematic estimates and decrease the dependency on modeling assumptions.

Regarding kinetics, incorporating force or pressure sensors in combination with the kinematic-based solution could improve the estimates. Our findings from Chapters 2 and 4 showed that the ground reaction moments in the frontal plane are the most challenging to assess. This moment is related to the center of pressure, which could potentially be more accurately obtained from in-shoe pressure insole measurements [236, 237]. In addition, foot pressure information could be used to solve the indeterminacy problem during the double support phase, which in this thesis was solved based on a gait event-based function in Chapters 2 and 3, and based on a dynamic-contact model in a musculoskeletal model in Chapter 4. Both methods require accurate assessment of the foot interaction with the ground, which could also be aided by in-shoe pressure information. In addition, new distribution models could be developed to map the measured foot pressure with the distribution of the GRF&M across the two feet. Integrating with in-shoe pressure insoles could remove the requirement for accurate upper body motion tracking and therefore result in a more convenient and possibly more accurate system. Ambulatory measurement of the GRF&M with the use of force and torque sensors has been proposed in the past [45, 47, 94]. However, the greatest limitation is the size and weight of the sensors

6.3. Modeling and Algorithms

that fulfill the range requirements of human motion. Further development efforts should be put towards less heavy and bulky force sensors [238, 239], which will be applicable for dynamic movements and will not influence the natural movement pattern [49].

6.2.3 Size and Power Autonomy of Sensors

In the last decades, the breakthrough in MEMS technology has enabled the miniaturization of previously heavy and bulky inertial sensors. Currently the size and power consumption of the sensors is continuously decreasing each year. Similar decreases in the size of batteries could potentially make possible unobtrusive continuous monitoring of movement in daily life. In addition, home and daily life application could benefit from energy harvesting technologies that have shown great potential in the recent years for powering up wearable devices [240, 241]. For instance, captured energy from various sources, such as solar [242], thermal [243], or kinetic [244] energy, could power small and fully autonomous wearable sensors. Finally, a significant step towards realization of motion wearables would be to incorporate the MEMS sensors into clothing. That would make human movement analysis technology completely seamless and more practical for daily life use.

6.3 Modeling and Algorithms

6.3.1 Subject-specific Anthropometry

Estimating kinetics based on kinematics requires knowledge of the mass and inertia values of each segment. In the context of this thesis, this was achieved via distribution of the person's mass using ratios found in generic anthropometric tables in the literature [107, 37]. In fact, age, sex, ethnicity, and body type may affect the estimates [245]. Camomilla *et al* reported that inertial parameter estimation are one of the least important sources of error in bottom-up inverse dynamics to assess joint moments [246]. However, this is not the case in top-down inverse dynamics as the ones used in this thesis. As demonstrated by the sensitivity analysis of Ren *et al* [39], the masses of the heaviest body segments, such as the thighs and torso, would contribute to considerable errors in kinetic estimates in a whole-body inverse dynamic technique. In contrast, discrepancies in radii of gyration would not be of significance in the estimation of moments. Therefore, in terms of segment mass parameters, a subject-specific approach could potentially improve the kinetic estimates. Commonly, hydrostatic weighting approaches (also known as water immersion) are used to derive the mass properties of a living body. In these techniques, the body segments are submerged step by step further into water, with the increase in water level measurements used to derive these quantities [247]. However, a more practical approach to derive the inertial parameters based on the volume of the segments could make use of three-dimensional scanning technologies [248]. Incorporating estimates of the subject's body composition measurements (e.g. fat, water, muscle percentage) could further facilitate the subject-specific assessment of the inertial parameters of the segments.

The segment lengths of the biomechanical model are manually measured with a

conventional tape and input in the motion capture system. This step may introduce errors in the position estimates of the inertial motion capture system. However, errors in segment lengths are also present in optical motion capture-based approaches, and only medical imaging-based estimates can provide a gold standard reference [249]. Therefore, in subject-specific models inputs from magnetic resonance images (MRI) or CT scans could be used to improve the input of the system. Moreover, Crabolu *et al.* demonstrated methods based on inertial measurements to estimate the joint center of rotation with potential application in deriving lengths of segments [250, 251].

6.3.2 Idealization of Biomechanical Models

All studies in this thesis utilized biomechanical models with several rigid-body and joint constraint assumptions. However, it is known that in reality, human body segments cannot be simply assumed to be linked by spherical, revolute or universal joints, but in many cases can also translate in three axes. These idealizations are introduced to decrease further errors in inertial and optical motion capture-derived kinematics that track the motion of the skin, rather than the bone. Applications that require very accurate movement tracking of the bones, in the tibiofemoral joint for example, could benefit from techniques in force-dependent kinematics [160, 252] or ultrasound-based bone motion tracking [253].

6.3.3 Sensor-to-Segment Calibration

The inertial motion capture system used in this thesis (Xsens MVN [104]) uses a sensor to segment calibration procedure based on a static upright pose, also called N-pose across the thesis. During this pose, it is assumed that the body segments have *a priori* known orientations. Despite the general agreement it may be difficult for a subject to perform that pose exactly as it is modelled, and therefore offsets may be introduced. In fact, this technique may introduce differences in the comparison to optical motion capture systems where commonly calibration based on anatomical landmarks from marker positions is used to derive the segment frames [109, 110]. In order to improve the definition of segment frames, functional calibration techniques could be used [254]. However, these methods typically apply only on finding the axes of joints with predominant motion across a plane, such as the mediolateral axis in the case of the knee joint. Therefore, the use of functional calibration may not be suitable for all joints and segments of the biomechanical model.

An approach that may improve this problem would be to manually input the initial orientations from digital photographs [255, 256] or from manual goniometer measurements [86]. However, this approach is also not error-free, since camera-based systems are known to be unreliable in the non-sagittal plane kinematics [22], while accuracy of goniometry may be influenced by the assessor's experience.

6.3.4 Consistent Inertial and Magnetic Motion Tracking

Tracking the human body motion with inertial and magnetic measurements is a field that has advanced quickly over the last two decades. Yet, the use of magnetic measurements is usually compromising the quality of the kinematic output and making

6.4. Biofeedback

it reliable only in environments with a homogeneous magnetic field [117, 32]. The latest version of the commercial Xsens MVN software, has shown promising results in reducing the effect of magnetic disturbances radically, providing full magnetic immunity to the technology. However, a large validation study across several subjects, movements and environments with various conditions is needed to better demonstrate the significance of this development. Further future developments in this field may utilize statistical models for sensor fusion, to maximize the quality of kinematics, regardless of environment of use [33].

6.4 Biofeedback

In Chapter 5 we proposed a real-time visual biofeedback system using an augmented reality headset. The potential of such devices is huge for biofeedback driven by one's own motion. Several features of the application presented in the study can be improved. For example the visualization of the feedback objects as well as their position in space could be optimized for a better user experience. The current validated version is especially tailored for treadmill applications. However, the wearable setup enables ambulatory overground application gait retraining. Minor adjustments in the visualization to provide smooth projection of holograms to the user while moving in space would be required.

Multimodal feedback was reported in the past to be the most effective [136]. Therefore, including additional audio and haptic feedback in the setup would be a step to make this wearable gait retraining application even more effective.

6.5 Towards healthcare application and beyond in the internet of moving things

Despite the challenges, there is no doubt that the future of healthcare can vastly benefit from wearable sensor data [257], regardless of their nature; heart rate, sleep duration and quality, step count and physical activity, or movement quality. However, before we reach the point of actual application we need to firstly ensure the highest quality possible to minimize the chance for erratic clinical decisions. Secondly, sensing setups should become less obstructive [258] in order to be applied in continuous daily life monitoring.

The internet of moving things is gradually evolving in many aspects; intelligent algorithms with few, low-power, low-cost, high-performance, miniature sensors incorporated into clothes could soon enable a completely seamless application of wearables. In this sense, motion and force data can be valuable for various purposes, including, but not limited to injury prevention, sports performance maximization, and rehabilitation. To reach that point and transfer the application of human movement analysis from artificial lab-like spaces to realistic daily life environments, further academic and industrial research is required.

6.6 Concluding Remarks

In this thesis, we have demonstrated the potential of inertial measurement units to obtain not only kinematics, but also kinetics of human movement (i.e. ground and joint reaction forces and moments). In addition, we have developed and evaluated a real-time wearable visual feedback setup to provide biofeedback on knee-load related kinematics i.e. foot progression angle.

To our knowledge, this was the first attempt to design and validate tools that leverage exclusively inertial sensor technology to assess complete ground reaction forces and moments during gait (Chapter 2), net knee joint moment variability in gait modifications (Chapter 3), and drive the kinematics of a musculoskeletal model capable of predicting internal loads (Chapter 4). Subsequently, in Chapter 5, we developed and evaluated the first ever fully-wearable visual biofeedback system for training the foot progression angle, with implications for applications of gait retraining in knee osteoarthritis.

The approaches presented in this thesis are valuable due to the fact that kinetics are predicted or inferred with no additional hardware costs on top of the kinematic sensors. In the discussion, we indicated a number of limitations of the current approaches and topics that could individually become the focus of future research, to reach both seamless and high performance ambulatory assessments, that will facilitate routine clinical adoption of human movement analysis.

Bibliography

- [1] Klette, R., Tee, G.: Understanding human motion: A historic review. In: Human Motion, pp. 1–22. Springer (2008) (Cited on page 3).
- [2] Αριστοτέλης: Ἀπαντα 20, Περὶ Ζώων Μορίων Δ, Περὶ Ζώων Κινήσεως, Περὶ Πορείας Ζώων. Κάκτος (1994) (Cited on page 3).
- [3] Aristotle: Aristotle: Parts of Animals. Movement of Animals. Progression of Animals (Loeb Classical Library No. 323). Harvard University Press (1937) (Cited on page 3).
- [4] Αρχιμήδης: Ἀπαντα 3, Επιπέδων Ισορροπιῶν, Ψαμμίτης, Τετραγωνισμός Παραβολής, Περὶ Των Οχουμένων. Κάκτος (2001) (Cited on page 3).
- [5] Archimedes: The Works of Archimedes (Dover Books on Mathematics). Dover Publications (2002) (Cited on page 3).
- [6] da Vinci, L., Richter, I.A., Kemp, M., Wells, T.: Leonardo da Vinci: Notebooks. Oxford World's Classics. Oxford University Press, USA (2008) (Cited on page 3).
- [7] Borelli, G.-A.: De Motu Animalium, (1680) (Cited on pages 3 and 4).
- [8] Newton, S. Isaac: Philosophiae Naturalis Principia Mathematica. Jussu Societatis Regiae ac Typis Josephi Streeter. Prostat apud plures bibliopolas (1687) (Cited on page 3).
- [9] da Vinci, L.: Leonardo's Anatomical Drawings (Dover Art Library). Dover Publications (2004) (Cited on page 4).
- [10] Hamill, J., Knutzen, K., Derrick, T.: Biomechanical Basis of Human Movement. LWW (2014) (Cited on page 5).
- [11] Beggs, J.S.: Kinematics. CRC Press (1983) (Cited on page 5).
- [12] Richards, J.: Biomechanics in Clinic and Research: An Interactive Teaching and Learning Course, 1e. Churchill Livingstone (2008) (Cited on pages 5 and 9).
- [13] Cappozzo, A., Della Croce, U., Leardini, A., Chiari, L.: Human movement analysis using stereophotogrammetry: Part 1: theoretical background. Gait & posture **21**(2), 186–196 (2005) (Cited on pages 5 and 43).

- [14] Corazza, S., Muendermann, L., Chaudhari, A., Demattio, T., Cobelli, C., Andriacchi, T.P.: A markerless motion capture system to study musculoskeletal biomechanics: visual hull and simulated annealing approach. *Annals of biomedical engineering* **34**(6), 1019–1029 (2006) (Cited on page 5).
- [15] Pfister, A., West, A.M., Bronner, S., Noah, J.A.: Comparative abilities of microsoft kinect and vicon 3d motion capture for gait analysis. *Journal of medical engineering & technology* **38**(5), 274–280 (2014) (Cited on page 5).
- [16] Fernández-Baena, A., Susín, A., Lligadas, X.: Biomechanical validation of upper-body and lower-body joint movements of kinect motion capture data for rehabilitation treatments. In: Intelligent Networking and Collaborative Systems (INCoS), 2012 4th International Conference On, pp. 656–661 (2012). IEEE (Cited on page 5).
- [17] Choppin, S., Lane, B., Wheat, J.: The accuracy of the microsoft kinect in joint angle measurement. *Sports Technology* **7**(1-2), 98–105 (2014). doi:10.1080/19346182.2014.968165 (Cited on page 5).
- [18] Eltoukhy, M., Kelly, A., Kim, C.-Y., Jun, H.-P., Campbell, R., Kuenze, C.: Validation of the microsoft kinect® camera system for measurement of lower extremity jump landing and squatting kinematics. *Sports Biomechanics* **15**(1), 89–102 (2016). doi:10.1080/14763141.2015.1123766 (Cited on page 5).
- [19] Eichelberger, P., Ferraro, M., Minder, U., Denton, T., Blasimann, A., Krause, F., Baur, H.: Analysis of accuracy in optical motion capture – a protocol for laboratory setup evaluation. *Journal of Biomechanics* **49**(10), 2085–2088 (2016). doi:10.1016/j.jbiomech.2016.05.007 (Cited on page 6).
- [20] Aurand, A.M., Dufour, J.S., Marras, W.S.: Accuracy map of an optical motion capture system with 42 or 21 cameras in a large measurement volume. *Journal of Biomechanics* **58**, 237–240 (2017). doi:10.1016/j.jbiomech.2017.05.006 (Cited on page 6).
- [21] OptiTrack - General FAQs. <http://optitrack.com/support/faq/general.html/>. (Accessed on 03/04/2018) (Cited on page 6).
- [22] McGinley, J.L., Baker, R., Wolfe, R., Morris, M.E.: The reliability of three-dimensional kinematic gait measurements: a systematic review. *Gait & posture* **29**(3), 360–369 (2009) (Cited on pages 6, 56, 82, and 94).
- [23] Chiari, L., Croce, U.D., Leardini, A., Cappozzo, A., Chiari, L., Croce, U.D., Cappozzo, A., Della Croce, U., Leardini, A., Chiari, L., Cappozzo, A.: Human movement analysis using stereophotogrammetry. *Gait & Posture* **21**(2), 226–237 (2005). doi:10.1016/j.gaitpost.2004.04.004 (Cited on pages 6, 37, and 67).
- [24] Roetenberg, D., Luinge, H., Slycke, P.: Xsens MVN: full 6DOF human motion tracking using miniature inertial sensors. Xsens Motion Technologies BV, Tech. Rep (March 2016) (2009) (Cited on pages 6, 20, 21, 24, 37, 44, 59, 60, and 75).
- [25] Roetenberg, D.: Inertial and Magnetic Sensing of Human Motion. University of Twente [Host] (2006) (Cited on page 8).

- [26] Sabatini, A.M.: Quaternion-based extended kalman filter for determining orientation by inertial and magnetic sensing. *IEEE Transactions on Biomedical Engineering* **53**(7), 1346–1356 (2006) (Cited on page 8).
- [27] Roetenberg, D., Luinge, H.J., Baten, C.T.M., Veltink, P.H.: Compensation of magnetic disturbances improves inertial and magnetic sensing of human body segment orientation. *IEEE Transactions on Neural Systems and Rehabilitation Engineering* **13**(3), 395–405 (2005). doi:10.1109/TNSRE.2005.847353 (Cited on pages 8, 22, 59, and 60).
- [28] Roetenberg, D., Baten, C.T.M., Veltink, P.H.: Estimating body segment orientation by applying inertial and magnetic sensing near ferromagnetic materials. *IEEE Transactions on Neural Systems and Rehabilitation Engineering* **15**(1), 469–471 (2007). doi:10.1109/TNSRE.2007.903946 (Cited on page 8).
- [29] Hol, J.D., Bellusci, G.: No Title. *Inertial Motion Capture Calibration* (2016) (Cited on page 8).
- [30] Bachmann, E.R., Duman, I., Usta, U., McGhee, R.B., Yun, X., Zyda, M.: Orientation tracking for humans and robots using inertial sensors. In: Computational Intelligence in Robotics and Automation, 1999. CIRA'99. Proceedings. 1999 IEEE International Symposium On, pp. 187–194 (1999). IEEE (Cited on page 8).
- [31] Skog, I., Hänel, P., Nilsson, J.-O., Rantakokko, J.: Zero-velocity detection — an algorithm evaluation. *IEEE transactions on bio-medical engineering* **57**(11), 2657–2666 (2010). doi:10.1109/TBME.2010.2060723 (Cited on page 8).
- [32] De Vries, W., Veeger, H., Baten, C., Van Der Helm, F.: Magnetic distortion in motion labs, implications for validating inertial magnetic sensors. *Gait & posture* **29**(4), 535–541 (2009) (Cited on pages 8, 37, 82, and 95).
- [33] Schepers, H.M., Giuberti, M., Bellusci, G.: Xsens MVN: Consistent Tracking of Human Motion Using Inertial Sensors (Cited on pages 8, 75, 77, 83, 91, and 95).
- [34] Whittaker, E.T.: *A Treatise on the Analytical Dynamics of Particles and Rigid Bodies* (Cambridge Mathematical Library). Cambridge University Press (1989) (Cited on page 8).
- [35] Zatsiorsky, V.: *Kinetics of Human Motion*. Human Kinetics (2002) (Cited on page 9).
- [36] Perry, J., Burnfield, J.: *Gait Analysis: Normal and Pathological Function*. Slack Incorporated (2010) (Cited on page 9).
- [37] Winter, D.A.: *Biomechanics and Motor Control of Human Movement - Fourth Edition* vol. 2nd, p. 383 (2009). doi:10.1002/9780470549148 (Cited on pages 9, 19, 26, 43, 46, 59, 63, and 93).
- [38] Challis, J.H.: The variability in running gait caused by force plate targeting. *Journal of Applied Biomechanics* **17**(1), 77–83 (2001) (Cited on pages 9 and 59).

- [39] Ren, L., Jones, R.K., Howard, D.: Whole body inverse dynamics over a complete gait cycle based only on measured kinematics. *Journal of Biomechanics* **41**(12), 2750–2759 (2008). doi:10.1016/j.jbiomech.2008.06.001 (Cited on pages 9, 10, 19, 24, 25, 26, 28, 33, 35, 36, 43, 46, 47, 49, 55, 59, 60, 64, and 93).
- [40] Oh, S.E., Choi, A., Mun, J.H.: Prediction of ground reaction forces during gait based on kinematics and a neural network model. *Journal of Biomechanics* **46**(14), 2372–2380 (2013). doi:10.1016/j.jbiomech.2013.07.036 (Cited on pages 9, 10, 19, 33, 35, 36, 43, and 59).
- [41] Choi, A., Lee, J.-M., Mun, J.H.: Ground reaction forces predicted by using artificial neural network during asymmetric movements. *International Journal of Precision Engineering and Manufacturing* **14**(3), 475–483 (2013). doi:10.1007/s12541-013-0064-4 (Cited on pages 9, 10, 19, 43, and 59).
- [42] Fluit, R., Andersen, M.S., Kolk, S., Verdonschot, N., Koopman, H.F.J.M.: Prediction of ground reaction forces and moments during various activities of daily living. *Journal of Biomechanics* **47**(10), 2321–2329 (2014). doi:10.1016/j.jbiomech.2014.04.030 (Cited on pages 9, 10, 19, 28, 33, 35, 36, 43, 44, 47, 59, and 70).
- [43] Skals, S., Jung, M.K., Damsgaard, M., Andersen, M.S.: Prediction of ground reaction forces and moments during sports-related movements. *Multibody System Dynamics*, 1–21 (2016). doi:10.1007/s11044-016-9537-4 (Cited on pages 9, 10, 19, 43, 44, 59, 64, and 70).
- [44] Shahabpoor, E., Pavic, A.: Measurement of walking ground reactions in real-life environments: A systematic review of techniques and technologies. *Sensors* **17**(9) (2017) (Cited on pages 10 and 43).
- [45] Veltink, P.H., Liedtke, C., Droog, E., Van Der Kooij, H.: Ambulatory measurement of ground reaction forces. *IEEE Transactions on Neural Systems and Rehabilitation Engineering* **13**(3), 423–427 (2005). doi:10.1109/TNSRE.2005.847359 (Cited on pages 10, 19, 43, 59, and 92).
- [46] Liu, T., Inoue, Y., Shibata, K.: A wearable ground reaction force sensor system and its application to the measurement of extrinsic gait variability. *Sensors* **10**(11), 10240–10255 (2010). doi:10.3390/s101110240 (Cited on pages 10 and 43).
- [47] Schepers, H.M., Koopman, H.F.J.M., Veltink, P.H.: Ambulatory assessment of ankle and foot dynamics. *IEEE Transactions on Biomedical Engineering* **54**(5), 895–902 (2007). doi:10.1109/TBME.2006.889769 (Cited on pages 10, 19, 43, 59, and 92).
- [48] Liedtke, C., Fokkenrood, S.a.W., Menger, J.T., van der Kooij, H., Veltink, P.H.: Evaluation of instrumented shoes for ambulatory assessment of ground reaction forces. *Gait and Posture* **26**(1), 39–47 (2007). doi:10.1016/j.gaitpost.2006.07.017 (Cited on pages 10, 19, 43, and 59).
- [49] Van Den Noort, J., Van Der Esch, M., Steultjens, M.P., Dekker, J., Schepers, M., Veltink, P.H., Harlaar, J.: Influence of the instrumented force shoe on

- gait pattern in patients with osteoarthritis of the knee. Medical and Biological Engineering and Computing **49**(12), 1381–1392 (2011). doi:10.1007/s11517-011-0818-z (Cited on pages 10, 19, 43, 59, and 93).
- [50] Savelberg, H.H.C.M., Lange, A.L.H.d.: Assessment of the horizontal, fore-aft component of the ground reaction force from insole pressure patterns by using artificial neural networks. Clinical Biomechanics **14**(8), 585–592 (1999). doi:10.1016/S0268-0033(99)00036-4 (Cited on pages 10 and 43).
- [51] Forner-Cordero, A., Koopman, H.J.F.M., van der Helm, F.C.T.: Inverse dynamics calculations during gait with restricted ground reaction force information from pressure insoles. Gait & Posture **23**(2), 189–199 (2006). doi:10.1016/j.gaitpost.2005.02.002 (Cited on pages 10 and 43).
- [52] Fong, D.T.-P., Chan, Y.-Y., Hong, Y., Yung, P.S.-H., Fung, K.-Y., Chan, K.-M.: Estimating the complete ground reaction forces with pressure insoles in walking. Journal of Biomechanics **41**(11), 2597–2601 (2008) (Cited on pages 10 and 43).
- [53] Rouhani, H., Favre, J., Crevoisier, X., Aminian, K.: Ambulatory assessment of 3D ground reaction force using plantar pressure distribution. Gait and Posture **32**(3), 311–316 (2010). doi:10.1016/j.gaitpost.2010.05.014 (Cited on pages 10, 19, 43, and 59).
- [54] Jung, Y., Jung, M., Lee, K., Koo, S.: Ground reaction force estimation using an insole-type pressure mat and joint kinematics during walking. Journal of Biomechanics **47**(11), 2693–2699 (2014). doi:10.1016/j.jbiomech.2014.05.007 (Cited on pages 10, 19, 43, and 59).
- [55] Sim, T., Kwon, H., Oh, S.E., Joo, S.-B., Choi, A., Heo, H.M., Kim, K., Mun, J.H.: Predicting complete ground reaction forces and moments during gait with insole plantar pressure information using a wavelet neural network. Journal of biomechanical engineering **137**(9), 091001 (2015) (Cited on pages 10 and 43).
- [56] Low, D.C., Dixon, S.J.: Footscan pressure insoles: Accuracy and reliability of force and pressure measurements in running. Gait and Posture **32**(4), 664–666 (2010). doi:10.1016/j.gaitpost.2010.08.002 (Cited on pages 10, 19, 43, and 59).
- [57] Sinusas, K.: Osteoarthritis: diagnosis and treatment. American family physician **85**(1) (2012) (Cited on page 12).
- [58] Guccione, A.A., Felson, D.T., Anderson, J.J., Anthony, J.M., Zhang, Y., Wilson, P., Kelly-Hayes, M., Wolf, P.A., Kreger, B.E., Kannel, W.B.: The effects of specific medical conditions on the functional limitations of elders in the framingham study. American journal of public health **84**(3), 351–358 (1994) (Cited on page 12).
- [59] Chronic diseases and health promotion. <http://www.who.int/chp/topics/rheumatic/en/>. (Accessed on 04/15/2018) (Cited on page 12).

- [60] Bitton, R.: The economic burden of osteoarthritis. *The American journal of managed care* **15**(8 Suppl), 230–5 (2009) (Cited on page 12).
- [61] Brooks, P.M.: Impact of osteoarthritis on individuals and society: how much disability? social consequences and health economic implications. *Current opinion in rheumatology* **14**(5), 573–577 (2002) (Cited on page 12).
- [62] Carr, A.J.: Beyond disability: measuring the social and personal consequences of osteoarthritis. *Osteoarthritis and Cartilage* **7**(2), 230–238 (1999) (Cited on page 12).
- [63] Blixen, C.E., Kippes, C.: Depression, social support, and quality of life in older adults with osteoarthritis. *Journal of Nursing Scholarship* **31**(3), 221–226 (1999) (Cited on page 12).
- [64] Johnson, V.L., Hunter, D.J.: The epidemiology of osteoarthritis. *Best practice & research Clinical rheumatology* **28**(1), 5–15 (2014) (Cited on page 12).
- [65] Statistics on regional population projections. http://ec.europa.eu/eurostat/statistics-explained/index.php/Statistics_onRegional_population_projections#An_aging_society_in_the_EU. (Accessed on 04/15/2018) (Cited on page 12).
- [66] OECD Obesity Update 2017. <http://www.oecd.org/health/obesity-update.htm> (Cited on page 12).
- [67] Felson, D.T., Anderson, J.J., Naimark, A., Walker, A.M., Meenan, R.F.: Obesity and knee osteoarthritis: the framingham study. *Annals of internal medicine* **109**(1), 18–24 (1988) (Cited on page 12).
- [68] Cushnaghan, J., Dieppe, P.: Study of 500 patients with limb joint osteoarthritis. i. analysis by age, sex, and distribution of symptomatic joint sites. *Annals of the rheumatic diseases* **50**(1), 8 (1991) (Cited on page 12).
- [69] Egloff, C., Hügle, T., Valderrabano, V.: Biomechanics and pathomechanisms of osteoarthritis. *Swiss Med Wkly* **142**(0) (2012) (Cited on page 12).
- [70] Yusuf, E.: Pharmacologic and non-pharmacologic treatment of osteoarthritis. *Current Treatment Options in Rheumatology* **2**(2), 111–125 (2016). doi:10.1007/s40674-016-0042-y (Cited on page 12).
- [71] Rönn, K., Reischl, N., Gautier, E., Jacobi, M.: Current surgical treatment of knee osteoarthritis. *Arthritis* **2011** (2011) (Cited on page 12).
- [72] Crawford, D.C., Miller, L.E., Block, J.E.: Conservative management of symptomatic knee osteoarthritis: a flawed strategy? *Orthopedic reviews* **5**(1) (2013) (Cited on page 12).
- [73] McAlindon, T.E., Bannuru, R., Sullivan, M., Arden, N., Berenbaum, F., Bierma-Zeinstra, S., Hawker, G., Henrotin, Y., Hunter, D., Kawaguchi, H., et al.: OARSI guidelines for the non-surgical management of knee osteoarthritis. *Osteoarthritis and cartilage* **22**(3), 363–388 (2014) (Cited on page 12).

- [74] Conaghan, P.G., Dickson, J., Grant, R.L.: Guidelines: care and management of osteoarthritis in adults: summary of nice guidance. *BMJ: British Medical Journal* **336**(7642), 502 (2008) (Cited on pages 12 and 75).
- [75] Guilak, F.: Biomechanical factors in osteoarthritis. *Best practice & research Clinical rheumatology* **25**(6), 815–823 (2011) (Cited on page 12).
- [76] Vincent, K.R., Conrad, B.P., Fregly, B.J., Vincent, H.K.: The pathophysiology of osteoarthritis: a mechanical perspective on the knee joint. *PM&R* **4**(5), 3–9 (2012) (Cited on page 12).
- [77] Zhao, D., Banks, S.A., Mitchell, K.H., D'Lima, D.D., Colwell, C.W., Fregly, B.J.: Correlation between the knee adduction torque and medial contact force for a variety of gait patterns. *Journal of Orthopaedic Research* **25**(6), 789–797 (2007). doi:10.1002/jor.20379 (Cited on pages 12, 43, and 75).
- [78] Kutzner, I., Trepczynski, A., Heller, M.O., Bergmann, G.: Knee adduction moment and medial contact force-facts about their correlation during gait. *PLoS ONE* **8**(12), 8–15 (2013). doi:10.1371/journal.pone.0081036 (Cited on pages 12 and 43).
- [79] Walter, J.P., D'Lima, D.D., Colwell, C.W., Fregly, B.J.: Decreased knee adduction moment does not guarantee decreased medial contact force during gait. *Journal of Orthopaedic Research* **28**(10), 1348–1354 (2010). doi:10.1002/jor.21142 (Cited on pages 12 and 55).
- [80] Fregly, B.J., D'Lima, D.D., Colwell, C.W.: Effective gait patterns for offloading the medial compartment of the knee. *Journal of Orthopaedic Research* **27**(8), 1016–1021 (2009). doi:10.1002/jor.20843 (Cited on pages 13 and 43).
- [81] Shull, P.B., Shultz, R., Silder, A., Dragoo, J.L., Besier, T.F., Cutkosky, M.R., Delp, S.L.: Toe-in gait reduces the first peak knee adduction moment in patients with medial compartment knee osteoarthritis. *Journal of Biomechanics* **46**(1), 122–128 (2013). doi:10.1016/j.jbiomech.2012.10.019 (Cited on pages 13, 43, 75, and 76).
- [82] Hunt, M.a., Takacs, J.: Effects of a 10-week toe-out gait modification intervention in people with medial knee osteoarthritis: A pilot, feasibility study. *Osteoarthritis and Cartilage* **22**(7), 904–911 (2014). doi:10.1016/j.joca.2014.04.007 (Cited on pages 13, 43, 75, and 76).
- [83] Guo, M., Axe, M.J., Manal, K.: The influence of foot progression angle on the knee adduction moment during walking and stair climbing in pain free individuals with knee osteoarthritis. *Gait & posture* **26**(3), 436–441 (2007) (Cited on pages 13, 43, and 75).
- [84] Fregly, B.J., Reinbolt, J.A., Rooney, K.L., Mitchell, K.H., Chmielewski, T.L.: Design of patient-specific gait modifications for knee osteoarthritis rehabilitation. *IEEE Transactions on Biomedical Engineering* **54**(9), 1687–1695 (2007). doi:10.1109/TBME.2007.891934. NIHMS150003 (Cited on pages 13, 43, and 75).

- [85] Schache, A.G., Fregly, B.J., Crossley, K.M., Hinman, R.S., Pandy, M.G.: The effect of gait modification on the external knee adduction moment is reference frame dependent. *Clinical Biomechanics* **23**(5), 601–608 (2008). doi:10.1016/j.clinbiomech.2007.12.008 (Cited on pages 13 and 56).
- [86] Hunt, M., Birmingham, T., Bryant, D., Jones, I., Giffin, J., Jenkyn, T., Vandrooort, A.: Lateral trunk lean explains variation in dynamic knee joint load in patients with medial compartment knee osteoarthritis. *Osteoarthritis and Cartilage* **16**(5), 591–599 (2008) (Cited on pages 13 and 94).
- [87] Hunt, M.a., Bennell, K.L.: Predicting dynamic knee joint load with clinical measures in people with medial knee osteoarthritis. *Knee* **18**(4), 231–234 (2011). doi:10.1016/j.knee.2010.05.014 (Cited on pages 13, 56, and 76).
- [88] Simic, M., Hunt, M.a., Bennell, K.L., Hinman, R.S., Wrigley, T.V.: Trunk lean gait modification and knee joint load in people with medial knee osteoarthritis: The effect of varying trunk lean angles. *Arthritis Care and Research* **64**(10), 1545–1553 (2012). doi:10.1002/acr.21724 (Cited on pages 13 and 43).
- [89] Messier, S.P., Gutekunst, D.J., Davis, C., DeVita, P.: Weight loss reduces knee-joint loads in overweight and obese older adults with knee osteoarthritis. *Arthritis & Rheumatology* **52**(7), 2026–2032 (2005) (Cited on page 13).
- [90] Coutts, F.: Gait analysis in the therapeutic environment. *Manual therapy* **4**(1), 2–10 (1999) (Cited on page 13).
- [91] Simon, S.R.: Quantification of human motion: gait analysis—benefits and limitations to its application to clinical problems. *Journal of biomechanics* **37**(12), 1869–1880 (2004) (Cited on page 13).
- [92] KNEEMO Initial Training Network. <https://www.kneemo.eu/>. (Accessed on 4/15/2018) (Cited on page 13).
- [93] Forner Cordero, A., Koopman, H.J.F.M., van der Helm, F.C.T.: Use of pressure insoles to calculate the complete ground reaction forces. *Journal of Biomechanics* **37**(9), 1427–1432 (2004). doi:10.1016/j.jbiomech.2003.12.016 (Cited on pages 19 and 59).
- [94] Liu, T., Inoue, Y., Shibata, K.: A wearable force plate system for the continuous measurement of triaxial ground reaction force in biomechanical applications. *Measurement Science and Technology* **21**(8) (2010). doi:10.1088/0957-0233/21/8/085804 (Cited on pages 19, 59, and 92).
- [95] van den Noort, J., van der Esch, M., Steultjens, M.P.M., Dekker, J., Schepers, M., Veltink, P.H., Harlaar, J.: Ambulatory measurement of the knee adduction moment in patients with osteoarthritis of the knee. *Journal of Biomechanics* **46**(1), 43–49 (2013). doi:10.1016/j.jbiomech.2012.09.030 (Cited on pages 19, 43, and 54).

- [96] Schepers, H.M., Veltink, P.H.: Estimation of ankle moment using ambulatory measurement of ground reaction force and movement of foot and ankle. Proceedings of the First IEEE/RAS-EMBS International Conference on Biomedical Robotics and Biomechatronics, 2006, BioRob 2006 **2006**, 399–401 (2006). doi:10.1109/BIOROB.2006.1639120 (Cited on page 19).
- [97] Audu, M.L., Kirsch, R.F., Triolo, R.J.: Experimental verification of a computational technique for determining ground reactions in human bipedal stance. *Journal of Biomechanics* **40**(5), 1115–1124 (2007). doi:10.1016/j.jbiomech.2006.04.016 (Cited on pages 19, 43, and 59).
- [98] Jung, Y., Jung, M., Ryu, J., Yoon, S., Park, S.K., Koo, S.: Dynamically adjustable foot-ground contact model to estimate ground reaction force during walking and running. *Gait and Posture* **45**, 62–68 (2016). doi:10.1016/j.gaitpost.2016.01.005 (Cited on page 19).
- [99] Villeger, D., Costes, A., Watier, B., Moretto, P.: An algorithm to decompose ground reaction forces and moments from a single force platform in walking gait. *Medical Engineering & Physics* **36**(11), 1530–1535 (2014). doi:10.1016/j.medengphy.2014.08.002 (Cited on pages 19, 24, and 25).
- [100] Luinge, H.J., Veltink, P.H.: Measuring orientation of human body segments using miniature gyroscopes and accelerometers. *Medical and Biological Engineering and Computing* **43**(2), 273–282 (2005). doi:10.1007/BF02345966 (Cited on pages 19, 43, 59, 60, and 75).
- [101] Zhang, J.-T., Novak, A.C., Brouwer, B., Li, Q.: Concurrent validation of xsens mvn measurement of lower limb joint angular kinematics. *Physiological Measurement* **34**(8), 63 (2013) (Cited on page 20).
- [102] Faber, G.S., Chang, C.C., Kingma, I., Dennerlein, J.T., van Dieën, J.H.: Estimating 3D L5/S1 moments and ground reaction forces during trunk bending using a full-body ambulatory inertial motion capture system. *Journal of Biomechanics* **49**(6), 904–912 (2016). doi:10.1016/j.jbiomech.2015.11.042 (Cited on page 20).
- [103] Logar, G., Munih, M.: Estimation of Joint Forces and Moments for the In-Run and Take-Off in Ski Jumping Based on Measurements with Wearable Inertial Sensors. *Sensors* **15**(5), 11258–11276 (2015). doi:10.3390/s150511258 (Cited on page 20).
- [104] Xsens MVN BIOMECH product webpage. <http://www.xsens.com/products/mvn-biomech/> (Cited on pages 20 and 94).
- [105] Xsens MVN tutorials: Preparing hardware MVN Link. <https://tutorial.xsens.com/video/preparing-hardware-mvn-link>. Accessed: 2016-12-07 (Cited on page 20).
- [106] Qualisys Oqus Video product webpage. <http://www.qualisys.com/cameras/oqus-video/> (Cited on pages 20, 26, and 44).

- [107] De Leva, P.: Adjustments to zatsiorsky-seluyanov's segment inertia parameters. *Journal of Biomechanics* **29**(9), 1223–1230 (1996). doi:10.1016/0021-9290(95)00178-6. 0021-92909600178-6 (Cited on pages 21, 23, 24, 36, 45, 55, and 93).
- [108] Xsens MVN tutorials: Taking Body Measurements. <https://tutorial.xsens.com/video/body-measurements> (Cited on page 20).
- [109] Wu, G., Siegler, S., Allard, P., Kirtley, C., Leardini, A., Rosenbaum, D., Whittle, M., D'Lima, D.D., Cristofolini, L., Witte, H., Schmid, O., Stokes, I.: {ISB} recommendation on definitions of joint coordinate system of various joints for the reporting of human joint motion—part i: ankle, hip, and spine. *Journal of Biomechanics* **35**(4), 543–548 (2002). doi:10.1016/S0021-9290(01)00222-6 (Cited on pages 26 and 94).
- [110] Wu, G., van der Helm, F.C.T., Veeger, H.E.J.D., Makhsous, M., Roy, P.V., Anglin, C., Nagels, J., Karduna, A.R., McQuade, K., Wang, X., Werner, F.W., Buchholz, B.: {ISB} recommendation on definitions of joint coordinate systems of various joints for the reporting of human joint motion—part ii: shoulder, elbow, wrist and hand. *Journal of Biomechanics* **38**(5), 981–992 (2005). doi:10.1016/j.jbiomech.2004.05.042 (Cited on pages 26 and 94).
- [111] Taylor, R.: Interpretation of the Correlation Coefficient: A Basic Review. *Journal of Diagnostic Medical Sonography* **6**(1), 35–39 (1990). doi:10.1177/875647939000600106 (Cited on pages 28 and 64).
- [112] Sprague, M.A., Geers, T.L.: Spectral elements and field separation for an acoustic fluid subject to cavitation. *Journal of Computational Physics* **184**(1), 149–162 (2003). doi:10.1016/S0021-9991(02)00024-4 (Cited on pages 28, 47, 49, and 64).
- [113] Hol, J.D., Bellusci, G.: Inertial Motion Capture Calibration. 20160258779, September 2016. <http://www.freepatentsonline.com/y2016/0258779.html> (Cited on page 36).
- [114] Cotton, S., Vanoncini, M., Fraisse, P., Ramdani, N., Demircan, E., Murray, A.P., Keller, T.: Estimation of the centre of mass from motion capture and force plate recordings: A study on the elderly. *Applied Bionics and Biomechanics* **8**(1), 67–84 (2011). doi:10.3233/ABB-2011-0006 (Cited on page 36).
- [115] Galli, M., Crivellini, M., Sibella, F., Montesano, a., Bertocco, P., Parisio, C.: Sit-to-stand movement analysis in obese subjects. *International journal of obesity and related metabolic disorders : journal of the International Association for the Study of Obesity* **24**(11), 1488–1492 (2000). doi:10.1038/sj.ijo.0801409 (Cited on page 36).
- [116] Cappozzo, A.: Gait analysis methodology. *Human Movement Science* **3**(1-2), 27–50 (1984). doi:10.1016/0167-9457(84)90004-6 (Cited on page 37).
- [117] Kok, M., Hol, J.D., Schön, T.B.: An Optimization-based Approach to Human Body Motion Capture Using Inertial Sensors. In: IFAC Proceedings Volumes (IFAC-PapersOnline), vol. 19, pp. 79–85 (2014) (Cited on pages 37, 91, and 95).

- [118] Sharma, L., Lou, C., Cahue, S., Dunlop, D.D.: The mechanism of the effect of obesity in knee osteoarthritis: The mediating role of malalignment. *Arthritis & Rheumatism* **43**(3), 568–575 (2000). doi:10.1002/1529-0131(200003)43:3;1-568::AID-ANR13;3.0.CO;2-E (Cited on page 37).
- [119] Giuberti, M.: Inertial sensing for human motion analysis: Processing, technologies, and applications. PhD thesis, Università di Parma. Dipartimento di Ingegneria dell'Informazione (2014) (Cited on page 38).
- [120] van den Noort, J.C., Steenbrink, F., Roeles, S., Harlaar, J.: Real-time visual feedback for gait retraining: toward application in knee osteoarthritis. *Medical & Biological Engineering & Computing* (2014). doi:10.1007/s11517-014-1233-z (Cited on pages 38, 76, 77, 85, and 86).
- [121] Fregly, B.J.: Gait Modification to Treat Knee Osteoarthritis. *HSS Journal* **8**(1), 45–48 (2012). doi:10.1007/s11420-011-9229-9 (Cited on page 43).
- [122] Haim, A., Rubin, G., Rozen, N., Goryachev, Y., Wolf, A.: Reduction in knee adduction moment via non-invasive biomechanical training: a longitudinal gait analysis study. *Journal of biomechanics* **45**(1), 41–45 (2012) (Cited on page 43).
- [123] Kinney, A.L., Besier, T.F., Silder, A., Delp, S.L., D'Lima, D.D., Fregly, B.J.: Changes in in vivo knee contact forces through gait modification. *Journal of Orthopaedic Research* **31**(3), 434–440 (2013) (Cited on page 43).
- [124] Rutherford, D., Hubley-Kozey, C., Deluzio, K., Stanish, W., Dunbar, M.: Foot progression angle and the knee adduction moment: a cross-sectional investigation in knee osteoarthritis. *Osteoarthritis and Cartilage* **16**(8), 883–889 (2008) (Cited on pages 43 and 75).
- [125] Heijink, A., Gomoll, A.H., Madry, H., Drobnič, M., Filardo, G., Espregueira-Mendes, J., Van Dijk, C.N.: Biomechanical considerations in the pathogenesis of osteoarthritis of the knee. *Knee Surgery, Sports Traumatology, Arthroscopy* **20**(3), 423–435 (2012) (Cited on page 43).
- [126] Andriacchi, T.P., Mündermann, A., Smith, R.L., Alexander, E.J., Dyrby, C.O., Koo, S.: A framework for the in vivo pathomechanics of osteoarthritis at the knee. *Annals of biomedical engineering* **32**(3), 447–457 (2004) (Cited on page 43).
- [127] Jackson, B., Wluka, A., Teichtahl, A., Morris, M., Cicuttini, F.: Reviewing knee osteoarthritis—a biomechanical perspective. *Journal of Science and Medicine in Sport* **7**(3), 347–357 (2004) (Cited on pages 43 and 75).
- [128] Mündermann, A., Dyrby, C.O., Hurwitz, D.E., Sharma, L., Andriacchi, T.P.: Potential strategies to reduce medial compartment loading in patients with knee osteoarthritis of varying severity: reduced walking speed. *Arthritis & Rheumatology* **50**(4), 1172–1178 (2004) (Cited on pages 43 and 75).
- [129] Takacs, J., Hunt, M.a.: The effect of contralateral pelvic drop and trunk lean on frontal plane knee biomechanics during single limb standing. *Journal of Biomechanics* **45**(16), 2791–2796 (2012). doi:10.1016/j.jbiomech.2012.08.041 (Cited on page 43).

- [130] Hunt, M.a., Simic, M., Hinman, R.S., Bennell, K.L., Wrigley, T.V.: Feasibility of a gait retraining strategy for reducing knee joint loading: Increased trunk lean guided by real-time biofeedback. *Journal of Biomechanics* **44**(5), 943–947 (2011). doi:10.1016/j.jbiomech.2010.11.027 (Cited on pages 43, 76, and 86).
- [131] Lin, C.-J., Lai, K.-A., Chou, Y.-L., Ho, C.-S.: The effect of changing the foot progression angle on the knee adduction moment in normal teenagers. *Gait & posture* **14**(2), 85–91 (2001) (Cited on pages 43 and 75).
- [132] Richards, R.E., van den Noort, J.C., van der Esch, M., Booij, M.J., Harlaar, J.: Effect of real-time biofeedback on peak knee adduction moment in patients with medial knee osteoarthritis: Is direct feedback effective? *Clinical Biomechanics* (2017) (Cited on pages 43, 75, 76, and 78).
- [133] Barrios, J.a., Crossley, K.M., Davis, I.S.: Gait retraining to reduce the knee adduction moment through real-time visual feedback of dynamic knee alignment. *Journal of Biomechanics* **43**(11), 2208–2213 (2010). doi:10.1016/j.jbiomech.2010.03.040. NIHMS150003 (Cited on pages 43, 75, 76, and 86).
- [134] Hunt, M.a., Schache, A.G., Hinman, R.S., Crossley, K.M.: Varus thrust in medial knee osteoarthritis: Quantification and effects of different gait-related interventions using a single case study. *Arthritis Care and Research* **63**(2), 293–297 (2011). doi:10.1002/acr.20341 (Cited on page 43).
- [135] Fregly, B.J., Reinbolt, J.A., Chmielewski, T.L.: Evaluation of a patient-specific cost function to predict the influence of foot path on the knee adduction torque during gait. *Computer methods in biomechanics and biomedical engineering* **11**(1), 63–71 (2008) (Cited on page 43).
- [136] Shull, P.B., Lurie, K.L., Cutkosky, M.R., Besier, T.F.: Training multi-parameter gaits to reduce the knee adduction moment with data-driven models and haptic feedback. *Journal of Biomechanics* **44**(8), 1605–1609 (2011). doi:10.1016/j.jbiomech.2011.03.016 (Cited on pages 43, 76, 80, 86, and 95).
- [137] Wheeler, J.W., Shull, P.B., Besier, T.F.: Real-time knee adduction moment feedback for gait retraining through visual and tactile displays. *Journal of biomechanical engineering* **133**(4), 041007 (2011). doi:10.1115/1.4003621 (Cited on pages 43, 76, and 86).
- [138] Gerbrands, T.a., Pisters, M.F., Vanwanseele, B.: Individual selection of gait retraining strategies is essential to optimally reduce medial knee load during gait. *Clinical Biomechanics* **29**(7), 828–834 (2014). doi:10.1016/j.clinbiomech.2014.05.005 (Cited on page 43).
- [139] Baker, R.: Gait analysis methods in rehabilitation. *Journal of neuroengineering and rehabilitation* **3**(1), 4 (2006) (Cited on page 43).
- [140] Brand, R.A., Crowninshield, R.D.: Comment on criteria for patient evaluation tools. *Journal of Biomechanics* **14**(9), 655 (1981) (Cited on page 43).

- [141] Simon, S.R.: Quantification of human motion: gait analysis—benefits and limitations to its application to clinical problems. *Journal of Biomechanics* **37**(12), 1869–1880 (2004). doi:10.1016/j.biomech.2004.02.047 (Cited on page 43).
- [142] Rouhani, H., Favre, J., Crevoisier, X., Aminian, K.: Ambulatory measurement of ankle kinetics for clinical applications. *Journal of Biomechanics* **44**(15), 2712–2718 (2011). doi:10.1016/j.biomech.2011.07.021 (Cited on page 43).
- [143] van den Noort, J.C., van der Esch, M., Steultjens, M.P.M., Dekker, J., Schepers, H.M., Veltink, P.H., Harlaar, J.: The knee adduction moment measured with an instrumented force shoe in patients with knee osteoarthritis. *Journal of Biomechanics* **45**(2), 281–288 (2012). doi:10.1016/j.biomech.2011.10.027 (Cited on page 43).
- [144] Karatsidis, A., Bellusci, G., Schepers, H.M., de Zee, M., Andersen, M.S., Veltink, P.H.: Estimation of ground reaction forces and moments during gait using only inertial motion capture. *Sensors (Switzerland)* **17**(1) (2017). doi:10.3390/s17010075 (Cited on pages 43, 44, 45, 46, 60, and 61).
- [145] MVN BIOMECH - Products - Xsens 3D motion tracking. <https://www.xsens.com/products/mvn-biomech/>. (Accessed on 10/20/2017) (Cited on page 44).
- [146] Qualisys Track Manager — Qualisys. <https://www.qualisys.com/software/qualisys-track-manager/>. (Accessed on 10/16/2017) (Cited on page 44).
- [147] OR6-7 Force Platform — Biomechanics Force Platform — Advanced Mechanical Technology Inc. — Multi-axis load cells and force sensors/platforms — amti.uk.com. <http://www.amti.uk.com/products/or6-7-force-platform.php>. (Accessed on 10/16/2017) (Cited on page 44).
- [148] Body Measurements — Xsens Video Tutorials. <https://tutorial.xsens.com/video/body-measurements>. (Accessed on 10/16/2017) (Cited on page 45).
- [149] Xsens MVN User Manual. <http://issuu.com/xsensmvn/docs/mvn/user-manual/71c37181653db5?e=14522406/12478179> (Cited on pages 45 and 77).
- [150] Kingma, I., De Looze, M.P., Toussaint, H.M., Klijnsma, H.G., Bruijnen, T.B.M.: Validation of a full body 3-D dynamic linked segment model. *Human Movement Science* **15**(6), 833–860 (1996). doi:10.1016/S0167-9457(96)00034-6 (Cited on page 46).
- [151] Damsgaard, M.: Analysis of musculoskeletal systems in the AnyBody Modeling System **14**, 1100–1111 (2006). doi:10.1016/j.simp.2006.09.001 (Cited on pages 47 and 55).
- [152] Lund, M.E., Andersen, M.S., Zee, M.D.: Scaling of musculoskeletal models from static and dynamic trials. *International Biomechanics* **2**(1), 0 (2015). doi:10.1080/23335432.2014.993706 (Cited on page 47).

- [153] Andersen, M.S., Damsgaard, M., Rasmussen, J.: Kinematic analysis of over-determinate biomechanical systems. *Computer Methods in Biomechanics and Biomedical Engineering* **12**(4), 371–384 (2009). doi:10.1080/10255840802459412 (Cited on pages 47, 63, and 75).
- [154] Kuo, A.D.: A least-squares estimation approach to improving the precision of inverse dynamics computations. *Journal of Biomechanical Engineering* **120**(1), 148–159 (1998) (Cited on pages 47 and 49).
- [155] Birmingham, T.B., Hunt, M.A., Jones, I.C., Jenkyn, T.R., Giffin, J.R.: Test-retest reliability of the peak knee adduction moment during walking in patients with medial compartment knee osteoarthritis. *Arthritis Care & Research* **57**(6), 1012–1017 (2007). doi:10.1002/art.22899 (Cited on page 54).
- [156] Davidson, P.L., Wilson, S.J., Wilson, B.D., Chalmers, D.J.: Estimating subject-specific body segment parameters using a 3-dimensional modeller program. *Journal of Biomechanics* **41**(16), 3506–3510 (2008). doi:10.1016/j.jbiomech.2008.09.021 (Cited on page 55).
- [157] Pandis, P., Bull, A.M.: A low-cost three-dimensional laser surface scanning approach for defining body segment parameters. *Proceedings of the Institution of Mechanical Engineers, Part H: Journal of Engineering in Medicine* **231**(11), 1064–1068 (2017). doi:10.1177/0954411917727031. PMID: 28814154 (Cited on page 55).
- [158] Creaby, M.: It's not all about the knee adduction moment: the role of the knee flexion moment in medial knee joint loading. *Osteoarthritis and cartilage* **23**(7), 1038–1040 (2015) (Cited on page 55).
- [159] Delp, S.L., Anderson, F.C., Arnold, A.S., Loan, P., Habib, A., John, C.T., Guendelman, E., Thelen, D.G.: OpenSim: Open-source software to create and analyze dynamic simulations of movement. *IEEE Transactions on Biomedical Engineering* **54**(11), 1940–1950 (2007). doi:10.1109/TBME.2007.901024 (Cited on pages 55 and 59).
- [160] Marra, M.a., Vanheule, V., Fluit, R., Koopman, B.H.F.J.M., Rasmussen, J., Verdonschot, N., Andersen, M.S.: A Subject-Specific Musculoskeletal Modeling Framework to Predict In Vivo Mechanics of Total Knee Arthroplasty. *Journal of Biomechanical Engineering* **137**(2), 020904 (2015). doi:10.1115/1.4029258 (Cited on pages 55, 63, and 94).
- [161] Pizzolato, C., Reggiani, M., Saxby, D.J., Ceseracciu, E., Modenese, L., Lloyd, D.G.: Biofeedback for gait retraining based on real-time estimation of tibiofemoral joint contact forces. *IEEE Transactions on Neural Systems and Rehabilitation Engineering* (2017) (Cited on pages 55, 76, and 86).
- [162] Yamaguchi, S., Kitamura, M., Ushikubo, T., Murata, A., Akagi, R., Sasho, T.: Effect of laterally wedged insoles on the external knee adduction moment across different reference frames. *PloS one* **10**(9), 0138554 (2015) (Cited on page 56).

- [163] Brandon, S.C., Deluzio, K.J.: Robust features of knee osteoarthritis in joint moments are independent of reference frame selection. *Clinical Biomechanics* **26**(1), 65–70 (2011) (Cited on page 56).
- [164] Wouda, F.J., Giuberti, M., Bellusci, G., Veltink, P.H.: Estimation of Full-Body Poses Using Only Five Inertial Sensors : An Eager or Lazy Learning Approach ? *Sensors* (Basel, Switzerland) (2016). doi:10.3390/s16122138 (Cited on pages 56 and 91).
- [165] von Marcard, T., Rosenhahn, B., Black, M.J., Pons-Moll, G.: Sparse inertial poser: Automatic 3d human pose estimation from sparse imus. In: *Computer Graphics Forum*, vol. 36, pp. 349–360 (2017). Wiley Online Library (Cited on pages 56 and 91).
- [166] Dell'Isola, A., Smith, S., Andersen, M., Steultjens, M.: Knee internal contact force in a varus malaligned phenotype in knee osteoarthritis (koa). *Osteoarthritis and cartilage* **25**(12), 2007–2013 (2017) (Cited on page 56).
- [167] Damsgaard, M., Rasmussen, J., Christensen, S.T., Surma, E., de Zee, M.: Analysis of musculoskeletal systems in the AnyBody Modeling System. *Simulation Modelling Practice and Theory* **14**(8), 1100–1111 (2006). doi:10.1016/j.simpat.2006.09.001 (Cited on pages 59, 61, and 63).
- [168] Erdemir, A., McLean, S., Herzog, W., van den Bogert, A.J.: Model-based estimation of muscle forces exerted during movements. *Clinical Biomechanics* **22**(2), 131–154 (2007). doi:10.1016/j.clinbiomech.2006.09.005 (Cited on page 59).
- [169] Rasmussen, J., Damsgaard, M., Voigt, M.: Muscle recruitment by the min/max criterion - A comparative numerical study. *Journal of Biomechanics* **34**(3), 409–415 (2001). doi:10.1016/S0021-9290(00)00191-3 (Cited on page 59).
- [170] Riemer, R., Hsiao-Wecksler, E.T., Zhang, X.: Uncertainties in inverse dynamics solutions: A comprehensive analysis and an application to gait. *Gait and Posture* **27**(4), 578–588 (2008). doi:10.1016/j.gaitpost.2007.07.012 (Cited on page 59).
- [171] Hatze, H.: The fundamental problem of myoskeletal inverse dynamics and its implications. *Journal of Biomechanics* **35**(1), 109–115 (2002). doi:10.1016/S0021-9290(01)00158-0 (Cited on page 59).
- [172] Zhang, J.-T., Novak, A.C., Brouwer, B., Li, Q.: Concurrent validation of Xsens MVN measurement of lower limb joint angular kinematics. *Physiological Measurement* **34**(8), 63–69 (2013). doi:10.1088/0967-3334/34/8/N63 (Cited on page 59).
- [173] Koning, B.H.W., Krogt, M.M.V.D., Baten, C.T.M., Bart, F.J.M.: Computer Methods in Biomechanics and Biomedical Engineering Driving a musculoskeletal model with inertial and magnetic measurement units **5842**(February 2017) (2015). doi:10.1080/10255842.2013.867481 (Cited on page 60).

- [174] Xsens: MVN User Manual by Xsens MVN - Issuu. http://issuu.com/xsensmvn/docs/mvn_user_manual_71c37181653db5?e=14522406/12478179. (Accessed on 02/03/2018) (2017) (Cited on page 60).
- [175] Skals, S., Rasmussen, K.P., Bendtsen, K.M., Yang, J., Andersen, M.S.: A Musculoskeletal Model Driven by Dual Microsoft Kinect Sensor Data. Multi-body System Dynamics (2017). doi:10.1007/s11044-017-9573-8 (Cited on pages 61 and 63).
- [176] de Zee, M., Hansen, L., Wong, C., Rasmussen, J., Simonsen, E.B.: A generic detailed rigid-body lumbar spine model. *Journal of Biomechanics* **40**(6), 1219–1227 (2007). doi:10.1016/j.jbiomech.2006.05.030 (Cited on pages 62 and 63).
- [177] Klein Horsman, M.D., Koopman, H.F.J.M., van der Helm, F.C.T., Prosé, L.P., Veeger, H.E.J.: Morphological muscle and joint parameters for musculoskeletal modelling of the lower extremity. *Clinical Biomechanics* **22**(2), 239–247 (2007). doi:10.1016/j.clinbiomech.2006.10.003 (Cited on pages 62 and 63).
- [178] Veeger, H.E.J., Van Der Helm, F.C.T., Van Der Woude, L.H.V., Pronk, G.M., Rozendal, R.H.: Inertia and muscle contraction parameters for musculoskeletal modelling of the shoulder mechanism. *Journal of Biomechanics* **24**(7), 615–629 (1991). doi:10.1016/0021-9290(91)90294-W (Cited on pages 62 and 63).
- [179] Veeger, H.E.J., Yu, B., An, K.-N., Rozendal, R.H.: Parameters for modeling the upper extremity. *Journal of Biomechanics* **30**(6), 647–652 (1997). doi:10.1016/S0021-9290(97)00011-0 (Cited on pages 62 and 63).
- [180] der Helm, F.C.T., Veeger, H.E.J., Pronk, G.M., der Woude, L.H.V., Rozendal, R.H.: Geometry parameters for musculoskeletal modelling of the shoulder system. *Journal of Biomechanics* **25**(2), 129–144 (1992). doi:10.1016/0021-9290(92)90270-B (Cited on pages 62 and 63).
- [181] Andersen, M.S., Damsgaard, M., MacWilliams, B., Rasmussen, J.: A computationally efficient optimisation-based method for parameter identification of kinematically determinate and over-determinate biomechanical systems. *Computer Methods in Biomechanics and Biomedical Engineering* **13**(2), 171–183 (2010). doi:10.1080/10255840903067080 (Cited on page 62).
- [182] Frankenfield, D.C., Rowe, W.A., Cooney, R.N., Smith, J.S., Becker, D.: Limits of body mass index to detect obesity and predict body composition. *Nutrition* **17**(1), 26–30 (2001). doi:10.1016/S0899-9007(00)00471-8 (Cited on page 63).
- [183] Silver, N.C., Dunlap, W.P.: Averaging correlation coefficients: should Fisher's z transformation be used? *Journal of Applied Psychology* **72**(1), 146 (1987) (Cited on page 64).
- [184] Leardini, A., Chiari, A., Della Croce, U., Cappozzo, A.: Human movement analysis using stereophotogrammetry Part 3. Soft tissue artifact assessment and compensation. *Gait and Posture* **21**(2), 212–225 (2005). doi:10.1016/j.gaitpost.2004.05.002 (Cited on page 67).

- [185] Eltoukhy, M., Kuenze, C., Andersen, M.S., Oh, J., Signorile, J.: Prediction of ground reaction forces for parkinson's disease patients using a kinect-driven musculoskeletal gait analysis model. *Medical Engineering and Physics* **50**, 75–82 (2017) (Cited on page 70).
- [186] Woolf, A.D., Pfleger, B.: Burden of major musculoskeletal conditions. *Bulletin of the World Health Organization* **81**, 646–656 (2003) (Cited on page 75).
- [187] Felson, D., Lawrence, R., Hochberg, M., et al: Osteoarthritis: New insights. part 2: treatment approaches. *Annals of Internal Medicine* **133**(9), 726–737 (2000). doi:10.7326/0003-4819-133-9-200011070-00015. /data/journals/aim/19968/0000605-200011070-00015.pdf (Cited on page 75).
- [188] Boutron, I., Tubach, F., Giraudeau, B., Ravaud, P.: Methodological differences in clinical trials evaluating nonpharmacological and pharmacological treatments of hip and knee osteoarthritis. *JAMA* **290**(8), 1062–1070 (2003). doi:10.1001/jama.290.8.1062. /data/journals/jama/4893/joc22095.pdf (Cited on page 75).
- [189] Sarzi-Puttini, P., Cimmino, M.A., Scarpa, R., Caporali, R., Parazzini, F., Zaninelli, A., Atzeni, F., Canesi, B.: Osteoarthritis: An overview of the disease and its treatment strategies. *Seminars in Arthritis and Rheumatism* **35**(1), 1–10 (2005). doi:10.1016/j.semarthrit.2005.01.013. Osteoarthritis in General and Specialist Practice in Italy: The AMICA Study (Cited on page 75).
- [190] Reeves, N.D., Bowling, F.L.: Conservative biomechanical strategies for knee osteoarthritis. *Nature Reviews Rheumatology* **7**(2), 113–122 (2011) (Cited on page 75).
- [191] Shull, P.B., Jirattigalachote, W., Hunt, M.a., Cutkosky, M.R., Delp, S.L.: Quantified self and human movement: A review on the clinical impact of wearable sensing and feedback for gait analysis and intervention. *Gait & Posture* **40**(1), 11–19 (2014). doi:10.1016/j.gaitpost.2014.03.189 (Cited on pages 75 and 76).
- [192] Chang, A., Hurwitz, D., Dunlop, D., Song, J., Cahue, S., Hayes, K., Sharma, L.: The relationship between toe-out angle during gait and progression of medial tibiofemoral osteoarthritis. *Annals of the rheumatic diseases* **66**(10), 1271–1275 (2007). doi:10.1136/ard.2006.062927 (Cited on page 75).
- [193] Simic, M., Wrigley, T.V., Hinman, R.S., Hunt, M.a., Bennell, K.L.: Altering foot progression angle in people with medial knee osteoarthritis: The effects of varying toe-in and toe-out angles are mediated by pain and malalignment. *Osteoarthritis and Cartilage* **21**(9), 1272–1280 (2013). doi:10.1016/j.joca.2013.06.001 (Cited on page 75).
- [194] Bergmann, J., McGregor, A.: Body-worn sensor design: what do patients and clinicians want? *Annals of biomedical engineering* **39**(9), 2299–2312 (2011) (Cited on page 75).

- [195] Kainz, H., Graham, D., Edwards, J., Walsh, H.P., Maine, S., Boyd, R.N., Lloyd, D.G., Modenese, L., Carty, C.P.: Reliability of four models for clinical gait analysis. *Gait & Posture* **54**, 325–331 (2017) (Cited on page 75).
- [196] Huang, Y., Jirattigalachote, W., Cutkosky, M.R., Zhu, X., Shull, P.B.: Novel Foot Progression Angle Algorithm Estimation via Foot-Worn, Magneto-Inertial Sensing. *IEEE Transactions on Biomedical Engineering* **63**(11), 2278–2285 (2016). doi:10.1109/TBME.2016.2523512 (Cited on pages 75, 82, and 91).
- [197] Xu, J., Bao, T., Lee, U.H., Kinnaird, C., Carender, W., Huang, Y., Sienko, K.H., Shull, P.B.: Configurable, wearable sensing and vibrotactile feedback system for real-time postural balance and gait training: proof-of-concept. *Journal of neuroengineering and rehabilitation* **14**(1), 102 (2017) (Cited on pages 75 and 86).
- [198] Richards, R., van den Noort, J.C., Dekker, J., Harlaar, J.: Gait retraining with real-time biofeedback to reduce knee adduction moment: Systematic review of effects and methods used. *Archives of Physical Medicine and Rehabilitation* **98**(1), 137–150 (2017). doi:10.1016/j.apmr.2016.07.006 (Cited on page 76).
- [199] Hunt, M.a., Takacs, J., Hart, K., Massong, E., Fuchko, K., Biegler, J.: Comparison of Mirror, Raw Video, and Real-Time Visual Biofeedback for Training Toe-Out Gait in Individuals With Knee Osteoarthritis. *Archives of Physical Medicine and Rehabilitation* **95**(10), 1912–1917 (2014). doi:10.1016/j.apmr.2014.05.016 (Cited on pages 76 and 85).
- [200] Segal, N.a., Glass, N.a., Teran-Yengle, P., Singh, B., Wallace, R.B., Yack, H.J.: Intensive Gait Training for Older Adults with Symptomatic Knee Osteoarthritis. *American Journal of Physical Medicine & Rehabilitation*, 1 (2015). doi:10.1097/PHM.0000000000000264 (Cited on page 76).
- [201] Richards, R., van der Esch, M., van den Noort, J.C., Harlaar, J.: The learning process of gait retraining using real-time feedback in patients with medial knee osteoarthritis. *Gait & posture* **62**, 1–6 (2018) (Cited on pages 76 and 78).
- [202] Dowling, A.V., Fisher, D.S., Andriacchi, T.P.: Gait Modification via Verbal Instruction and an Active Feedback System to Reduce Peak Knee Adduction Moment. *Journal of Biomechanical Engineering* **132**(7), 071007 (2010). doi:10.1115/1.4001584 (Cited on pages 76 and 86).
- [203] Shull, P.B., Silder, A., Shultz, R., Dragoo, J.L., Besier, T.F., Delp, S.L., Cutkosky, M.R.: Six-week gait retraining program reduces knee adduction moment, reduces pain, and improves function for individuals with medial compartment knee osteoarthritis. *Journal of Orthopaedic Research* **31**(7), 1020–1025 (2013). doi:10.1002/jor.22340 (Cited on page 76).
- [204] Chen, D.K.Y., Haller, M., Besier, T.F.: Wearable lower limb haptic feedback device for retraining foot progression angle and step width. *Gait & Posture* **55**(Supplement C), 177–183 (2017). doi:10.1016/j.gaitpost.2017.04.028 (Cited on pages 76, 78, 80, 85, and 86).

- [205] Ferrigno, C., Stoller, I.S., Shakoor, N., Thorp, L.E., Wimmer, M.A.: The feasibility of using augmented auditory feedback from a pressure detecting insole to reduce the knee adduction moment: a proof of concept study. *Journal of biomechanical engineering* **138**(2), 021014 (2016) (Cited on pages 76 and 86).
- [206] Seuter, M., Opitz, L., Bauer, G., Hochmann, D.: Live-feedback from the imus: Animated 3d visualization for everyday-exercising. In: Proceedings of the 2016 ACM International Joint Conference on Pervasive and Ubiquitous Computing: Adjunct, pp. 904–907 (2016). ACM (Cited on page 76).
- [207] The leader in Mixed Reality Technology — HoloLens. <https://www.microsoft.com/en-us/hololens>. (Accessed on 08/25/2017) (Cited on pages 76 and 77).
- [208] Geijtenbeek, T., Steenbrink, F., Otten, B., Even-Zohar, O.: D-flow: immersive virtual reality and real-time feedback for rehabilitation. In: Proceedings of the 10th International Conference on Virtual Reality Continuum and Its Applications in Industry, pp. 201–208 (2011). ACM (Cited on page 77).
- [209] Van den Bogert, A.J., Geijtenbeek, T., Even-Zohar, O., Steenbrink, F., Hardin, E.C.: A real-time system for biomechanical analysis of human movement and muscle function. *Medical & biological engineering & computing* **51**(10), 1069–1077 (2013) (Cited on page 77).
- [210] Xsens MVN Analyze - Products - Xsens 3D motion tracking. <https://www.xsens.com/products/xsens-mvn-analyze/>. (Accessed on 12/23/2017) (Cited on page 77).
- [211] Xsens MTw Awinda - Products - Xsens 3D motion tracking. <https://www.xsens.com/products/mtw-awinda/>. (Accessed on 2018-04-07) (Cited on page 77).
- [212] Billboarding and tag-along - Windows Mixed Reality - Microsoft. https://developer.microsoft.com/en-us/windows/mixed-reality/billboarding_and_tag-along. (Accessed on 2018-01-24) (Cited on page 78).
- [213] Grownay, E., Meglan, D., Johnson, M., Cahalan, T., An, K.-N.: Repeated measures of adult normal walking using a video tracking system. *Gait & Posture* **6**(2), 147–162 (1997) (Cited on page 82).
- [214] Kadaba, M., Ramakrishnan, H., Wootten, M., Gainey, J., Gorton, G., Cochran, G.: Repeatability of kinematic, kinetic, and electromyographic data in normal adult gait. *Journal of Orthopaedic Research* **7**(6), 849–860 (1989) (Cited on page 82).
- [215] Steinwender, G., Saraph, V., Scheiber, S., Zwick, E.B., Uitz, C., Hackl, K.: Intrasubject repeatability of gait analysis data in normal and spastic children. *Clinical Biomechanics* **15**(2), 134–139 (2000) (Cited on page 82).
- [216] Tsushima, H., Morris, M.E., McGinley, J.: Test-retest reliability and inter-tester reliability of kinematic data from a three-dimensional gait analysis system. *Journal of the Japanese Physical Therapy Association* **6**(1), 9–17 (2003) (Cited on page 82).

- [217] Eve, L., McNee, A., Shortland, A.: Extrinsic and intrinsic variation in kinematic data from the gait of healthy adult subjects. *Gait & Posture* **24**, 56–57 (2006) (Cited on page 82).
- [218] Gorton, G., Hebert, D., Goode, B.: Assessment of the kinematic variability between twelve shriners motion analysis laboratories part 2: short-term follow up. *Gait Posture* **16**(S1), 65–6 (2002) (Cited on page 82).
- [219] Gorton, G.E., Hebert, D.A., Gannotti, M.E.: Assessment of the kinematic variability among 12 motion analysis laboratories. *Gait & Posture* **29**(3), 398–402 (2009). doi:10.1016/j.gaitpost.2008.10.060 (Cited on page 82).
- [220] Murphy, A., McGinley, J., Tirosh, O.: Reliability of kinematic gait measurements in adult hemiplegic stroke. *Proceedings of the 12th annual gait and clinical movement analysis society* (2007) (Cited on page 82).
- [221] Schwartz, M.H., Trost, J.P., Wervey, R.A.: Measurement and management of errors in quantitative gait data. *Gait & posture* **20**(2), 196–203 (2004) (Cited on page 82).
- [222] Xia, H., Xu, J., Wang, J., Hunt, M.A., Shull, P.B.: Validation of a smart shoe for estimating foot progression angle during walking gait. *Journal of biomechanics* **61**, 193–198 (2017) (Cited on pages 82 and 91).
- [223] Hill, P., Group, I.S.B.S.: Practical Software Project Estimation: A Toolkit for Estimating Software Development Effort & Duration. McGraw-Hill Education (2010). <https://books.google.gr/books?id=mW6phtfWZ-EC> (Cited on page 85).
- [224] Uhlrich, S.D., Silder, A., Beaupre, G.S., Shull, P.B., Delp, S.L.: Subject-specific toe-in or toe-out gait modifications reduce the larger knee adduction moment peak more than a non-personalized approach. *Journal of biomechanics* **66**, 103–110 (2018) (Cited on page 85).
- [225] Berryman, N., Gayda, M., Nigam, A., Juneau, M., Bherer, L., Bosquet, L.: Comparison of the metabolic energy cost of overground and treadmill walking in older adults. *European Journal of Applied Physiology* **112**(5), 1613–1620 (2012). doi:10.1007/s00421-011-2102-1 (Cited on page 86).
- [226] Clark, R.a., Pua, Y.-H., Bryant, A.L., Hunt, M.a.: Validity of the Microsoft Kinect for providing lateral trunk lean feedback during gait retraining. *Gait & Posture* **38**(4), 1064–1066 (2013). doi:10.1016/j.gaitpost.2013.03.029 (Cited on page 86).
- [227] Wouda, F.J., Giuberti, M., Bellusci, G., Maartens, E., Reenalda, J., Van Beijnum, B.-J.F., Veltink, P.H.: Estimation of vertical ground reaction forces and sagittal knee kinematics during running using three inertial sensors. *Frontiers in physiology* **9**, 218 (2018) (Cited on page 91).
- [228] Mousas, C.: Full-body locomotion reconstruction of virtual characters using a single inertial measurement unit. *Sensors* **17**(11), 2589 (2017) (Cited on page 92).

- [229] Holden, D., Saito, J., Komura, T.: A deep learning framework for character motion synthesis and editing. *ACM Transactions on Graphics (TOG)* **35**(4), 138 (2016) (Cited on page 92).
- [230] Weenk, D., Roetenberg, D., van Beijnum, B.-J.J.F., Hermens, H.J., Veltink, P.H.: Ambulatory Estimation of Relative Foot Positions by Fusing Ultrasound and Inertial Sensor Data. *IEEE Transactions on Neural Systems and Rehabilitation Engineering* **23**(5), 817–826 (2015). doi:10.1109/TNSRE.2014.2357686 (Cited on page 92).
- [231] Kortier, H.G., Antonsson, J., Schepers, H.M., Gustafsson, F., Veltink, P.H.: Hand pose estimation by fusion of inertial and magnetic sensing aided by a permanent magnet. *IEEE Transactions on Neural Systems and Rehabilitation Engineering* **23**(5), 796–806 (2015). doi:10.1109/tnsre.2014.2357579 (Cited on page 92).
- [232] Mourikis, A.I., Roumeliotis, S.I.: A multi-state constraint kalman filter for vision-aided inertial navigation. In: *Robotics and Automation, 2007 IEEE International Conference On*, pp. 3565–3572 (2007). IEEE (Cited on page 92).
- [233] Supej, M.: 3d measurements of alpine skiing with an inertial sensor motion capture suit and GNSS RTK system. *Journal of Sports Sciences* **28**(7), 759–769 (2010). doi:10.1080/02640411003716934 (Cited on page 92).
- [234] Bo, A.P.L., Hayashibe, M., Poignet, P.: Joint angle estimation in rehabilitation with inertial sensors and its integration with kinect. In: *Engineering in Medicine and Biology Society, EMBC, 2011 Annual International Conference of the IEEE*, pp. 3479–3483 (2011). IEEE (Cited on page 92).
- [235] SteamVR. <http://store.steampowered.com/steamvr>. (Accessed on 03/11/2018) (Cited on page 92).
- [236] Chesnin, K.J., Selby-Silverstein, L., Besser, M.P.: Comparison of an in-shoe pressure measurement device to a force plate: concurrent validity of center of pressure measurements. *Gait & posture* **12**(2), 128–133 (2000) (Cited on page 92).
- [237] Han, T.R., Paik, N.J., Im, M.S.: Quantification of the path of center of pressure (cop) using an f-scan in-shoe transducer. *Gait & posture* **10**(3), 248–254 (1999) (Cited on page 92).
- [238] Brookhuis, R.A., Lammerink, T.S., Wiegerink, R.J., de Boer, M.J., Elwenspoek, M.C.: 3d force sensor for biomechanical applications. *Sensors and actuators A: physical* **182**, 28–33 (2012) (Cited on page 93).
- [239] Brookhuis, R.A., Droogendijk, H., de Boer, M.J., Sanders, R.G., Lammerink, T.S., Wiegerink, R.J., Krijnen, G.J.: Six-axis force–torque sensor with a large range for biomechanical applications. *Journal of micromechanics and microengineering* **24**(3), 035015 (2014) (Cited on page 93).

- [240] Mitcheson, P.D.: Energy harvesting for human wearable and implantable bio-sensors. In: 2010 Annual International Conference of the IEEE Engineering in Medicine and Biology. IEEE (2010). doi:10.1109/emb.2010.5627952. <https://doi.org/10.1109/emb.2010.5627952> (Cited on page 93).
- [241] Magno, M., Boyle, D.: Wearable energy harvesting: From body to battery. In: 2017 12th International Conference on Design & Technology of Integrated Systems In Nanoscale Era (DTIS). IEEE (2017). doi:10.1109/dtis.2017.7930169. <https://doi.org/10.1109/dtis.2017.7930169> (Cited on page 93).
- [242] Lin, K., Yu, J., Hsu, J., Zahedi, S., Lee, D., Friedman, J., Kansal, A., Raghunathan, V., Srivastava, M.: Heliomote: Enabling long-lived sensor networks through solar energy harvesting. In: Proceedings of the 3rd International Conference on Embedded Networked Sensor Systems. SenSys '05, pp. 309–309. ACM, New York, NY, USA (2005). doi:10.1145/1098918.1098974. <http://doi.acm.org/10.1145/1098918.1098974> (Cited on page 93).
- [243] Leonov, V.: Thermoelectric energy harvesting of human body heat for wearable sensors. IEEE Sensors Journal **13**(6), 2284–2291 (2013). doi:10.1109/jsen.2013.2252526 (Cited on page 93).
- [244] Khaligh, A., Zeng, P., Zheng, C.: Kinetic energy harvesting using piezoelectric and electromagnetic technologies—state of the art. IEEE Transactions on Industrial Electronics **57**(3), 850–860 (2010). doi:10.1109/tie.2009.2024652 (Cited on page 93).
- [245] Pavol, M.J., Owings, T.M., Grabiner, M.D.: Body segment inertial parameter estimation for the general population of older adults. Journal of biomechanics **35**(5), 707–712 (2002) (Cited on page 93).
- [246] Camomilla, V., Cereatti, A., Cutti, A.G., Fantozzi, S., Stagni, R., Vannozzi, G.: Methodological factors affecting joint moments estimation in clinical gait analysis: a systematic review. Biomedical engineering online **16**(1), 106 (2017) (Cited on page 93).
- [247] Park, S.J., Kim, C.-B., Park, S.C.: Anthropometric and biomechanical characteristics on. Applied human science **18**(3), 91–99 (1999) (Cited on page 93).
- [248] Clarkson, S., Wheat, J., Heller, B., Choppin, S.: Assessing the suitability of the microsoft kinect for calculating person specific body segment parameters. In: Computer Vision - ECCV 2014 Workshops, pp. 372–385. Springer (2015) (Cited on page 93).
- [249] Kainz, H., Hoang, H.X., Stockton, C., Boyd, R.R., Lloyd, D.G., Carty, C.P.: Accuracy and reliability of marker-based approaches to scale the pelvis, thigh, and shank segments in musculoskeletal models. Journal of Applied Biomechanics **33**(5), 354–360 (2017). doi:10.1123/jab.2016-0282 (Cited on page 94).
- [250] Crabolu, M., Pani, D., Raffo, L., Cereatti, A.: Estimation of the center of rotation using wearable magneto-inertial sensors. Journal of biomechanics **49**(16), 3928–3933 (2016) (Cited on page 94).

- [251] Crabolu, M., Pani, D., Raffo, L., Conti, M., Crivelli, P., Cereatti, A.: In vivo estimation of the shoulder joint center of rotation using magneto-inertial sensors: MRI-based accuracy and repeatability assessment. *Biomedical engineering online* **16**(1), 34 (2017) (Cited on page 94).
- [252] Andersen, M.S., de Zee, M., Damsgaard, M., Nolte, D., Rasmussen, J.: Introduction to force-dependent kinematics: theory and application to mandible modeling. *Journal of Biomechanical Engineering* **139**(9), 091001 (2017) (Cited on page 94).
- [253] Niu, K.: Ultrasound based skeletal motion capture: the development and validation of a non-invasive knee joint motion tracking method (2018). doi:10.3990/1.9789036544825 (Cited on page 94).
- [254] Favre, J., Aissaoui, R., Jolles, B.M., de Guise, J.A., Aminian, K.: Functional calibration procedure for 3d knee joint angle description using inertial sensors. *Journal of Biomechanics* **42**(14), 2330–2335 (2009). doi:10.1016/j.jbiomech.2009.06.025 (Cited on page 94).
- [255] Schmitt, H., Kappel, H., Moser, M.T., Cardenas-Montemayor, E., Engelleiter, K., Kuni, B., Clarius, M.: Determining knee joint alignment using digital photographs. *Knee Surgery, Sports Traumatology, Arthroscopy* **16**(8), 776–780 (2008). doi:10.1007/s00167-008-0570-6 (Cited on page 94).
- [256] Specogna, A., Birmingham, T., DaSilva, J., Milner, J., Kerr, J., Hunt, M., Jones, I., Jenkyn, T., Fowler, P., Giffin, J.: Reliability of lower limb frontal plane alignment measurements using plain radiographs and digitized images. *The Journal of Knee Surgery* **17**(04), 203–210 (2010). doi:10.1055/s-0030-1248222 (Cited on page 94).
- [257] Veltink, P., van Beijnum, F., van Beijnum, B., Klaassen, B., Hermens, H., Droog, A., Weusthof, M., Lorusso, F., Tognetti, A., Reenalda, J., Reenalda, J., Nikamp, C.D.M., Nikamp-Simons, C., Baten, C., Buurke, J., Held, J., Luft, A., Luinge, H., De Toma, G., Mancuso, C., Paradiso, R.: In: Aminian, K. (ed.) Daily-life tele-monitoring of motor performance in stroke survivors. *Internation Symposium on 3D Analysis of Human Movement*, pp. 159–162. Ecole Polytechnique Federale de Lausanne (2014) (Cited on page 95).
- [258] Klaassen, B., van Beijnum, B.J.F., Hermens, H.J.: Usability in telemedicine systems—a literature survey. *International Journal of Medical Informatics* **93**, 57–69 (2016). doi:10.1016/j.ijmedinf.2016.06.004 (Cited on page 95).

Summary

Human movement analysis is an important field enabling us to understand the nature of several musculoskeletal disorders. The way we move affects the mechanical loads applied on our joints, which may gradually result in structural changes. For example, in the case of knee osteoarthritis, increased knee joint loading may lead to progression of the disease and worsening of the symptoms. However, the low availability and increased complexity of traditional movement analysis systems are one of the leading causes of poor clinical adoption of treatments that consider the human body mechanics. Therefore, new assessment methods have to be developed based on ambulatory, fast to setup, easy to use, and reliable instrumentation.

In the first chapter, we initially provide an introduction about the history and influencers of the field of human movement analysis. Subsequently we present how human movement analysis is performed in terms of both kinematics and kinetics and describe the limitations of the current systems. Next, we describe the clinical relevance of biomechanics in knee osteoarthritis; a leading cause of disability in the elderly population worldwide. Biomechanical loading is one of the risk factors, which could be potentially modulated via gait modification treatments. However, today's laboratory-based human movement analysis systems impede the clinical adoption of biomechanics in clinical practice. One of the causes is that such systems are not widely available in every clinic due to their complexity, time-consuming setups, data collections, and post-processing. Ideally, ambulatory systems that could capture both kinematics and kinetics would be used during the daily life or in a clinical environment easier, faster and with similar performance. However, to date a practical and reliable solution to capture the kinetics is missing from ambulatory approaches. The goals of this thesis were to develop techniques using inertial sensor-based kinematics to assess kinetics, as well as demonstrate the capability of inertial sensors to drive real-time biofeedback aiming at reducing the knee joint loading. This work was performed within KNEEMO project, an EU-funded Initial Training Network aiming at investigating biomechanical interventions in knee osteoarthritis.

In the second chapter, we propose a method to estimate the external ground reaction forces and moments during gait tasks using only inertial measurement units. The reconstructed kinematics available through a commercial inertial motion capture system together with anthropometric measurements are used to as input in a whole-body inverse dynamics approach, deriving the total external force and moment applied on the body. A known problem in such approaches is the indeterminacy occurring between the feet in the bipedal phase. An empirical gait event-driven function called smooth transition assumption has been utilized to solve this problem. We compared the ground reaction force and moment estimates derived from either in-

ertial or optical motion capture input against a gold standard force plate reference. The agreement between the estimated and reference GRF&M was categorized over a self-selected walking speed as excellent for the vertical ($\rho = 0.992$, rRMSE = 5.3%), anterior ($\rho = 0.965$, rRMSE = 9.4%) and sagittal ($\rho = 0.933$, rRMSE = 12.4%) GRF&M components and as strong for the lateral ($\rho = 0.862$, rRMSE = 13.1%), frontal ($\rho = 0.710$, rRMSE = 29.6%), and transverse GRF&M ($\rho = 0.826$, rRMSE = 18.2%).

In chapter three, we developed and validated the afore-mentioned method further in estimating knee joint moments during gait modifications. The examined gait modifications have been proposed to alter the knee joint loading, reflected by the joint moments, and therefore are assumed to be ways to unload the knee joint without external orthotic devices. Our analysis focused on the estimation of knee adduction and flexion moments assessed with the use of inertial sensors only, and compared these estimates to the ones obtained from a conventional inverse dynamics approach using optical motion capture and force plates. The accuracy analysis showed that moments obtained from the proposed method presented moderate to strong correlations for the knee adduction and flexion moment ($\rho=0.64$ to 0.72 and $\rho= 0.80$ to 0.84 , respectively), over the stance phase. In addition, knee adduction moment changes from a baseline due to gait modification were quantified with mean differences less than 0.2 % of body weight times body height between the proposed and reference approach in toe-in, toe-out, and lateral trunk lean walking patterns. These findings are encouraging for the further clinical adoption of inertial motion capture systems in assessing kinetics.

Chapter four takes a step towards integrating existing highly detailed musculoskeletal models with inertial motion capture. Recent techniques in musculoskeletal modeling allow the estimation of loads from motion while distributing the loads across a number of muscles using fatigue minimization principles. The significant advantage of such a technique is that it can be applied in several activities without dependence on a database. Available musculoskeletal models typically operate using reduced number of degrees of freedom and different segment definitions with respect to what commercial inertial motion capture systems use. Therefore, a method to reduce the number of degrees of freedom is proposed based on solving over-determinate inverse kinematics of a few virtual markers driven by the inertial model. For evaluation we compared the lower limb kinematics and kinetics of three different systems: 1) inertial motion capture with predicted ground reaction forces 2) optical motion capture with predicted ground reaction forces and 3) optical motion capture with measured ground reaction forces. The sagittal plane joint angles of ankle, knee, and hip presented excellent Pearson correlations ($\rho = 0.95$, 0.99 , and 0.99 , respectively) and root-mean-squared-differences of $4.1 \pm 1.3^\circ$, $4.4 \pm 2.0^\circ$, and $5.7 \pm 2.1^\circ$, respectively showcasing the robustness of inertial motion capture to assess joint angles. In addition, the ground and joint reaction forces and moments from the first and second kinematically-driven models provided in most cases similar performance to the third reference model demonstrating that inertial motion capture can be considered as an input option for musculoskeletal models and kinetics predictions outside laboratory environments.

In the fifth chapter, we investigate the second objective of the thesis, focusing on a wearable biofeedback system for gait retraining applications. The foot progression angle (FPA) has been selected as the most conveniently assessable and effective

parameter to alter knee joint moments. A visual feedback system has been implemented with the use of augmented reality. The recent advances in this field allow accurate placement of virtual objects in the environment of use. Using the capabilities of the device we adjust the color and spatial properties of the objects in such a way that they convey information about the performed and targeted movement in real-time. The wearable system tracked FPA with an accuracy of 2.4 degrees RMS and ICC=0.94 across all target angles and subjects, when compared to an optical motion capture reference. In addition, the effectiveness of the biofeedback, reflected by the number of steps with FPA value ± 2 degrees from the target, was found to be around 50% in both wearable and laboratory approaches. These findings demonstrate that retraining of the FPA using wearable inertial sensing and visual feedback is feasible with effectiveness matching closely an established laboratory method. The proposed wearable setup may reduce the complexity of gait retraining applications and facilitate their transfer to routine clinical practice.

Finally, in the last chapter, we described the major insights of this research, including the limitations and sources of error, and provided directions for future development, validation and use of the proposed techniques. The research described in this thesis is only a first step to assess full kinetics using inertial sensors and several improvements should be introduced to reach clinical or daily life use. Reducing the number and size of sensors, as well as finding alternative power sources would facilitate the unobtrusive use. Regarding performance, methods to improve the sensor-to-segment calibration and scaling of the biomechanical models should be found. As for the biofeedback application, multimodal feedback should be explored to maximize the effect of gait retraining applications.

Samenvatting

Bewegingsanalyse is een belangrijke methode dat ons staat stelt om de aard van verschillende spier- en skeletaandoeningen te begrijpen. De manier waarop we bewegen heeft invloed op hoe ons lichaam wordt belast, wat kan leiden tot structurele lichaamsveranderingen. In het geval van knie artrose kan een verhoogde belasting van het kniegewicht bijvoorbeeld leiden tot progressie van de ziekte en verergering van de symptomen. De slechte beschikbaarheid en de toegenomen complexiteit van traditionele bewegingsanalyse-systeem zijn één van de belangrijkste oorzaken van een slechte klinische acceptatie van dergelijke conservatieve biomechanische behandelingen. Daarom moeten nieuwe beoordelingsmethoden worden ontwikkeld op basis van ambulante, snel in te stellen, eenvoudig te gebruiken en betrouwbare instrumenten.

In het eerste hoofdstuk geven we een inleiding over de geschiedenis en de invloedrijke personen van bewegingsanalyse. Vervolgens presenteren we hoe menselijke bewegingsanalyse wordt uitgevoerd op basis van kinematica en kinetica. Bovendien beschrijven we de klinische relevantie van biomechanica bij knieartrose; een belangrijke oorzaak van invaliditeit bij de oudere bevolking wereldwijd. Biomechanische belasting is een van de risicofactoren, die potentieel kan worden gemoduleerd via aanpassingen van het looppatroon. De huidige laboratoriumgebaseerde analysesystemen voor menselijke bewegingen belemmeren echter de klinische acceptatie van op biomechanica gebaseerde diagnostiek in de klinische routine. Een van de belangrijkste oorzaken is dat dergelijke systemen niet in alle klinieken beschikbaar zijn vanwege hun complexiteit, tijdrovende opstellingen, dataverzamelingen en nabewerking. Idealiter zouden ambulante systemen die zowel kinematica als kinetica zouden kunnen meten, tijdens het dagelijkse leven of in een klinische omgeving gemakkelijker, sneller en met vergelijkbare prestaties gebruikt kunnen worden. Tot nu toe ontbreekt echter een praktische en betrouwbare oplossing om de kinetica te meten in ambulante methodes. De doelstellingen van deze studie waren om technieken te ontwikkelen met behulp van inertiële sensor-gebaseerde kinematica om de kinetica te beoordelen, evenals het vermogen van inertiële sensoren om real-time biofeedback aan te sturen gericht op het verminderen van de belasting op het kniegewicht. Dit werk werd uitgevoerd binnen het KNEEMO-project, een door de EU gefinancierd Initial Training Network dat zich richt op het onderzoeken van biomechanische interventies bij artrose van de knie.

In het tweede hoofdstuk stellen we een methode voor om de externe grondreactiekrachten en momenten (GRF&M) tijdens loopbewegingen te schatten met behulp van alleen inertiële sensoren. De gereconstrueerde kinematica die beschikbaar is via een commercieel inertieel bewegingsanalysesysteem, samen met antropometri-

sche metingen, worden gebruikt als invoer voor een inverse dynamica benadering voor het hele lichaam, die de totale externe kracht en het moment op het lichaam berekend. Een bekend probleem bij dergelijke benaderingen is de onbepaaldheid die optreedt wanneer meer dan één segment een interactie heeft met de omgeving. Een empirische looppatroon functie genaamd 'smooth transition assumption' is gebruikt om dit probleem op te lossen. We vergelijken de geschatte grondreactiekachten en momenten die zijn afgeleid van ofwel inertiële- of optische bewegingsanalysesystemen tegen een gouden standaard krachtplaatreferentie. De overeenkomst tussen de geschatte en referentie GRF&M was gecategoriseerd tijdens een zelfgekozen loopsnelheid als uitstekend voor de verticale ($\rho = 0.992$, rRMSE = 5.3 %), anteriore ($\rho = 0.965$, rRMSE = 9.4 %) en sagittale ($\rho = 0.933$, rRMSE = 12.4 %) componenten van de GRF&M en als sterk voor de laterale ($\rho = 0.862$, rRMSE = 13.1 %), frontale ($\rho = 0.710$, rRMSE = 29.6 %), en transversale GRF&M ($\rho = 0.826$, rRMSE = 18.2 %).

In hoofdstuk drie ontwikkelen en valideren we deze methode verder in het schatten van kniegewichtmomenten tijdens aanpassingen van het looppatroon. De onderzochte aanpassingen van het looppatroon zijn voorgesteld om de belasting van het kniegewicht, weerspiegeld door de gewichtsmomenten, te veranderen en daarom wordt aangenomen dat dit manieren zijn om het kniegewicht zonder externe orthetische apparaten te ontladen. Onze analyse concentreerde zich op de schatting van de knie-adductie- en flexiemomenten alleen met het gebruik van inertiële sensoren, en we vergelijken deze schattingen met die van een conventionele inverse dynamica-benadering met behulp van optische bewegingsanalyse en krachtplaten. De nauwkeurigheidsanalyse liet zien dat momenten verkregen uit de voorgestelde methode matige tot sterke correlaties voor het adductiemoment ($\rho = 0.64$ tot 0.72) en en het flexiemoment ($\rho = 0.80$ tot 0.84, respectievelijk) vertoonden over de standfase. Bovendien werd het adductiemoment van de knie ten opzichte van een baseline als gevolg van aanpassingen van het looppatroon gekwantificeerd met gemiddelde verschillen van minder dan 0.2% lichaamsge wicht maal de lichaamshoogte tussen de voorgestelde en referentiebenadering in drie van de vier looppatronen. Deze bevindingen zijn bemoedigend voor de verdere klinische acceptatie van inertiële bewegingsregistratiesystemen bij het beoordelen van de kinetica.

Hoofdstuk vier neemt een stap in de richting van meer gedetailleerde spier- en skelet modellen aangedreven door inertiële bewegingsregistratie. Recente technieken voor het modelleren van het bewegingsapparaat maken het mogelijk belastingen te schatten en de belastingen over een aantal spieren te verdelen met behulp van vermoeiingsminimalisatieprincipes. Het grote voordeel van een dergelijke techniek is dat deze voor verschillende activiteiten kan worden toegepast zonder afhankelijk te zijn van een database. Beschikbare musculoskeletale modellen werken meestal met een verminderd aantal vrijheidsgraden en verschillende segmentdefinities met betrekking tot wat commerciële inertiële bewegingsanalyse systemen gebruiken. Daarom wordt een methode voorgesteld om de vrijheidsgraden te verminderen op basis van het oplossen van de overbepaalde inverse kinematica van een paar virtuele markeringen die worden aangestuurd door het inertiële model. Voor de evaluatie vergelijken we de kinematica en kinetica van de onderste ledematen van drie verschillende systemen: 1) inertiële bewegingsregistratie met voorspelde grondreactiekachten 2) optische bewegingsregistratie met voorspelde grondreactiekachten en 3) optische bewegingsregistratie met gemeten grondreactiekachten. De sagittale vlakke gewichtshoeken

van enkel, knie en heup presenteerden uitstekende Pearson-correlaties (respectievelijk $\rho = 0.95$, 0.99 en 0.99) en root-mean-squared-verschillen van $4.1 \pm 1.3^\circ$, $4.4 \pm 2.0^\circ$ en $5.7 \pm 2.1^\circ$ en tonen respectievelijk de robuustheid van inertiële motion capture om gewichtshoeken te beoordelen. Bovendien leverden de grond- en gewichtsreactiekrachten en momenten van de eerste en tweede kinematisch aangedreven modellen in de meeste gevallen een vergelijkbare prestatie als het derde referentiemodel, wat aantoon dat inertiële bewegingsregistratie kan worden beschouwd als een inputoptie voor musculoskeletale modellen en kinetiekvoorspellingen buiten laboratoriumomvingen.

In het vijfde hoofdstuk onderzoeken we het tweede doel van het proefschrift, namelijk een draagbaar biofeedbacksysteem voor looptrainingstoepassingen. De voetverloophoek is gekozen als de meest eenvoudige en effectieve manier om kniegewichtmomenten te veranderen. Een visueel feedbacksysteem kan worden geïmplementeerd met behulp van augmented reality. De recente ontwikkelingen op dit gebied maken een nauwkeurige plaatsing van virtuele objecten in de gebruiksomgeving mogelijk. Met behulp van de netwerk mogelijkheden van het apparaat kunnen we de kleur- en spatiële eigenschappen van de objecten op een zodanige manier aanpassen dat ze informatie over de uitgevoerde en gerichte beweging in realtime tonen. We tonen aan dat een dergelijk raamwerk net zo effectief kan worden gebruikt als een systeem in een bewegingslaboratorium. Het draagbare systeem volgde FPA met een nauwkeurigheid van 2.4 graden RMS en $ICC = 0.94$ over alle doelhoeken en proefpersonen in vergelijking met een referentie voor optische bewegingsvastlegging. Bovendien bleek de effectiviteit van de biofeedback, weerspiegeld door het aantal stappen met FPA-waarde ± 2 graden ten opzichte van het doel, rond de 50% te liggen in zowel draagbare als laboratoriumbenaderingen. Deze bevindingen tonen aan dat coaching van de FPA met behulp van draagbare inertiële sensoren en visuele feedback haalbaar is met vergelijkbare effectiviteit als een gevestigde laboratoriummethode. De voorgestelde draagbare opstelling kan de complexiteit van looptrainingstoepassingen verminderen en de overdracht ervan naar routinematige klinische praktijken vergemakkelijken.

Tot slot, in het laatste hoofdstuk, hebben we de belangrijkste inzichten van dit onderzoek beschreven, inclusief de beperkingen en bronnen van fouten, en richtlijnen gegeven voor toekomstige ontwikkeling, validatie en gebruik van voorgestelde technieken. Het onderzoek beschreven in dit proefschrift is slechts een eerste stap in het evalueren van de complete kinetiek met behulp van inertiële sensoren en er moeten verschillende verbeteringen worden doorgevoerd om het klinische of dagelijkse leven te bereiken. Het verminderen van het aantal en de grootte van sensoren, evenals het vinden van alternatieve energiebronnen, zou het onopvallende gebruik vergemakkelijken. Wat de prestaties betreft, moeten methoden worden gevonden om de kalibratie van sensor tot segment en de schaal van de biomechanische modellen te verbeteren. Wat de toepassing van biofeedback betreft, moeten meerdere feedbackmodaliteiten worden onderzocht om het effect van looptrainingstoepassingen te maximaliseren.

Acknowledgements

Day #1295: The chapters are completed. It's now the moment to share my words of thanks. The last 3+ years of my PhD work have been full of ups and downs, but I have always been fortunate to have people around who supported me and helped me move forward, each one of them in their own special way. My apologies in advance if I have missed mentioning someone by the end of this section.

To begin with, I would like to express my deepest gratitude to my supervisor prof. dr. ir. Peter H. Veltink, who provided me with his persistent guidance and support through the entire trajectory of my doctoral research. Without his helpful advice and in-depth knowledge on ambulatory sensing topics, the completion of this dissertation would not be possible.

I am grateful to my second supervisor, prof. dr. ir. Jaap Harlaar, who despite the physical distance between Enschede and Amsterdam provided invaluable suggestions and insights into the clinical aspects of my research, in order to define the right research questions.

My deepest appreciation goes to my co-supervisor Giovanni Bellusci for the enormous support, time and effort put in my supervision. His excellent advice on inertial motion tracking and long-term guidance have been crucial for the completion of my doctoral research.

I would like to express my sincere gratitude to Martin Schepers, for sharing his experience and detailed advice on human motion analysis and ambulatory sensing, and for making time to meet and provide valuable feedback and comments on my research.

I am deeply indebted to Henk Luinge, who initially gave me the opportunity for this PhD position hosted by Xsens and provided me with his unlimited guidance on the first crucial year of my doctoral trajectory.

Special thanks also to the project partners from Aalborg University, Michael Skipper Andersen and Mark de Zee. Michael, I am grateful for all the essential lessons on biomechanics over Skype&Paint, as well as the AnyBody debugging sessions, without which I would not have gone this far. Mark, thank you for your support with hosting and supporting our data collection in the lab and for always providing constructive suggestions on my research.

The fifth Chapter is a product of our fruitful collaboration with VUMC Amsterdam. Many thanks to Rosie Richards for sharing her insights into gait retraining and clinical biomechanics and the invaluable help in the VR lab. I am grateful to Josien van den Noort for the illuminating discussions on her experience on ambulatory methods and knee osteoarthritis topics.

This dissertation is part of the EU-funded KNEEMO Initial Training Network,

which was coordinated by Glasgow Caledonian University. For that reason, I am sincerely grateful to Prof. Martijn Steultjens, Prof. Jim Woodburn and Denise Scullion for the excellent organization of the network and training events and for making the funding possible.

KNEEMO fellows, thanks for the cheerful meetings in Amsterdam, Glasgow, Münster, Aalborg, Odense, Salzburg, and Brisbane, as well as for all the online and offline knowledge sharing!

During my PhD, my weeks were split between Xsens and BSS. In this way, I obtained twice as many colleagues and friends that helped me overcome the challenges.

On the Xsens side, I have to express my gratitude to Jason who at the latest stage of my PhD has been a constant source of encouragement. "Mate", thanks for your positive attitude and sharing your advice on use of statistics and English language. I am grateful to Sara for the enormous help with the data collection in Aalborg, which was an essential task for this dissertation. The last study would not be possible without the key assistance of Fabian with C# issues. Many thanks to all the colleagues at Xsens for their dedication in delivering outstanding inertial motion capture technology!

From BSS, I am grateful to Bert-Jan for all the help with supervision of student projects and wide-ranging discussions. I would like to sincerely thank both secretaries, Wies and Sandra, for making my PhD path easier through all these years. Next, I would like to thank my first year officemates, Dirk and Fokke for all the useful advice during the crucial planning period of my PhD. Thanks to Tom for the Illustrator tips and all interesting discussions. Thanks to Ed and Marcel for the technical support and coffee breaks. Thanks to all the BSS members for the lunch walks and useful Dutch lessons!

I have been fortunate to be involved in the daily supervision of the graduation assignments of two excellent students, Kwan and Kevin. I am grateful for their help to understand the endless capabilities of HoloLens that was later used in Chapter 5.

The idea to pursue my PhD was born in Xanthi at the time of my Diploma graduation in November 2014. My special gratitude goes to my Diploma thesis supervisor Georgios Ch. Sirakoulis and his former student Kostas Nizamis, who both encouraged me to apply for this PhD position in Twente.

Paranymphs, Frank and Matteo, thank you both for accepting to be next to me for the defence. Frank, I am grateful for all the constructive feedback and coping with me as an officemate at both BSS and Xsens on a daily basis for the last three years. Matteo, thank you for sharing your interdisciplinary advice on topics ranging from inertial sensors, machine learning and cooking!

My family has been since ever a source of support and encouragement for which I am extremely grateful. Μητέρα και πατέρα, Κώστα και Μπάμπη, σας ευχαριστώ θερμά για την απέραντη υποστήριξη!

Last, but definitely not least, I am eternally grateful to Federica for sharing all the beautiful moments with me, but also for all the unlimited support and care through all the life challenges during my PhD period!

Biography



Angelos Karatsidis was born in Didymoteicho, Greece in 1990. In 2008 he started studying Electrical and Computer Engineering in the Democritus University of Thrace, in Greece from where he obtained his Diploma degree in 2014. In his diploma thesis, he investigated hardware implementations of computer vision algorithms for the identification of crowd motion behavior.

His first contact with biomedical technology came during his internship with SciFY NPC in Athens, where he explored assistive input devices and technologies for patients with limited mobility.

Driven by his interests in motion analysis and biomedical technology, in February 2015 he moved to the Netherlands to pursue his PhD, hosted in a mixed industrial and academic setup at Xsens and the department of Biomedical Signals and Systems of the University of Twente. His doctoral project was part of KNEEMO, a Marie Skłodowska-Curie research and training network funded by the EU, investigating biomechanical interventions for knee osteoarthritis. Within this interdisciplinary network, he studied the use of wearable inertial sensors to estimate joint loading, as well as drive biofeedback via augmented reality for the purpose of gait retraining.

Angelos is a student member of IEEE (Institute of Electrical and Electronics Engineers), and ISB (International Society of Biomechanics), and alumnus member of EESTEC (Electrical Engineering STudents European assoCiAtion).

Since February 2018, he works as a research engineer at Xsens, on topics related to inertial motion tracking models and applications.

List of Publications

Published peer-reviewed journal publications

Karatsidis, A., Bellusci, G., Schepers, H. M., de Zee, M., Andersen, M. S., & Veltink, P. H. (2016). Estimation of ground reaction forces and moments during gait using only inertial motion capture. *Sensors*, 17(1), 75.
<http://dx.doi.org/10.3390/s17010075>

Karatsidis, A., Richards, R. E., Konrath, J. M., van den Noort, J. C., Schepers, H. M., Bellusci, G., Harlaar, J., Veltink, P. H. (2018) Validation of wearable visual feedback for retraining foot progression angle using inertial sensors and an augmented reality headset, *Journal of NeuroEngineering and Rehabilitation*, 15(1), 78
<http://dx.doi.org/10.1186/s12984-018-0419-2>

Submitted peer-reviewed journal publications

Karatsidis, A., Schepers, H. M., Bellusci, G., de Zee, M., Andersen, M. S., & Veltink, P. H. Assessment of knee adduction and flexion moments using inertial sensors in knee unloading gait modifications

Karatsidis, A., Jung, M., Schepers, H. M., Bellusci, G., de Zee, M., Veltink, P. H., & Andersen, M. S. Musculoskeletal model-based inverse dynamic analysis under ambulatory conditions using inertial motion capture

Oral, Poster, and Online Presentations

Karatsidis, A., Bellusci, G., Schepers, H. M., de Zee, M., Andersen, M. S., & Veltink, P. H. (2016). From inertial motion capture to ground reaction forces and moments, Vereniging voor Bewegingswetenschappen Nederland (VvBN) PhD-day 2016, 9 November 2016, Maastricht, The Netherlands

Karatsidis, A., Bellusci, G., Schepers, H. M., de Zee, M., Andersen, M. S., & Veltink, P. H. (2017). Estimating the complete ground reaction forces and moments during walking using inertial motion capture, 6th Dutch Bio-Medical Engineering Conference, 26 & 27 January 2017, Egmond aan Zee, The Netherlands

Karatsidis, A., Bellusci, G., Schepers, H. M., de Zee, M., Andersen, M. S., & Veltink, P. H. (2017). Net knee moment estimation using exclusively inertial measurement units, XXVI Congress of the International Society of Biomechanics, ISB 2017, 23-27 July 2017, Brisbane, Australia

Marreiros, S., **Karatsidis, A.**, Schepers, H. M., Bellusci, G., H. M., de Zee, M., Andersen, M. S. (2017). Comparing Performance of Two Methods to Process Inertial Data in Gait Analysis, XXVI Congress of the International Society of Biomechanics, ISB 2017, 23-27 July 2017, Brisbane, Australia

Paulich, M., **Karatsidis, A.**, Gopalakrishnan A. (2017) Outdoor Motion Capture and Musculoskeletal Simulations, Online Webinar by Xsens Technologies B.V. and AnyBody Technology A/S, 30 November 2017
<https://youtu.be/8kfpHmG-f1Q>



ISBN 978-90-365-4602-7